EFFECT OF HYDROGENATED VEGETABLE OIL (HVO) – DIESEL BLEND ON DIESEL SPRAY FLAME UNDER LOW OXYGEN CONCENTRATION AND HIGH DENSITY SURROUNDING GAS

POP-PAUL EWPHUN

A THESIS SUBMITTED IN PARTIAL FULFILLMENT
OF THE REQUIREMENTS FOR THE DEGREE OF
MASTER OF ENGINEERING IN AUTOMOTIVE ENGINEERING
(INTERNATIONAL PROGRAM)
INTERNATIONAL COLLEGE
KING MONGKUT'S INSTITUTE OF TECHNOLOGY LADKRABANG
ACADEMIC YEAR 2016
KMITL-2016-IC-M-004-002

Thesis	Effect of Hydrogenated Vegetable Oil (HVO) – Diesel Blend On Diesel Spray Flame under Low Oxygen Concentration and High Density Surrounding Gas
Student	Mr. Pop-Paul Ewphun
Student ID.	57610029
Degree	Master of Engineering
Program	Automotive Engineering (International Program)
Year	2016
Thesis Advisor	Asst. Prof. Dr. Chinda Charoenphonphanich
	Dr. Nuwong Chollacoop
	Prof. Dr. Hidenori Kosaka

ABSTRACT

This research investigates effect of Hydrotreated vegetable oil – diesel blend to combustion characteristics under EGR and supercharged conditions. Hydrotreated vegetable oil (HVO) is a second generation biofuel that can be a candidate to replace diesel. It can produced from various feedstocks and has a similar viscosity, density and heating value as diesel. However, HVO still has limitations in the CI engine due to its low lubricity and poor low-temperature flow properties. These must be improved by blending it with commercial diesel. The combination of high ambient pressure and high EGR rate is an effective method of reducing emissions of both of NO_x and soot. Injection and spray characteristic are require in order to clearly explain combustion characteristics. A single hole injector was tested with five different fuels commercial diesel, HVO - diesel blends by mass: 20%, 50%, 80% and pure HVO under constant injection pressure and injection duration to investigate the effects of HVO percentage on injection, spray and combustion characteristics under simulate CI engine condition.

Injection characteristic were investigated using Zeuch's method. The experiments were carried out on constant volume chamber. Test fuel is injected into a constant volume chamber filled with test fuel at certain pressure. Chamber pressure was generated by filling test fuel into the

chamber by hand pump until back pressure setting point to simulate the ambient pressure of a CI engine at TDC. As the mass of the fuel in the chamber increases due to injected fuel, the chamber pressure increases proportionally. The results showed that increasing HVO blending percentages not only decreased bulk modulus and injection delay, but also increase injection rate, discharge coefficient, Reynolds number and input energy.

Spray characteristic were investigated using shadowgraph technique. The experiments were carried out on constant volume combustion chamber. Series of spray image were captured by high speed VDO camera then analyzed by image processing. Ambient pressure was generated by filling nitrogen gas into the chamber until back pressure setting point to simulate the ambient pressure of a CI engine at TDC. The results showed that increasing HVO blending percentages not only slightly decreased spray penetration and spray velocity, but also increase spray cone angle.

Combustion characteristics were investigated using heat release rate analysis, two color method, soot concentration measurement and NO_x concentration measurement. The experiments were carried out on a rapid compression expansion machine to simulate the ambient condition of a CI engine at TDC. Synthetic gas with oxygen concentrations of 21%, 15% and 10% were used to simulate EGR conditions. Ambient pressure were varied to supercharged conditions. The results showed that increasing HVO blending percentages decreased ignition delay, flame temperature, soot concentration and NO_x concentration. Heat release at oxygen concentration of 10% dramatically dropped due to a shortened ignition delay, which resulted in less combustion. A decreased oxygen concentration from applied EGR conditions not only increased ignition delay, heat release, flame temperature and NO_x concentration, but also increased soot concentration. A combination of EGR and supercharged conditions by increasing ambient pressure and decreasing oxygen concentrations resulted in increased heat release, decreased flame temperature, ignition delay and soot concentration, compared to EGR conditions.

Keywords: Hydrotreated vegetable oil, Injection characteristic, Isothermal spray visualization, Combustion characteristic, Two-color method

ACKNOWLEDGEMENT

Initially, I would like to express, first and foremost, to my advisor, Asst. Prof. Chinda Charoenphonphanich and co-advisor, Dr. Nuwong Chollacoop and Prof. Hidenori Kosaka for their spacious advice, guidance and encouragement throughout my thesis.

I am extremely grateful to thank National Metal and Materials Technology Center (MTEC), THAILAND for the financial and measuring equipment support in my research and Academic Cooperation Agreement Program (ACAP) for given a chance to be an exchange student at Tokyo Institute of Technology.

I would like to sincerely thank to Prof. Hidenori Kosaka and Assoc. Prof Susumu Sato who has given a chance to perform the experiment in their laboratory. I have learned many things under his kind guidance during I spent my special time in Tokyo Institute of Technology.

I would also like to thank my thesis committee, Asst. Prof. Preechar Karin and Assoc.Prof. Kanit Wattanavichien for their comment and suggestion.

I wish to express my gratitude to assistance from my senior, junior and friends at KMITL Automotive Technology Laboratory, Dr. Prathan Srichai, Mr. Sombat Marasri, Mr. Panuwat Kangkaya, Mr. Jiramed Boonsakda, Mr. Sukit Saranghaeyo and Mr. Veerayut Wongpattharaworakul for their sincere advice and technical support such as the electronic program, equipment some comment and suggestion. I am pleased to have this opportunity to thank many colleagues and bachelor subordinate who have helped me with this dissertation.

I also wish to express my gratitude to assistance from my senior, junior and friends at Tokyo Institute of Technology Advanced Thermo-Fluid Dynamics Laboratory, Mr. Athiwat Butmarasri, Mr. Dittapoom Shinabuth, Mr. Jaeok Bae, Mr. Jaehoon Jeong, Ms. Zhong Peiying, Mr. Hiroki Nakazawa and Mr. Hiroki Sato for their sincerely support during my experiment in Tokyo Institute of Technology.

I am also wish to thank PTT Research & Technology Institute for providing test fuels and Hi-Tech Resources. Co., Ltd for support the high speed video camera.

CONTENTS

LIST OF FIGURE

LIST OF TABLE

CHAPTER 1
Introduction

1.1 Background

Currently, the world is faced with fossil fuel depletion and numerous environmental problems. Many researchers are trying to develop new, clean energy sources for vehicles such as electricity, fuel cell, etc. Unfortunately, it is difficult to replace conventional vehicles due to cost, energy sources, distance between refueling and vehicle performance. Internal combustion and hybrid engines will likely play a role in powering light-duty vehicles at least until 2050 [1].

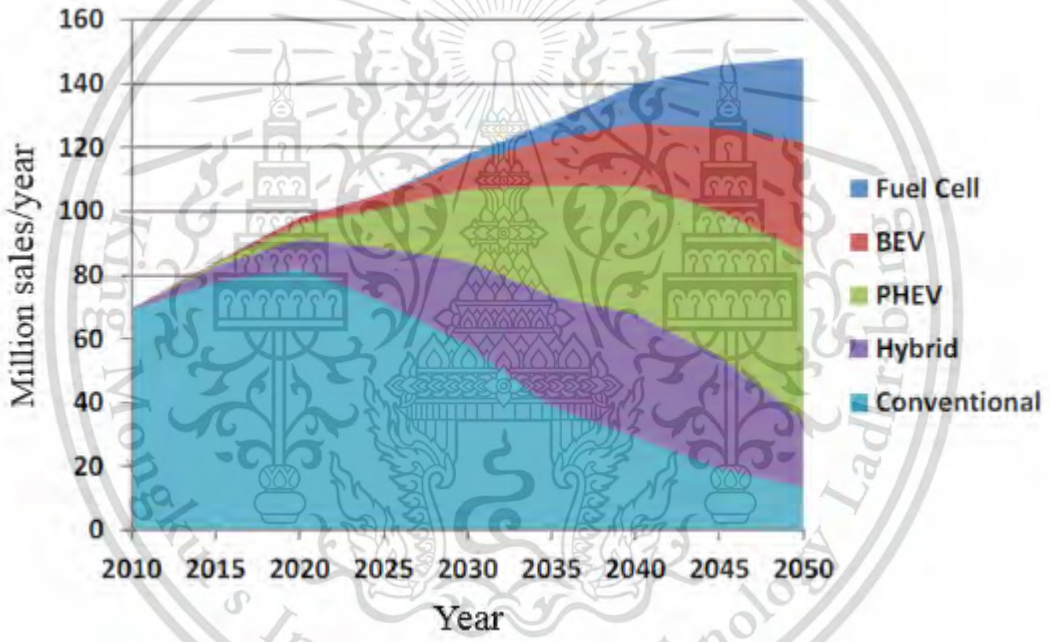

Fig. 1.1 Life cycle of technology light-duty vehicle [1]

Compression ignition (CI) engines provide higher thermal efficiency compared to other internal combustion engines [2]. However, large amounts of NO_x and soot are produced during combustion [3]. Soot and NO_x emission can be reduced by using Hydrotreated vegetable oil (HVO) without the need of engine and control modification [4].

HVO is a second generation biofuel that produce from vegetable oil by using hydrotreating process to remove oxygen from structure. HVO can be a candidate to replace diesel. It can produced from various many kind of vegetable oil without compromising fuel quality, difference form FAME (fatty acid methyl ester) that can produce from limit feedstocks [4]. HVO

has a similar physical and chemical fuel property such as viscosity, density and heating value as diesel [5].

The high cetane number of HVO decreases HC emissions and fuel consumption by increasing the advanced heat release rate and shortening ignition delay [6]. Other advantages of using HVO include advanced combustion phase, shortened combustion duration, and improved thermal efficiency [7].

Moreover NO_x emission in using HVO were almost same level as using commercial diesel but in case of using FAME show significantly higher NO_x emission [8]. Increasing NO_x emission from using FAME cause from the higher fuel injection volume when comparing with diesel due to the lower heating value and higher bulk modulus of elasticity, thus the higher NO_x emission. HVO has almost same heating value with diesel fuel, while its H/C ratio is higher due to the molecular structure of paraffinic hydrocarbon, the higher H/C ratio of BHD could suppress the NO_x emission [9]. However, HVO still has limitations in the CI engine due to its low lubricity and poor low-temperature flow properties. These problems must be improved by blending it with commercial diesel [10, 11].

Another importance issued for CI engine research is thermal efficiency improvement. Thermal efficiency can be improve applying a supercharged condition simulating the operation of a turbo charger in a CI engine, the result is an increased ambient pressure and thermal efficiency. Increased ambient pressure and density also increase heat release from promoted oxygen enhancement. Further, it increases NO_x emission [12].

By applying exhaust gas recirculation (EGR) NO_x emission can be reduce. EGR is a simple, effective method to reduce NO_x emission [13]. This results from decreased oxygen concentration and flame temperatures [14]. On the other hand, EGR decreases heat release due to decreased combustion reaction intensity [15]. It also increases the heat capacity of ambient gas [16].

The combination of high ambient pressure and high EGR rate is an effective method of reducing emissions of both of NO_x and soot [17]. Increasing ambient pressure can extend the limit of the EGR ratio by shortening ignition delay and reducing misfiring by enhanced air fuel mixing [18]. At high boost pressure and EGR up to 30%, no significant effects on performance or thermal efficiency reduction is observed [19].

To date, no study has been performed on the effect of HVO as an alternative fuel with regard to flame temperature under simulated EGR and supercharged conditions. Flame temperature is useful information to explain combustion phenomena, especially for NO_x and soot emissions.

However, Injection and spray characteristic have strongly effect on combustion characteristics [20]. For that reason Injection and spray

characteristic are require in order to clearly perform combustion characteristics as show in Fig. 1.2.

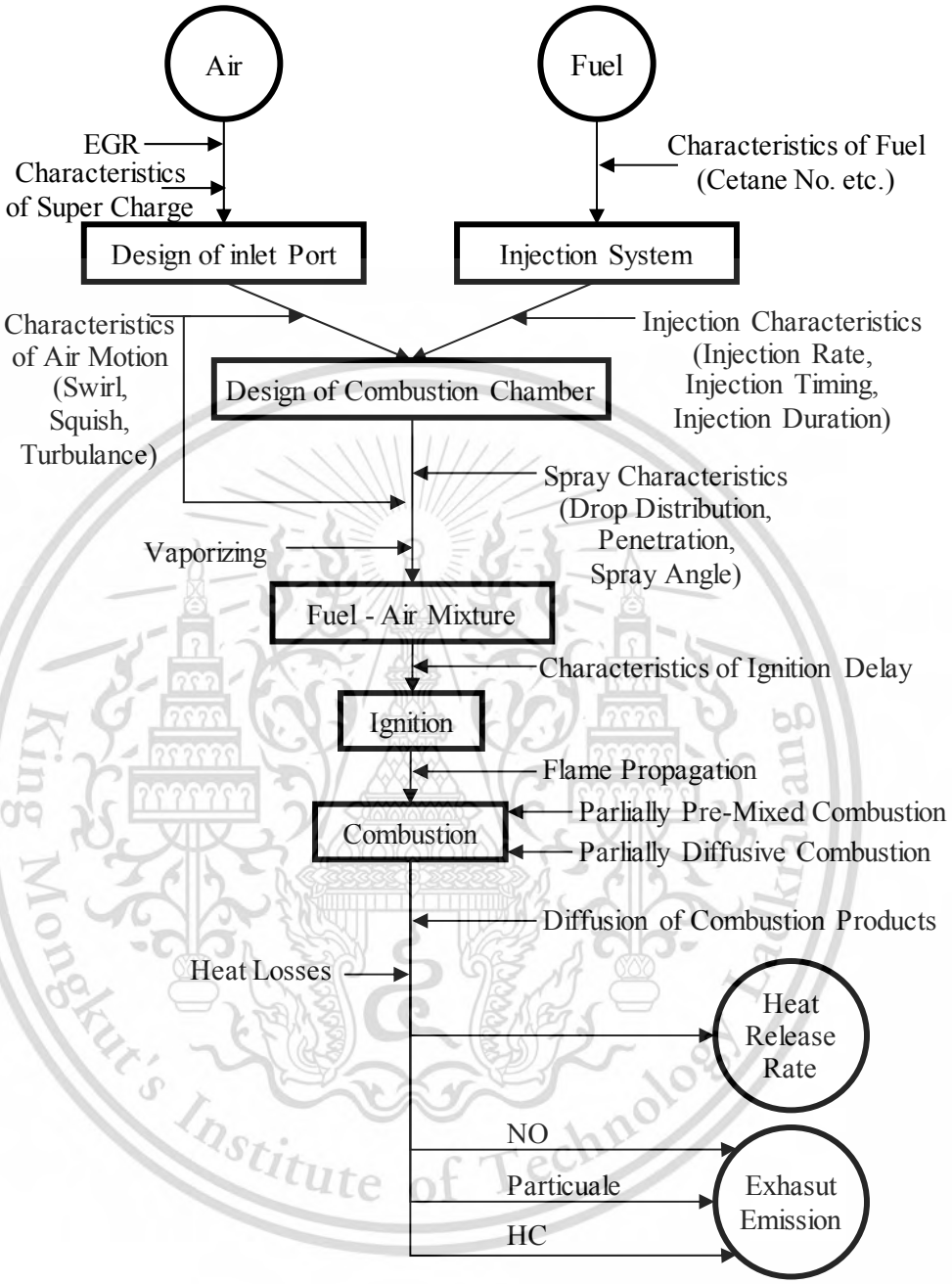

Fig. 1.2 Block diagram of diesel combustion [19]

1.2 Objectives

To investigate effect of HVO - diesel blends 20%, 50%, 80% and HVO on injection, spray and combustion characteristic of diesel spray flame under low oxygen concentration and high density surround gas.

1.3 Scope of work

1.3.1 Fuel property test

These fuel samples will be tested fuel properties such as density, surface tension, viscosity, cetane number, heating value.

1.3.2 Injection characteristic experiment

In this experiment was investigated injection characteristic by Zuech method. Injection characteristic was analysis terms of bulk modulus, injection delay, injection duration, injection quantity, injection rate, discharge coefficient, discharge coefficient compare to Reynolds number and input energy.

1.3.3 Spray characteristic experiment

In this experiment was investigated spray characteristic by high speed photography from shadow graph technic. Spray characteristic was analysis terms of spray penetration, spray velocity, spray cone angle and spray volume.

1.3.4 Combustion characteristic experiment

In this experiment was investigated combustion characteristics under EGR and supercharged conditions using heat release rate analysis, two color method, soot concentration measurement and NO_x concentration measurement. Oxygen concentrations were varied to simulate the effect of EGR under naturally aspirated conditions. EGR and supercharged simulated by varying oxygen concentrations at ambient pressure under a constant total equivalent ratio.

CHAPTER 2

Literature review

2.1 Diesel engine

Diesel engine is internal combustion engine that use the heat of compression to start combustion process. Fuel was injected into the combustion chamber during the final steps of compression stroke. It was developed by Rudolf Diesel in 1897 based on Carnot's cycle, which was invented by Sardis Sardi Carnot. Diesel engine is different from the gasoline engine that used spark plug to ignite. Diesel engine ignite by compressed of air and fuel under high pressure and temperature [21].

2.1.1 Diesel engine operation

Principle of the diesel engine is compress air to a higher temperature then inject fuel. Rapidly compression made pressure and temperature increased without heat loss (Adiabatic compression). The fuel is inject in to combustion chamber then vaporizes and the mixture ignites by itself. Pressure rise from combustion transfer to piston and connecting rod made crack shaft rotated.

Diesel engine is a compression ignition engine of a two or four stroke type. However, in automotive application, diesel engines are four stroke type. The 4 cycle consists of, intake, compression, power, and exhaust as show in Fig. 2.1.

1. Intake stroke: Piston move down from top dead canter (TDC) to bottom dead canter (BDC) during intake valve open and exhaust valve close. The fresh air is drawn in to cylinder.

2. Compression stroke: Piston move up from BDC. In this timing both intake valve and exhaust valve are close. The cylinder pressure and temperature increase corresponding to compression.

3. Power stroke: Piston moves up almost TDC. At the end of the compression stroke fuel is injected into the combustion chamber. In this timing both intake valve and exhaust valve are close. The cylinder pressure increased from combustion is converted into mechanical energy through the piston to the crankshaft.

4. Exhaust stroke: Piston move up from BDC to TDC during intake valve close and exhaust valve open. The exhaust is push out of cylinder.

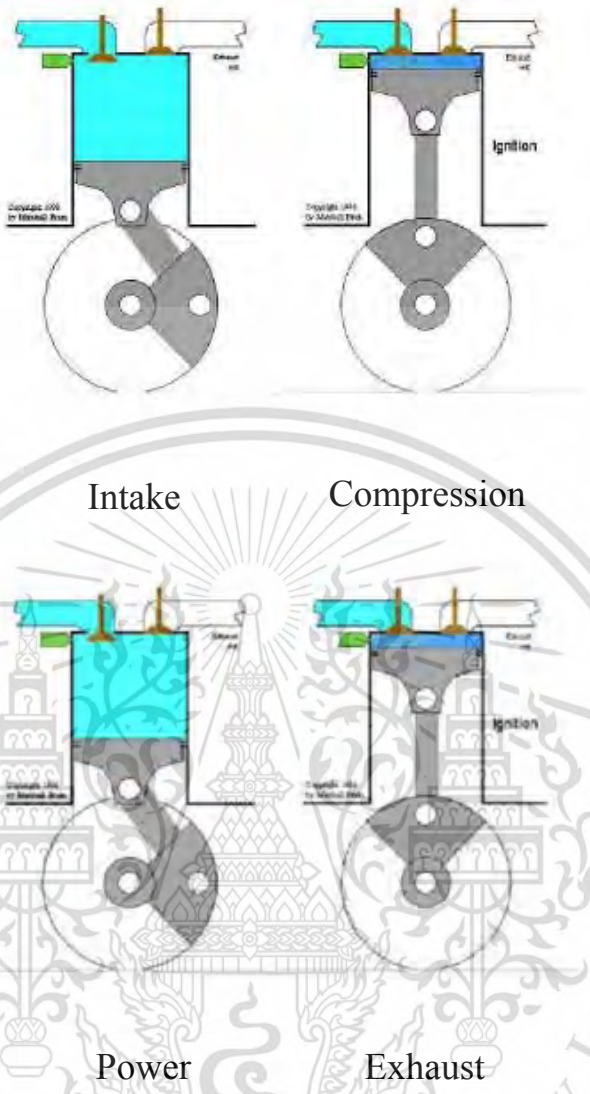

Fig. 2.1 4 Stroke operating cycle [21]

2.1.2 Diesel engine characteristic

Diesel engines provide higher thermal efficiency compared to other internal combustion engines. Moreover, there is no any controversy for diesel engine in heavy duty applications. Another advantageous of diesel engine is operability to use with variety fuels. However, configuration of general diesel engines are manufactured considering using of diesel fuel produced from crude oil. To develop the new fuel technology compatible for diesel engine it is essential to understand the features of common diesel engine. Those features are roughly classified into six groups as Fuel injection characteristic, Fuel spray characteristic, Combustion

characteristic, Engine performance characteristic, Ecology characteristic and Economy characteristic [22].

Fig 2.2 show the relationship of diesel engine characteristics with each other. It is show that injection and fuel spray characteristics relate to combustion, engine performance, ecology and economy. All these characteristics depend on basic parameters such as fuel type or injection system type and on various process characteristics such as the injection process, fuel spray development, atomization, mixture formation, ignition and combustion. The diesel engine characteristics may be influenced by various geometrical and setup parameters either mechanically or electronically controlled fuel injection system.

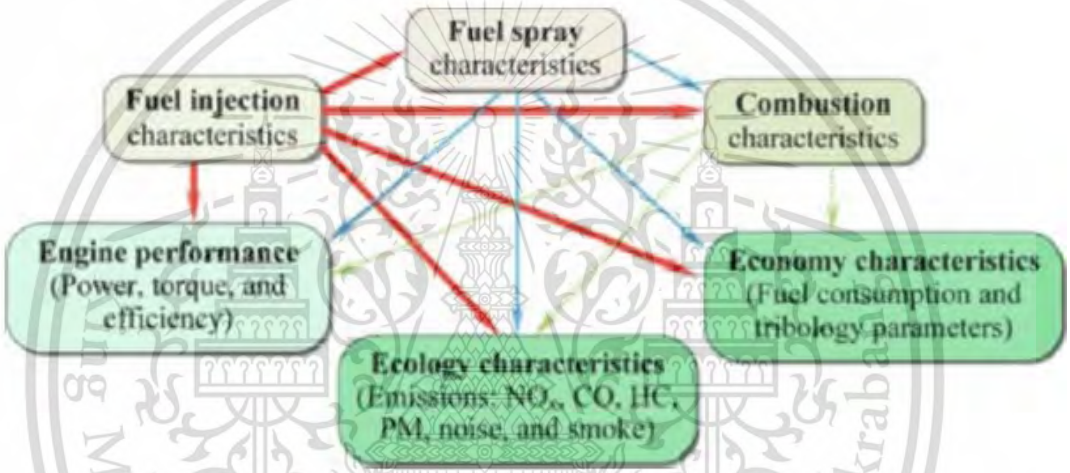

Fig. 2.2 Relationship of diesel engine characteristics [22]

Injection characteristics, spray characteristics and combustion likely play an importance role on engine combustion performance, emission and economy characteristic

2.2 Diesel combustion

2.2.1 Diesel combustion process

In diesel engine, fuel is injected directly into combustion chamber at TDC. However the fuel will not immediately combustion. Mixing time of fuel and air mixture is require. Fig. 2.3 shows the relationship between heat release rate from start of injection (SOI) to end of combustion.

Ignition delay (a to b) is the period between the start of fuel injection into the combustion chamber and start of combustion. Specifically, the

point that heat release rates curves recovers from negative value due to evaporation of fuel into the hot environment.

Premixed combustion (b to c). In this phase combustion of the fuel which already mixed with air during the ignition delay period occurs rapidly in a short time. The burning mixture is added to fuel that ready for burning and burns during this phase, the high heat release rate characteristic of this phase result.

Mixing controlled combustion (c to d). When fuel and air that mixed during the ignition delay have been consumed, the heat release rate is controlled by the rate at which mixture becomes available for burning. While several processes are involved liquid fuel atomization, vaporization, mixture formation, chemical reaction the rate of burning is controlled in this phase primarily by the mixture of fuel and air. The heat release rate may or may not reach a second peak in this phase; it decrease as this phase progresses.

Late combustion (d to e). Heat release continues at lower rate. There are several reasons for this phenomena. A small fraction of the fuel may not yet have burned. A fraction of the fuel energy present in soot and fuel rich combustion product. The cylinder charge mixing in this period promotes more complete combustion and less dissociated gases. The kinetics of the final burnout process become slower as the temperature of the cylinder gases fall.

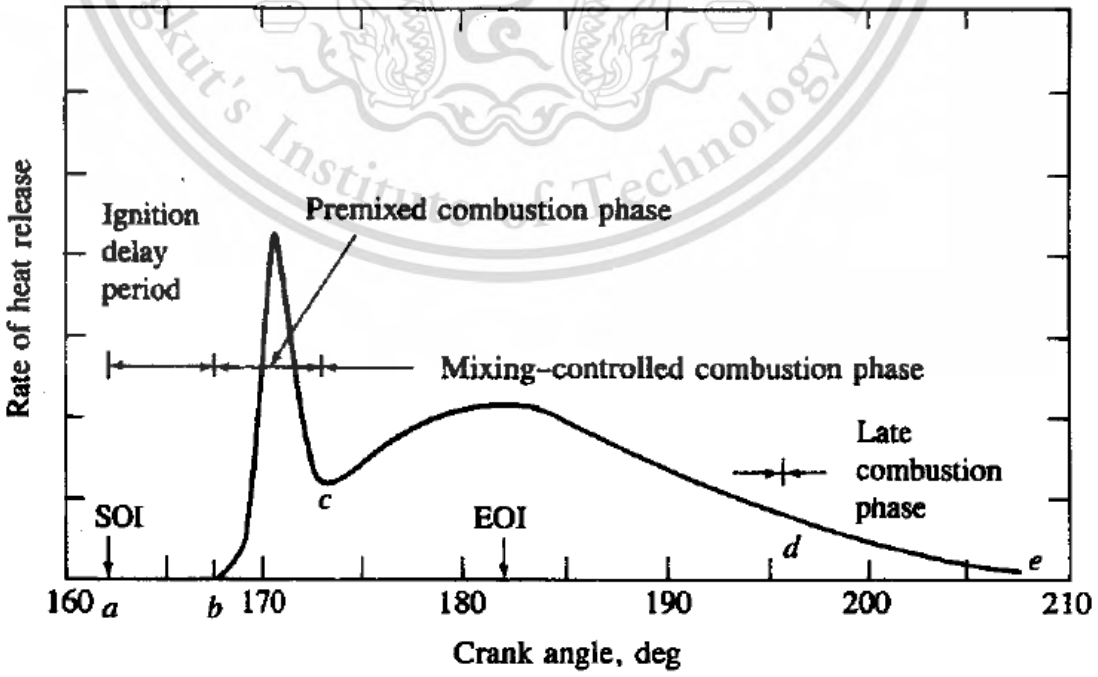

Fig. 2.3 Diesel combustion process [23]

2.3 Fuel injection system

2.3.1 Common rail system

Common rail system as show in Fig. 2.4 [24] has been developed for the modern diesel engines. Supply Pump supply high pressure fuel into the common rail, which is equipped with pressure sensors. Pressure sensor control fuel pressure inside common rail to suit with the engine operating condition.

Electronic Control Unit (ECU) control operating of common rail system based on information from various sensors such as the crankshaft positioning sensor, throttle positioning sensor, intake temperature. Electric Driver Unit (EDU) receive information from ECU to control injector suit with load and speed. ECU also controls the Suction Control Valve of supply pumps to match with engine operation. Resulting the engine is able to unequal inject fuel in each cylinder. From that reason improved engine performance, less vibration, long life time, low maintenance costs and low exhaust emissions.

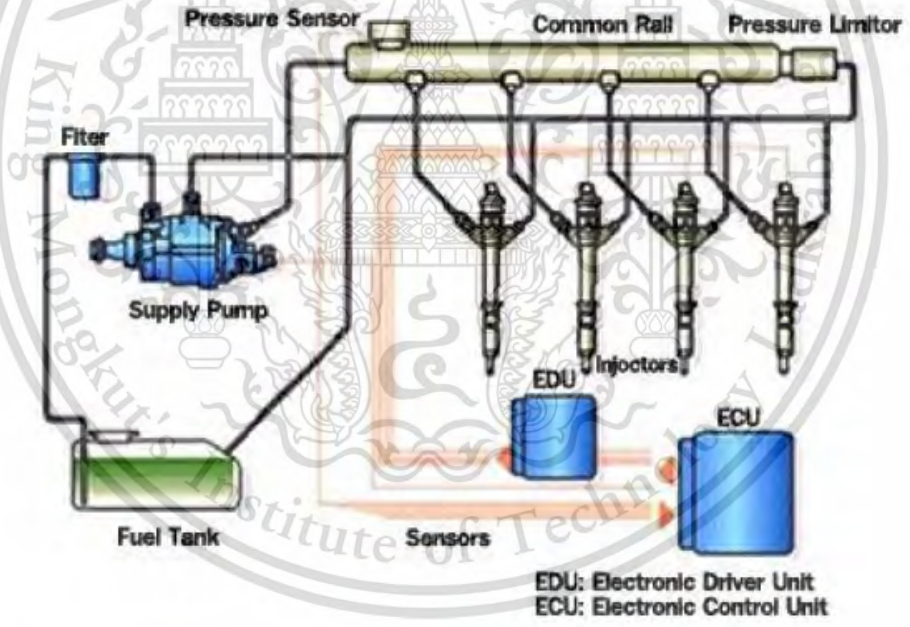

Fig. 2.4 Main component of common rail system [24]

2.4 Hydrotreated vegetable oil

Hydrotreated vegetable oil (HVO) is the second generation biofuel that can be produced from many kinds of vegetable oil by using hydrotreating process, the triglyceride is hydrogenated in the first step and broken down into various intermediates, mainly monoglycerides, diglycerides, and carbonxylic acids. These intermediates are then converted into alkanes by different pathways: decarboxylation, decarbonylation (both removing a

carbon atom from the initial intermediate), and hydrodeoxygenation (with no carbon removal) at the temperatures at temperature above 300–360 ºC and pressure at least 3 MPa. Propane, water, carbon monoxide and carbon dioxide are produced as side-products. HVO is a mixture of normal paraffin and iso-paraffin with shorter chain-length. However, there are some disadvantages that may limit to use HVO from previous study such as poor low-temperature properties, as displayed by cloud point, pour point and cold filter plugging point (CFPP) [11]. Therefore, an improvement process as isomerization process is can be used to solve that problem then HVO would be iso-HVO.

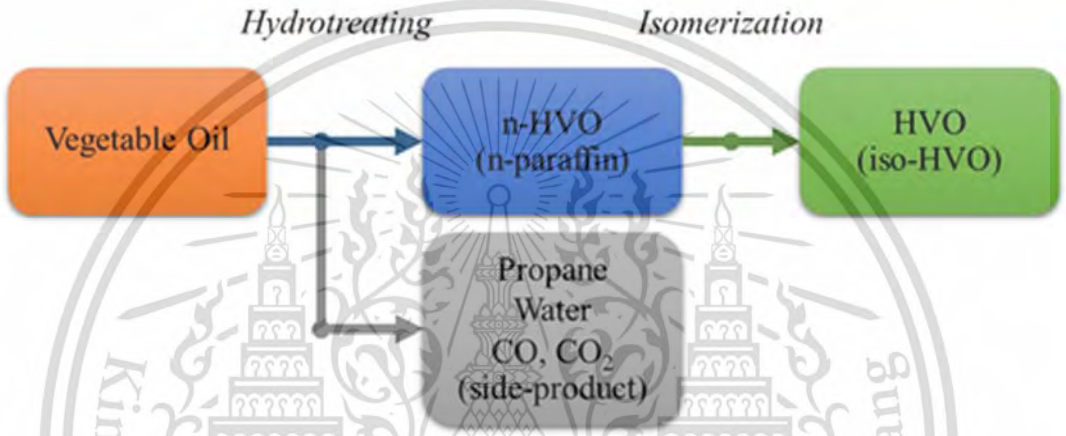

Fig. 2.5 HVO production process

HVO can be a candidate to replace diesel. It can produced from various many kind of vegetable oil without compromising fuel quality, difference form FAME (fatty acid methyl ester) that can produce from limit feedstocks as show in Table 2.1 [4].

Table 2.1 Comparison between FAME and HVO production [3]

Large scale production	Process	Product	Feedstocks: Volume availability and price	Product quality	Production plant investments
≈ 1995 …	Esterification	Biodiesel Ester FAME	-	-	+
2007 …	Hydrotreating	Renewable diesel C_nH_{2n+2} HVO	+	+ + +	-
≈ 2015 …	Gasification + Fischer-Tropsch	Renewable diesel C_nH_{2n+2} FT-BTL	+ + +	+ + +	- - -

C_nH_{2n+2} is a general formula for paraffinic hydrocarbons. + sign indicates benefit, - sign indicates disadvantage

HVO has a similar viscosity, density and heating value as diesel as show in Table 2.2 [5].

Table 2.2 HVO (NEx BTL) properties in comparison with different fuel [5]

FUEL PROPERTIES *)	NExBTL biodiesel	GTL diesel	FAME (RME)	EN590 /2005
Density @15°C [kg/m3]	775...785	770....785	≈ 885	≈ 835
Viscosity @40°C [mm2/s]	2.9...3.5	3.2...4.5	≈ 4.5	≈ 3.5
Cetane number	84...99 **)	73...81	≈ 51	≈ 53
Distillation 10 vol% [°C]	260...270	≈ 260	≈ 340	≈ 200
Distillation 90 vol% [°C]	295...300	325...330	≈ 355	≈ 350
Cloud point [°C]	- 5...- 30	0...- 25	≈ - 5	≈ - 5
Lower heating value [MJ/kg]	≈ 44	≈ 43	≈ 38	≈ 43
Lower heating value [MJ/litres]	≈ 34	≈ 34	≈ 34	≈ 36
Polyaromatics [wt%]	0	0	0	≈ 4
Oxygen [wt%]	0	0	≈ 11	0
Sulfur [mg/kg]	≈ 0	< 10	< 10	< 10

Sugiyama *et al.* [6] Study on combustion characteristic and emission of HVO compare to diesel by using 2.2 liter common rail, turbo charger CI engine on engine and chassis dynamometer. This experiment showed that high cetane number of HVO decreases emissions and fuel consumption by increasing the advanced heat release rate and shortening ignition delay as show in Fig. 2.6.

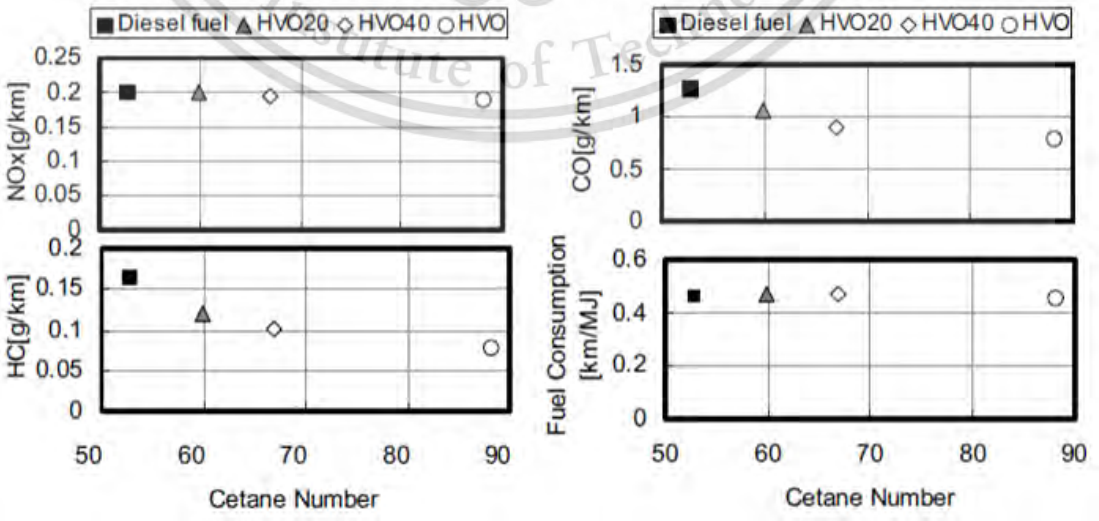

Fig. 2.6 Result of using HVO in vehicle [6]

Jaroonjitsathian *et al*. [7] Study effect of HVO, GTL, HVO and GTL blend with diesel 50% on engine performance and emission characteristic by using 2.5 liter common rail, turbo charge CI engine without any modification on engine dynamometer. The study, conducted on pilot and main injection at 1170 RPM. HVO and GTL, showed shorter ignition delays as show in Fig. 2.7, advanced combustion phase and shortened combustion duration as show in Fig. 2.8 due to a higher cetane number and a higher thermal efficiency compared to diesel.

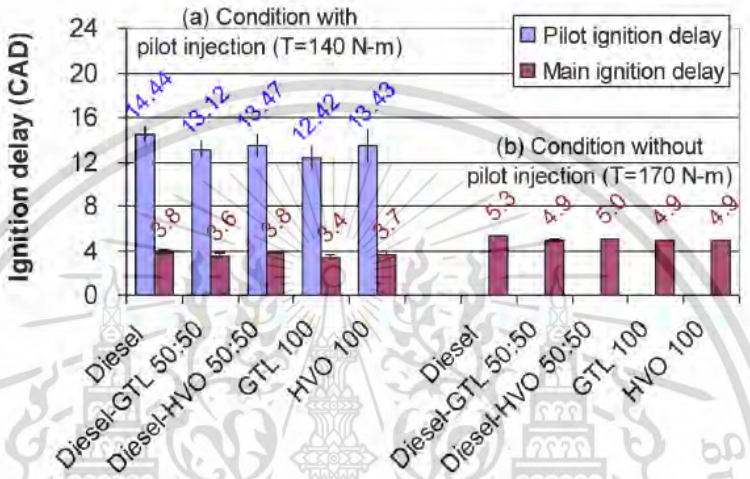

Fig. 2.7 Comparison of ignition delay [7]

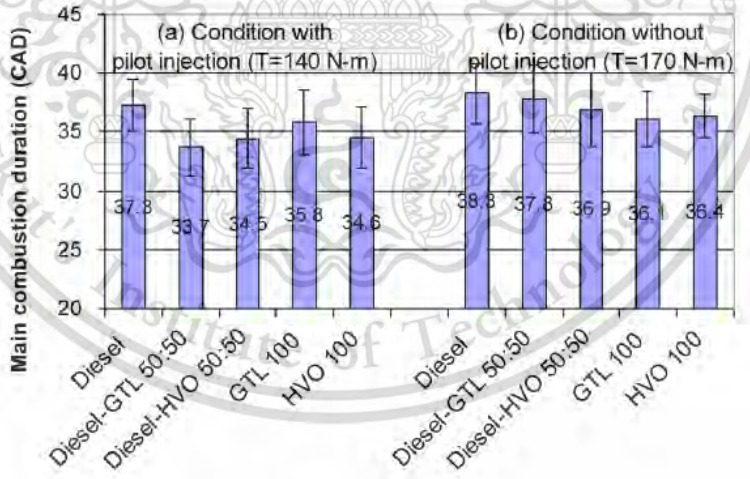

Fig. 2.8 Comparison of combustion duration [7]

Mizushima *et al*. [8] Study effect of FAME, HVO, BTL, HVO and BTL blend with diesel on NO_x emission by using 6.0 liter common rail, turbo charge CI vehicle equipped with portable emission measurement system. The study, conducted by using real road driving test. HVO show almost same NO_x emission level as using commercial diesel but in case of using FAME show significantly higher NO_x emission as show in Fig. 2.9.

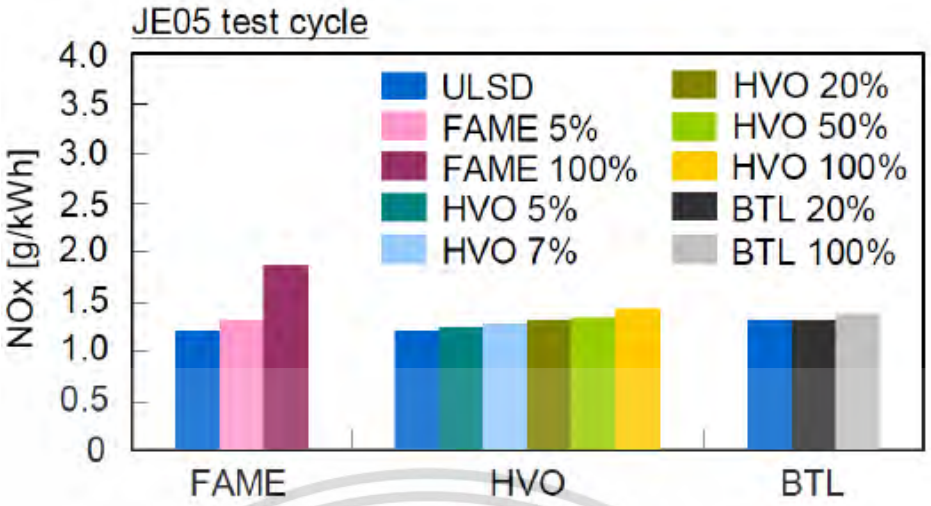

Fig. 2.9 Comparison of NO_x emission [8]

Increasing NO_x emission from using FAME cause from the higher fuel injection volume when comparing with diesel due to the lower heating value and higher bulk modulus of elasticity, thus the higher NO_x emission. HVO has almost the same heating value with diesel fuel, while its H/C ratio is higher due to the molecular structure of paraffinic hydrocarbon, the higher H/C ratio of HVO could suppress the NO_x emission [9].

However, HVO still has limitations in the CI engine due to its low lubricity and poor low-temperature flow properties. These must be improved by blending it with commercial diesel [10, 11].

2.5 Exhaust gas recirculation

Exhaust gas recirculation (EGR) is a simple, effective method to reduce NO_x emission [13]. The exhaust gases mainly consist of nitrogen, carbon dioxide and the mixture has higher specific heat ratio compared to air in atmosphere. Re-circulated exhaust gas mixed with fresh air entering the combustion chamber with carbon dioxide and water vapor present in engine exhaust. As a consequence of this air displacement, lower oxygen concentration in the intake mixture is prepare for combustion. Reduced oxygen concentration for combustion lowers the effective air–fuel ratio. This effective reduction in air–fuel ratio affects exhaust emissions substantially. In addition, mixing of exhaust gases with intake air increases specific heat of intake mixture, which results in the reduction of flame temperature.

Kitamura *et al.* [12] Investigate effect of oxygen concentration by change oxygen concentration in Constant volume combustion chamber (CVCC). The result show that decreased oxygen concentration effect to NO_x emission reduction as show in Fig. 2.10.

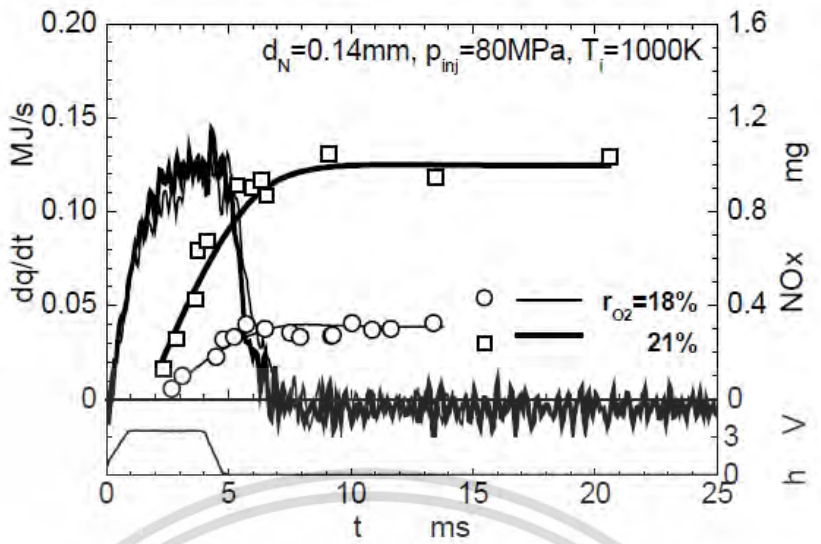

Fig. 2.10 Effect of oxygen concentration on heat release rate and NOx [12]

Jing *et al.* [25] Investigate effect of oxygen concentration by change oxygen concentration on flame temperature in CVCC. The result show that decreased oxygen concentration effect to flame temperatures reduction as show in Fig. 2.11.

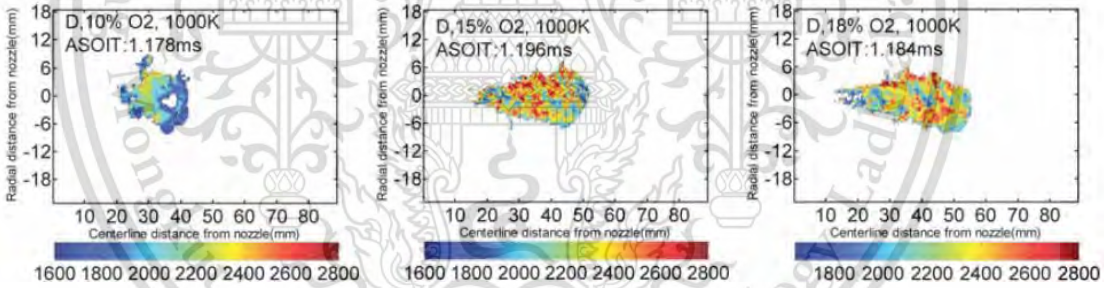

Fig. 2.11 Effect of oxygen concentration on flame temperature [25]

EGR is effective method to reduce NO_x emission from decreased oxygen concentration and flame temperatures. However EGR also decreases heat release due to decreased combustion reaction intensity.

Zhang *et al.* [15] Investigate effect of oxygen concentration by change oxygen concentration 21%, 18%, 15% 12% and 10% in CVCC. The result show that lower oxygen concentration extend ignition delay and reduce heat release rate due to decreased combustion reaction intensity as show in Fig. 2.12. Decreasing reaction intensity with can be explain in function of OH chem-iluminescence as show in Fig. 2.13.

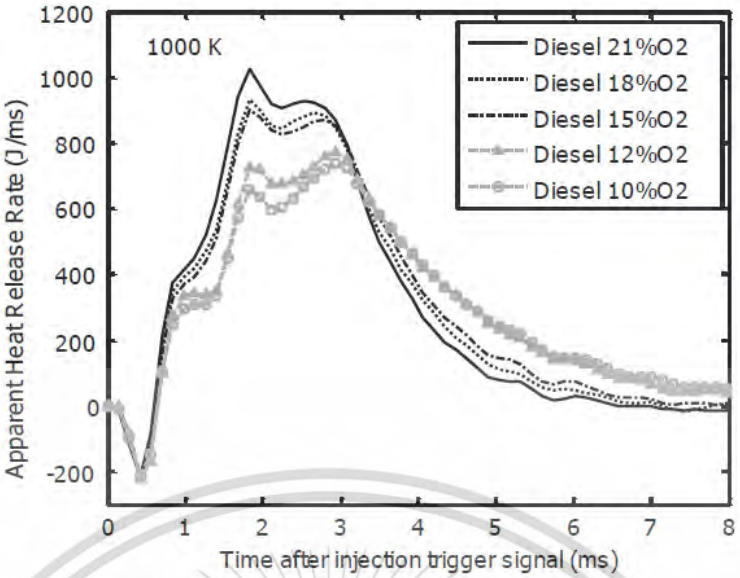

Fig. 2.12 Effect of oxygen concentration on heat release rate [15]

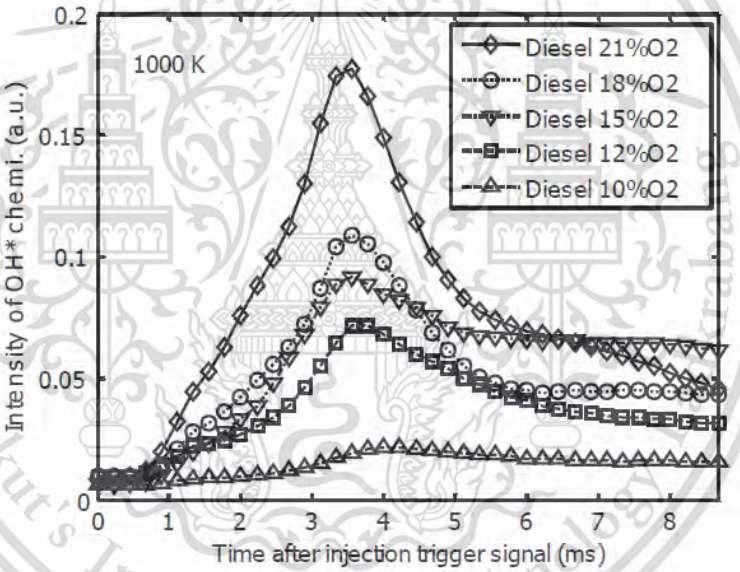

Fig. 2.13 Effect of oxygen concentration on OH* chemiluminescence [15]

2.6 Supercharged condition

By applying a supercharged condition simulating the operation of a turbo charger in a CI engine, the result is an increased ambient pressure and thermal efficiency. Increased ambient pressure and density also increase heat release from promoted oxygen enhancement. Further, it increases NO_x emission.

Kitamura *et al.* [12] Investigate effect of ambient pressure on heat release rate and NO_x emission in CVCC. The result show that increased ambient pressure and thermal efficiency. Increasing ambient pressure

increased heat release rate and also NO_x emission from promoted oxygen enhancement as show in Fig. 2.14.

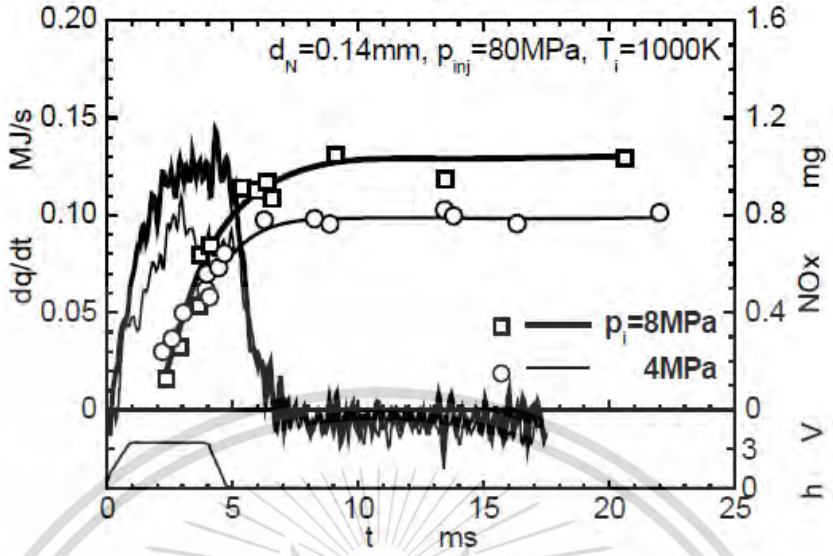

Fig. 2.14 Effect of ambient pressure on heat release rate and NO_x [12]

Adachi *et al.* [17] Study effect of high boost and high EGR on NO_x reduction. The experimental was done one heavy duty diesel engine equip with high-pressure loop EGR system (HP-EGR), low-pressure loop EGR system (LP-EGR) and back pressure control valve (BPCV) as shown in Fig. 2.15. HP-EGR is the EGR gas returns to intake pipe after passage through the compressor of a turbocharger from the exhaust manifold before the turbocharger turbine. LP-EGR is the EGR gas returns from the exhaust pipe after the turbocharger to the atmospheric intake pipe before the turbocharger compressor. BPCV which controls the exhaust pressure. The result show that combination of high ambient pressure and high EGR rate is an effective method of reducing emissions of both of NO_x and soot as show in Fig. 2.16.

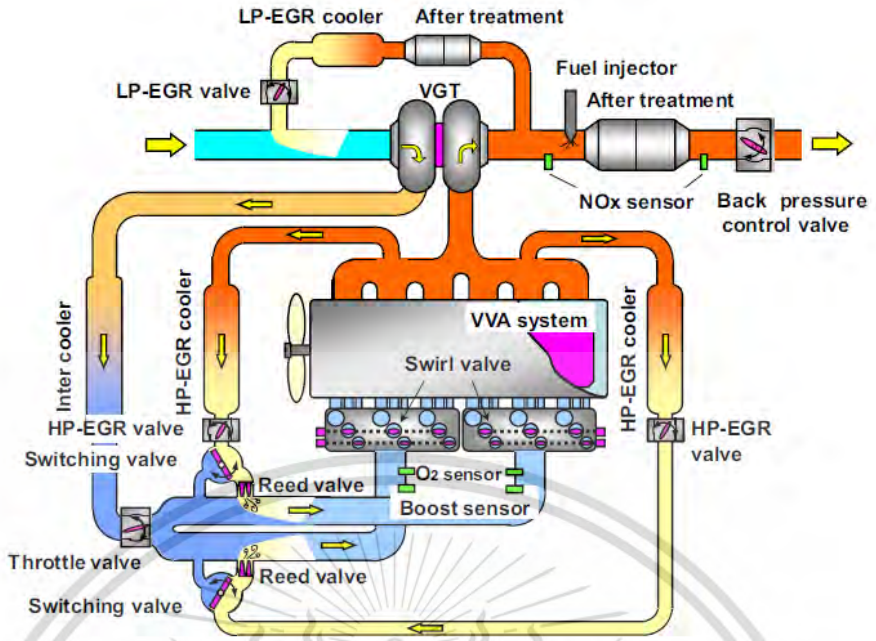

Fig. 2.15 Diagram of engine equip HP-EGR and LP-EGR [17]

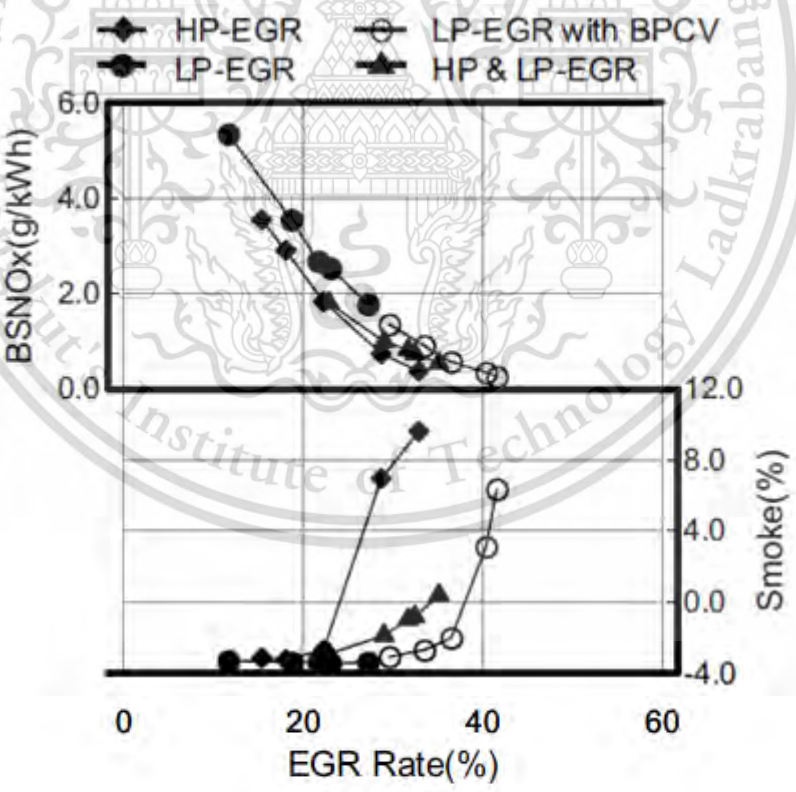

Fig. 2.16 Effect of high boost and high EGR on emission [17]

Uchida *et al.* [18] Study effect of EGR application method to combustion pressure and heat release rate by using 1.3 liter single cylinder CI engine. The study, conducted on replace EGR method and additional

EGR method. For replace EGR method intake pressure was kept at constant and varying EGR ratio. For additional EGR method intake pressure increase proportional to EGR ratio. Fig. 2.17 shows the combustion pressure and heat release for replaced EGR. Ignition delay increasing proportionally with EGR ratio. At retarded injection timings misfires occurred at high EGR conditions due to the increased inert gas and reduced mixing time. On the other hand, for Additional EGR the effect of EGR ratio on combustion was different from replaced EGR. Ignition delay was decreased and the heat release rate was improved as much as the without EGR condition. Ignition delay was increased at a very low EGR ratio. Moreover, heat release rates during the diffusion combustion period were slightly increased compared with the without EGR condition as show in Fig. 2.18.

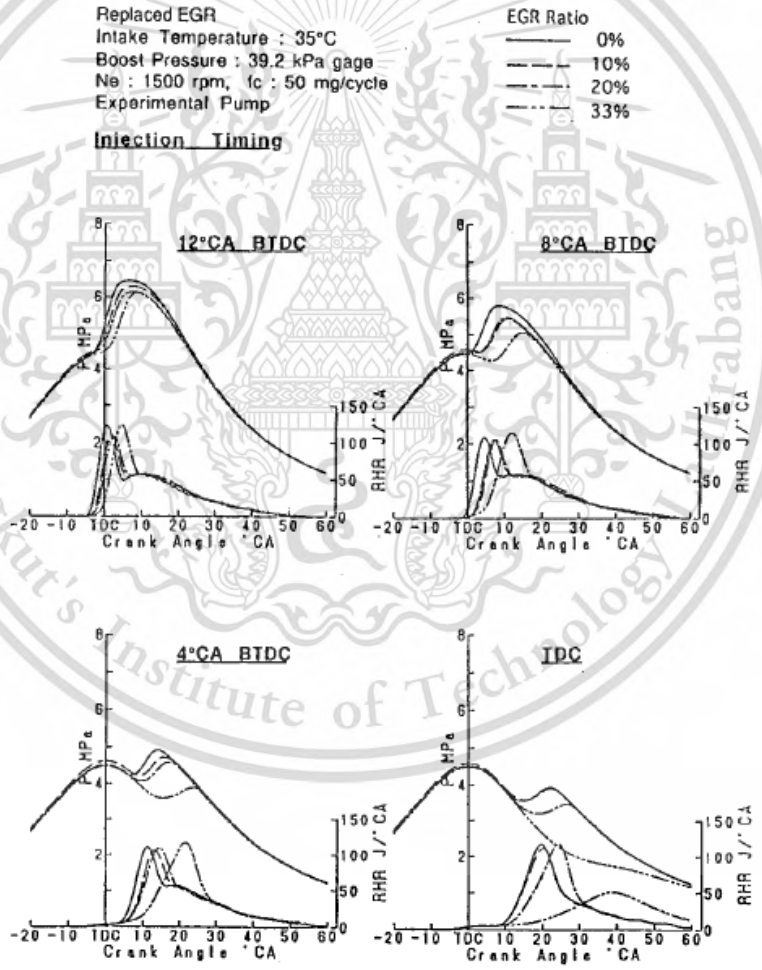

Fig. 2.17 Effect of replaced EGR on combustion pressure and heat release rate [18]

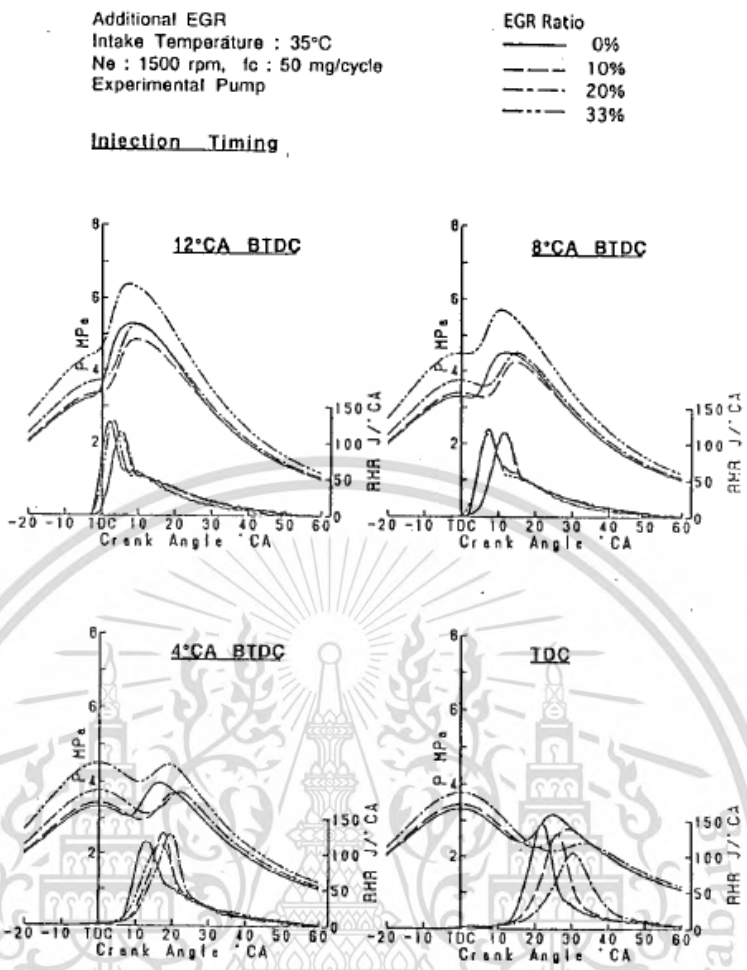

Fig. 2.18 Effect of additional EGR on combustion pressure and heat release rate [18]

Aoyagi *et al.* [19] Study effect of EGR percentage under high boost condition to heat release rate by using 2.0 liter common rail, turbo charge single cylinder CI engine on engine dynamometer. The study, conducted on full load with varies EGR percentage at 1200 RPM. No significant heat release rate reduction was observed in this experiment at EGR up to 30% as show in Fig. 2.19.

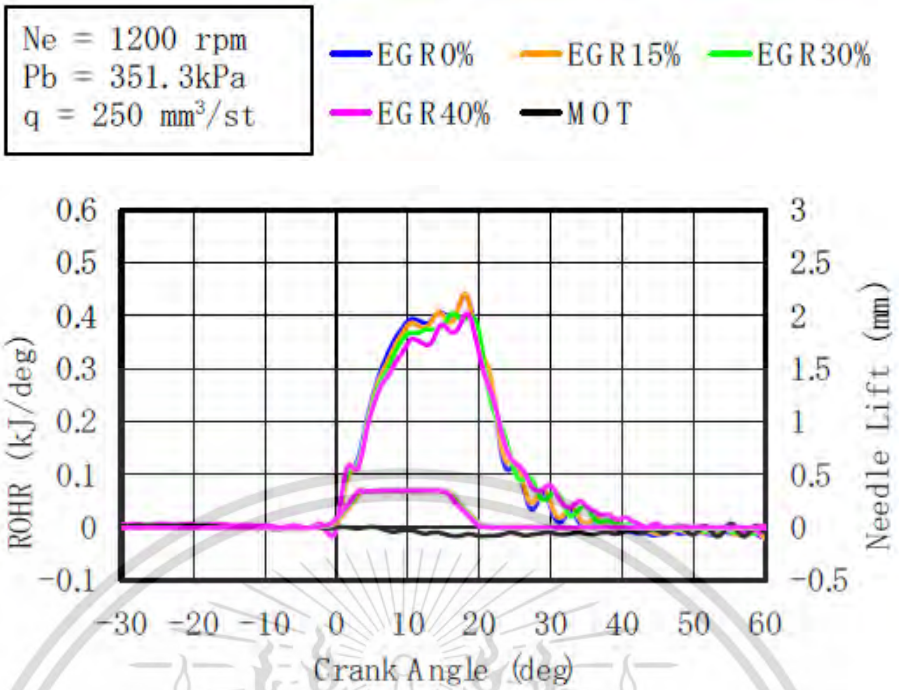

Fig. 2.19 Effect of oxygen concentration on heat release rate under high boost condition [19]

2.7 Research gap

From high cetane of HVO might be beneficial at high EGR ratio. The combination of EGR and supercharged condition made simultaneously reduce exhaust emissions and improve thermal efficiency is possible.

To date, no study has been performed on the effect of HVO as an alternative fuel on injection, spray and combustion characteristic of diesel spray flame under low oxygen concentration and high density surround gas.

CHAPTER 3

Experimental procedure

3.1 Test fuels

The experiment was conducted using five different fuels- commercial diesel, HVO - diesel blends by mass: 20% (H20), 50% (H50), 80% (H80) and pure HVO. In this research density were tested by density meter. Kinematic viscosity were tested by viscometer. Heating value were tested by bomb calorimeter. Surface tension were tested by tensiometer. Carbon, Hydrogen and Oxygen content were tested by gas chromatography. Distillation temperature were tested by distillation tower.

Table 3.1 Fuels properties

Properties	Standard	Diesel	H20	H50	H80	HVO
Density @ 30°C (g/cm3)	ASTM D4052	0.824	0.814	0.800	0.787	0.778
Kinematic viscosity @ 40°C (mm2/s)	ASTM D445	3.24	3.09	2.90	2.74	2.64
Heating value (MJ/Kg)	ASTM D240	45.86	46.04	46.38	46.55	46.86
Surface tension (mN/m)	ASTM D1590	26.38	25.89	25.56	24.91	24.84
Carbon content (%)	ASTM D5291	85.73	85.43	84.98	84.53	84.24
Hydrogen content (%)	ASTM D5291	13.22	13.59	14.14	14.68	15.05
Oxygen content (%)	ASTM D5599	0.00	0.00	0.00	0.00	0.00
Distillation T10 (°C)	ASTM D86-11b	207.7	210.7	216.3	223.1	227.4
Distillation T50 (°C)	ASTM D86-11b	287.9	284.5	281.4	279.2	278.2
Distillation T90 (°C)	ASTM D86-11b	352.3	345.2	327.4	303.5	293.2
Derived cetane index	ASTM D4737	60.43	63.37	68.32	73.44	76.89

Comparison of diesel densities at 303 K to H20, H50, H80 and HVO showed decreases of 1.15%, 2.87%, 4.49% and 5.53%, respectively. Viscosity decreases at 40°C were recorded at 4.54%, 10.34%, 15.30% and 18.49%, respectively. Heating value increases were recorded at 0.39%, 1.12%, 1.15% and 2.18%, respectively. Surface tension decreases were recorded at 1.86%, 3.11%, 5.57% and 5.84%, respectively. Distillation T10 increases were recorded at 1.44%, 4.14%, 7.45% and 9.49%, respectively. Distillation T50 decreases were recorded at 1.18%, 2.26%, 3.02% and 3.37%, respectively. Distillation T90 decreases were recorded at 2.02%, 7.07%, 13.86% and 16.76%, respectively. Derived cetane index increases were recorded at 4.87%, 13.06%, 21.53% and 27.24%, respectively. Mean increasing HVO blend percentage, density decrease, viscosity decrease, heating value increase, distillation T10 increase, distillation T50 decrease, distillation T90 decrease and derived cetane index increases as are shown in Table 3.1. From the physical and chemical property of HVO and HVO blend fuel tend to be good candidate to replace diesel.

3.2 Injection characteristics

3.2.1 Methods of injection experiment

Using the Zeuch method [26] to determine amount of fuel injection. Principle of Zeuch's injection rate, the test fuel is injected into a constant volume chamber filled with test fuel at certain pressure. As the mass of the fuel in the chamber increases due to injected fuel, the chamber pressure increases proportionally. Bulk modulus is defined as the fuel's resistance to compression as shown in Equation (1)

$$K = V\frac{dP}{dV} \qquad (1)$$

Where K is bulk modulus, dV is change of chamber volume and dP is pressure rise from compression of the plunger. Bulk modulus and pressure increase from injected fuel rate can be determined using Equation (2)

$$\dot{m}_f = \frac{dm}{dt} = \rho\frac{V}{K}\frac{dP}{dt} \qquad (2)$$

Fig. 3.1 shows measurement method from injection rate profile calculated using Equation (2). Injection delay is the period from the start of energizing (SOE) to the start of injection (SOI). Specifically, the point that injection rate recovers from negative value due to the volume change

from needle lift. Injection duration is the period from SOI to the end of injection (EOI), or the point that injection rate decreases to negative value. Injection quantity is calculated by integration under curve area from SOI to EOI. Measured mass flow is calculated by averaging injection rates from 1 ms to 3 ms due to avoid the effect of transient opening and closing of injector.

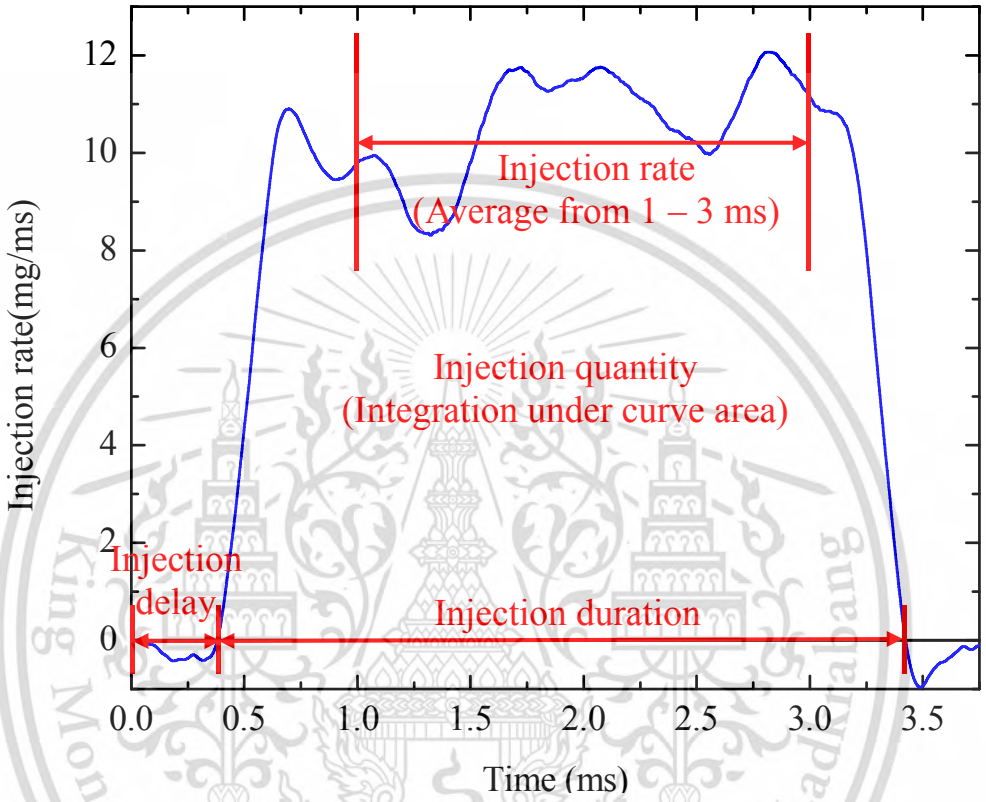

Fig. 3.1 Measurement method of injection experiment

Discharge coefficient (*Cd*) is the ratio of measured injection rate to theoretical injection rate from the Bernoulli equation, where $\dot{m}_f$ is measured injection rate, $\dot{m}_{th}$ is theoretical injection rate, n is number of orifice, S is nozzle outlet cross section area and ΔP is pressure difference between injection pressure and back pressure, as shown in Equation (3) [27].

$$Cd = \frac{\dot{m}_f}{\dot{m}_{th}} = \frac{\dot{m}_f}{n \times S\sqrt{2\Delta P \times \rho}} \qquad (3)$$

The fuel exit effective velocity is calculated using Equation (4) where $\dot{m}_f$ is measured injection rate, n is number of orifice and S is nozzle outlet cross section area [28].

$$V_{ef} = \frac{\dot{m}_f}{n \cdot S \cdot \rho} \qquad (4)$$

Reynolds number is calculated using Equation (5) where V_{ef} is the fuel effective velocity at the orifice outlet, D_0 is the nozzle outlet diameter and v is the kinematic viscosity.

$$Re = \frac{V_{ef} \cdot D_0}{v} \qquad (5)$$

Input energy under constant energizing time is determined as injection quantity multiplied by heating value as shown in Equation (6)

$$Input\ energy = Injection\ quantity \cdot Heating\ value \qquad (6)$$

3.2.2 Experimental setup of injection experiment

A schematic diagram of the experiment is show in Fig. 3.2. In this experiment, the Zeuch chamber with volume capacity 40 cm^2 was selected to clearly determine pressure signal and electric noise [18]. A single hole 0.2 mm cylindrical nozzle was equipped with solenoid injector and installed in the chamber to inject test fuel. Back pressure was generated by compress test fuel into the chamber by hand pump until back pressure setting point. A static pressure transducer was installed to measure back pressure. Pressure increase from the injected fuel was measured by a piezoelectric dynamic pressure tranducer (Kistler 6053CC60) and amplified by charge amplifier (Kistler 5011). The pressure increase from the injected fuel was recorded by oscilloscope (RIGOL DS1052E) with sampling rate $2x10^8$ sampling / sec. 2nd generation common rail pump drive by three phase motor controlled by inverter. Injection pressure was kept constant by motor revolution and the suction control valve. Injection duration and trigger was controlled by micro controller which actuated Electric Drive Unit (EDU) to inject fuel.

Fuel bulk modulus was measured by filling the chamber with test fuel using a hand pump until reaching the back pressure setting point, and then supplying nitrogen gas to the pneumatic cylinder to push the plunger. The movement of the plunger caused chamber volume reduction which led to a pressure increase. All experiments were conducted at room temperature.

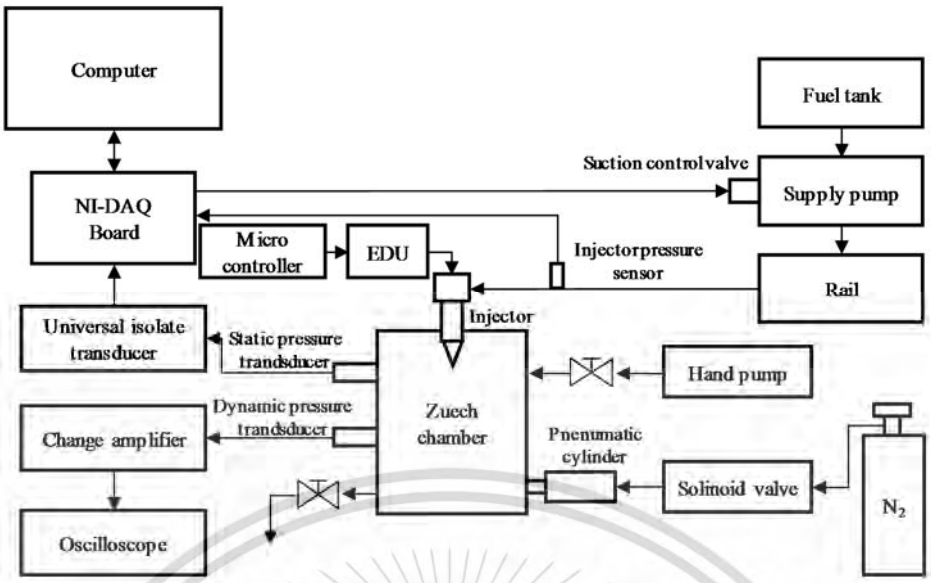

Fig. 3.2 Schematic diagram of injection experiment

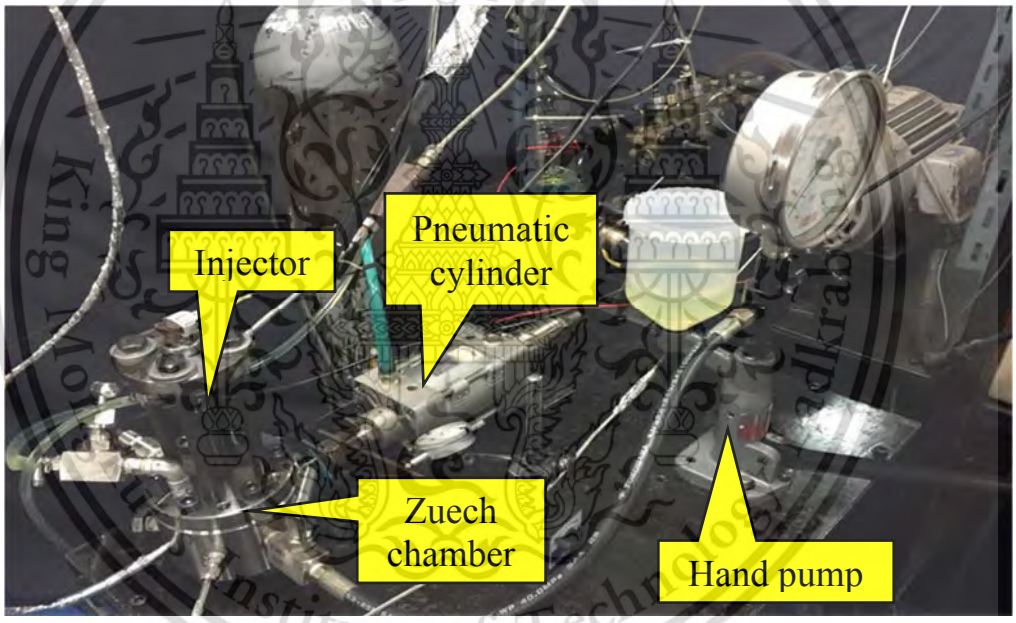

Fig. 3.3 Injection characteristic experimental equipment

This experiment was conducted using five different fuels- commercial diesel, HVO - diesel blends by mass: 20% (H20), 50% (H50), 80% (H80) and pure HVO. Further, the testing was done at ambient temperature with single hole diameter 0.2 mm, 0.8 mm orifice length solenoid injector, 2.0 ms energizing time, 100 MPa injection pressure, 4 MPa back pressure (to simulate pressure inside the combustion chamber) at TDC of compression ignition engine. Bulk modulus measurement was done with 7.0 mm plunger diameter and 2.0 mm plunger displacement .All tests were repeated 10 times, as shown in Table 3.2.

Table 3.2 Test conditions of injection experiment

Parameter	Conditions
Test fuel	Diesel, H20, H50, H80, HVO
Nozzle orifice diameter	Single hole 0.2mm
Energizing time	2.0 ms
Injection pressure	100 MPa
Back pressure	4.0 MPa
Plunger diameter	7.0 mm
Plunger displacement	2.0 mm
Repeat	10 Times / Condition

3.3 Spray characteristics

3.3.1 Methods of spray experiment.

Image processing was used to determine the boundary of spray image as show in Fig. 3.4. The image processing method start from binarization of the images from a threshold of intensity, by the Otsu's method. Spray penetration (S) is defined as 80% intensity from tip of spray image to avoid evaporate of liquid spray. Spray velocity is calculated from spray penetration a in each frame divided by time. Spray cone angle is defined as maximum angle each side of spray at S/2 from injector tip [29]

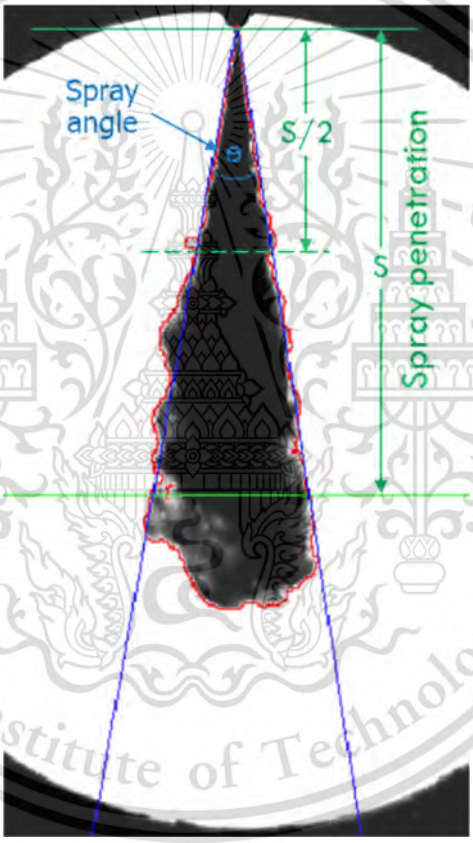

Fig. 3.4 Image processing method

Spray volume (V) described by Equation (7) [30]. The spray volume calculate by using basic geometry, Spray penetration (S) and spray cone angle (θ).

$$V = (\pi/3)S^3[tan^3(\theta/2)]\frac{1+2tan(\theta/2)}{[1+2tan(\theta/2)]^3} \qquad (7)$$

3.4.2 Experimental setup spray experiment

A schematic diagram of the experiment is show in Fig. 3.5. In this experiment, the cylindrical constant volume combustion chamber (CVCC) with 80 mm diameter quart windows. A single hole 0.2 mm cylindrical nozzle was equipped with solenoid injector and installed in the chamber to inject test fuel. Ambient pressure was generated by filling nitrogen gas into the chamber until back pressure setting point. A static pressure transducer was installed to measure ambient pressure. A 2nd generation common rail pump drive by three phase motor controlled by inverter. Injection pressure was kept constant by motor revolution and the suction control valve. Injection duration and trigger was controlled by micro controller which actuated Electric Drive Unit (EDU) to inject fuel. Series of spray image were captured by high speed VDO camera (Photron UX100) with lens at 10,000 frame per second (fps) and 640x480 pixels then analyzed by image processing. High speed VDO camera was triggered with injector command. All experiments were conducted at room temperature.

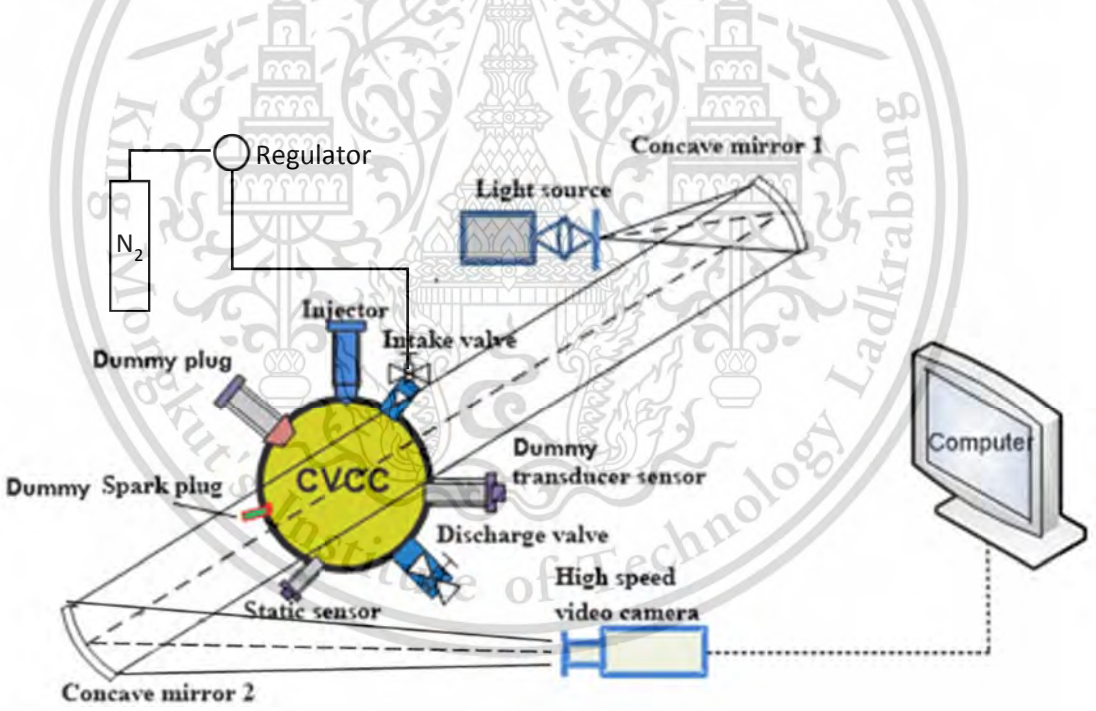

Fig. 3.5 Schematic diagram of spray experiment

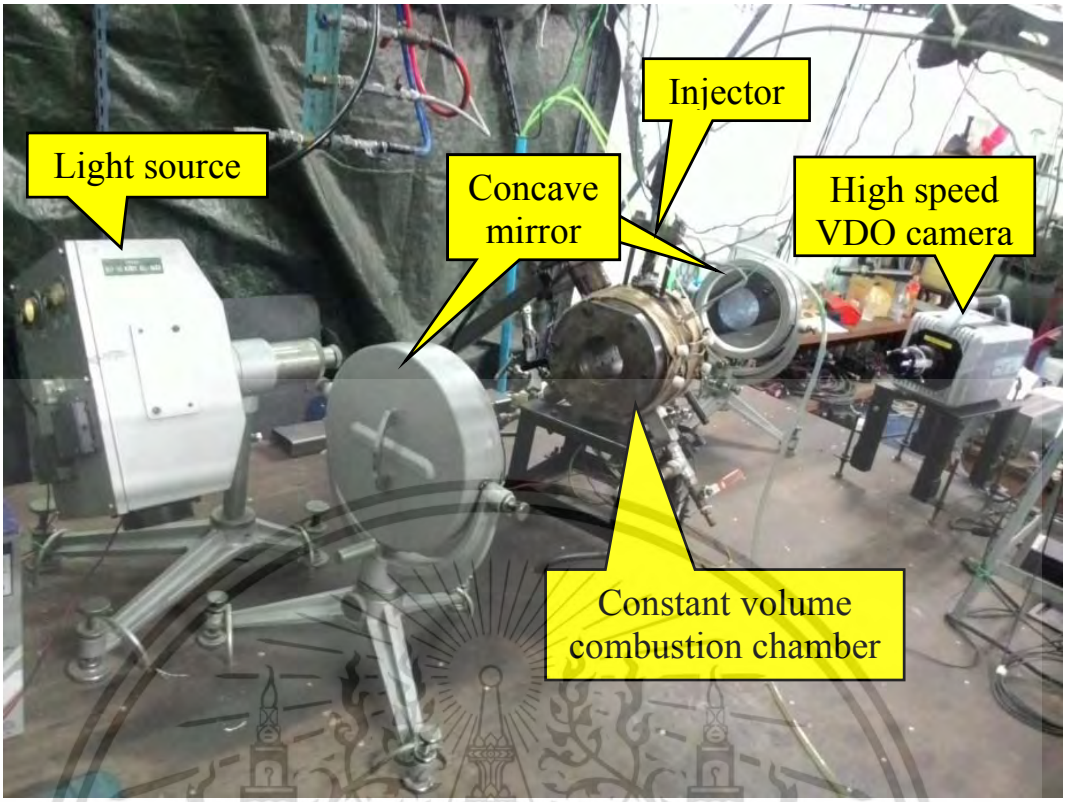

Fig. 3.6 Spray characteristic experimental equipment

This experiment was conducted using five different fuels- commercial diesel, HVO - diesel blends by mass: 20% (H20), 50% (H50), 80% (H80) and pure HVO. Further, the testing was done at ambient temperature with single hole diameter 0.2 mm, 0.8 mm orifice length solenoid injector, 2.0 ms energizing time, 100 MPa injection pressure, 4 MPa back pressure (to simulate pressure inside the combustion chamber) at TDC of compression ignition engine. All tests were repeated 10 times, as shown in Table 3.3.

Table 3.3 Test conditions of spray experiment

Parameter	Conditions
Test fuel	Diesel, H20, H50, H80, HVO
Nozzle orifice diameter	Single hole 0.2mm
Energizing time	2.0 ms
Injection pressure	100 MPa
Back pressure	4.0 MPa
Repeat	10 Times / Condition

3.4 Combustion characteristics

3.4.1 Methods of combustion experiment

Ignition delay is defined as the interval between the start of injection (SOI) and the start of combustion (SOC). Specifically, the point that heat release rate curves recovers from negative value due to evaporation of fuel into the hot environment [23] as show in Fig. 3.7.

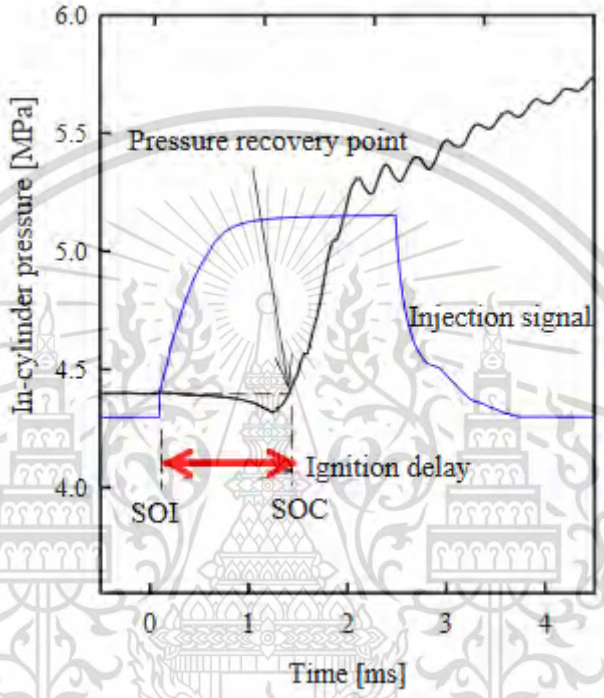

Fig. 3.7 Definition of ignition delay by combustion pressure and injection signal [31]

Heat release rate was calculated from combustion pressure rise after fuel injection by applying the first law of thermodynamics [23], as shown in Equation (8) where γ is the specific heat ratio, P is the chamber pressure, dV/dt is the rate of volume change in chamber and dP/dt is the rate of pressure change in chamber.

$$\frac{dQ}{dt} = \frac{\gamma}{\gamma - 1} \cdot P \cdot \frac{dV}{dt} + \frac{1}{\gamma - 1} \cdot V \cdot \frac{dP}{dt} \qquad (8)$$

Heat release is calculated by integration under the curve area of heat release rate from the start of combustion to the point at which the heat release rate decreases to a negative value.

Flame temperatures were measured by the two color method based on thermal radiation of soot particle in two different wave lengths [32]. Monochromatic radiation from non-black body, explained by Equation (9) where ε is the emissivity, λ is the wavelength, C_1 is the first Planck constant, C_2 is the second Planck constant and T flame is the flame temperature.

$$I_{(\lambda,T)} = \varepsilon_\lambda \frac{C_1}{\pi\lambda^5} exp^{(-C_2/\lambda T)} \qquad (9)$$

The monochromatic radiant intensity can also be explained in terms of the apparent temperature (T_a), as shown in Equation (10).

$$I_{(\lambda,T)} = \frac{C_1}{\pi\lambda^5} exp^{(-C_2/\lambda T_a)} \qquad (10)$$

Monochromatic radiant intensity in Equation (9) and (10) are equal. By replacing $\varepsilon\lambda$ from Equation (9) with Equation (10), Equation (11) is obtained.

$$\varepsilon_\lambda = 1 - exp^{(-KL/\lambda)} \qquad (11)$$

The measurement of soot particle radiations in two wavelengths enables solution for KL and T, based on Equation (12) where K is the absorption coefficient and L is the path.

$$KL = -\lambda^a \ln\left[1 - exp\left\{\frac{C_2}{\lambda}\left(\frac{1}{T_a} - \frac{1}{T}\right)\right\}\right] \qquad (12)$$

Before the two color method can be applied to measure flame temperature, it is necessary to calibrate high speed camera for flame brightness measurement. Black body furnace and pyrometer are used to accurately determine the reference temperature. Distance between black body furnace and high speed camera was set same as measurement distance used in the experiment. The visible light can be converted by CCD detector in the high speed camera into three color bands, red, green and blue. Any two of the three color bands can be used for the calculation of temperature and KL factor. Two wavelengths that used in this experiment are blue (501 nm) and red (612 nm). Then flame temperature can be calculated by using MATLAB base on Equation (12).

Soot concentration is determined by passing exhaust gas from a combustion unit chamber to filter paper to collect soot emissions. It is then measured with a smoke meter.

NO_x concentration is investigated by passing exhaust gas from a combustion unit chamber through a pressure reduction tube then supplying it to a NO_x analyzer.

3.4.2 Experimental setup of combustion experiment

Combustion characteristics experimental were done on a rapid compression expansion machine (RCEM) [33], shown in Fig. 3.8 The RCEM combustion chamber has 86.0 mm bore with a 151.5 mm diameter. Ambient pressure was arrived at by mixing O_2 and N_2 in a mixing tank at 453K, then filling synthetic gas into the combustion chamber until the setting pressure. It was then compressed by piston from BDC to TDC within 30 ms and kept at TDC for 150 ms to provide a constant volume condition. A single hole 0.2 mm diameter exit orifice was equipped with solenoid injector to injected test fuel with 100 MPa into the combustion chamber. A static pressure transducer was installed to measure ambient pressure at BDC. Pressure increase from combustion was measured by a piezoelectric dynamic pressure tranducer (AVL GU22CK) and amplified by charge amplifier (Kistler 5011B). The pressure increase from the injected fuel was recorded by oscilloscope (YOKOGAWA DL750) with a sampling rate of $1x10^6$ sampling/sec. The flame image was captured by high speed camera (NAC GX-1) with lens (Nikkor 55 mm f/2.8) at 10,000 frame per second (fps) and 464x464 pixels. Soot concentration was measured by passing through exhaust gas from combustion to filter paper in order to collect soot emissions. It was then measured by smoke meter (SOKKEN GSM-3). NO_x concentration was measured by passing through exhaust gas after smoke filter through a pressure reduction pipe then supplying normal pressure chemiluminescence to a NO_x analyzer (SHIMADZU NOA7000).

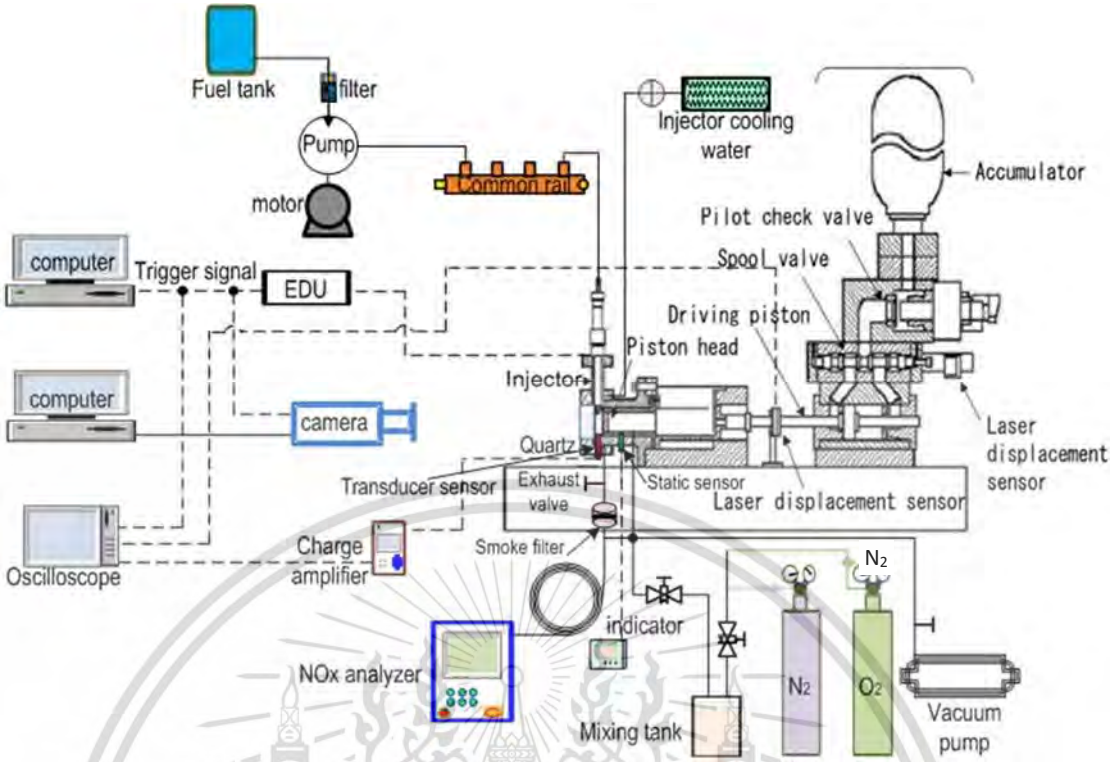

Fig. 3.8 Schematic diagram of combustion experiment

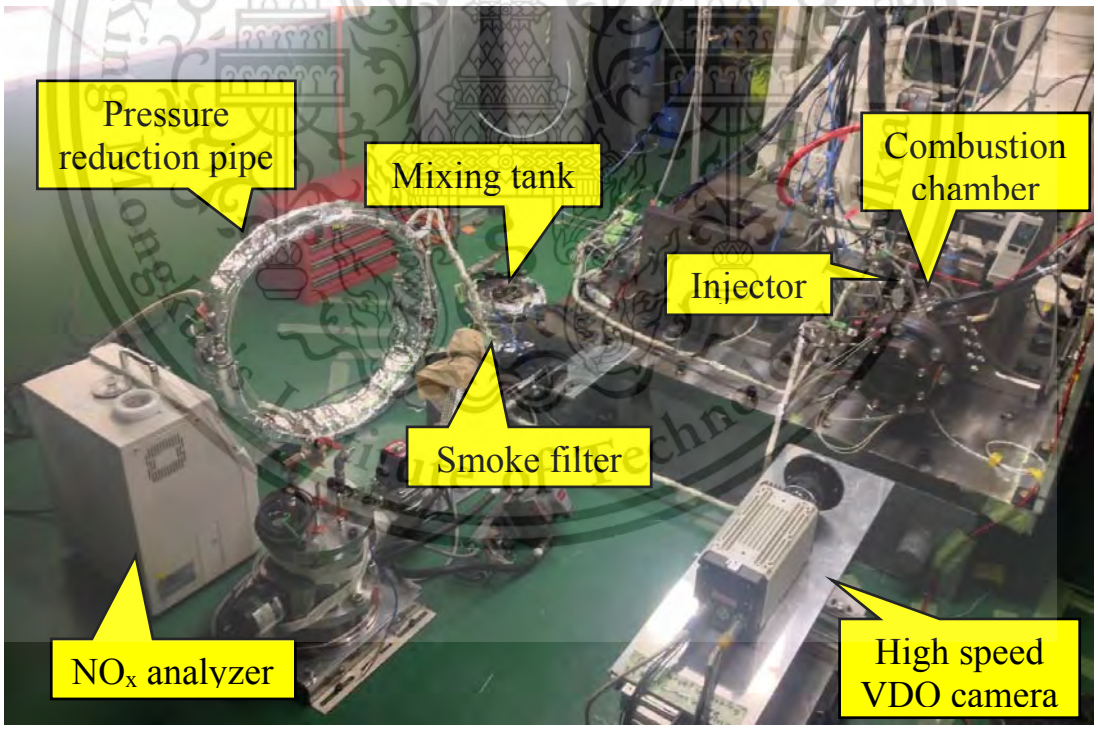

Fig. 3.9 Combustion characteristic experimental equipment

Table 3.4 shows test conditions in this experiment. The experiment was conducted using five different fuels- commercial diesel, HVO - diesel blends by mass: 20% (H20), 50% (H50), 80% (H80) and pure HVO. Other conditions were a nozzle exit orifice diameter of 0.2mm; solenoid injector

2.0 ms energizing time, to reduce the effect of transient opening condition and closing; 100 MPa injection pressure, to avoid cavitation from high pressure; and 800K ambient gas temperature. Oxygen concentrations of 21%, 15% and 10% at 4.0 MPa were used to simulate the effect of EGR under naturally aspirated conditions by varying oxygen concentrations under constant total gas amount. For oxygen concentrations of 15% at 5.6 MPa and 10% at 8.4 MPa, the effect was investigated of EGR and supercharged by varying oxygen concentrations at ambient pressure under a constant equivalent ratio. All tests were repeated 10 times for each test condition.

Table 3.4 Test conditions of combustion experiment

Parameter	Conditions
Test fuel	Diesel, H20, H50, H80, HVO
Nozzle orifice diameter	Single hole 0.2mm
Energizing time	2.0 ms
Injection pressure	100 MPa
Ambient gas temperature	800 K
Oxygen concentration	21, 15 and 10%
Ambient pressure	Naturally aspirated: 4.0MPa Supercharged :5.6and 8.4MPa
Repeat	10 Times / Condition

CHAPTER 4

Results and Discussions

4.1 Injection characteristics

In this experiment, injection characteristics were conducted using five different fuels- commercial diesel, H20, H50, H80 and HVO. Other conditions were a nozzle exit orifice diameter of 0.2mm, solenoid injector 2.0 ms energizing time, 100 MPa injection pressure and 4.0 MPa back pressure. Result of injection characteristics experimental are present in terms of bulk modulus, injection rate profile, injection delay, injection duration, injection quantity, injection rate, discharge coefficient, discharge coefficient compared to Reynolds number and input energy.

4.1.1 Bulk modulus

Fig. 4.1 shows the effects of blending percentages of HVO into diesel fuel on bulk modulus under constant chamber pressure and volume. The bulk modulus was calculated using Equation (1). Diesel shows the highest bulk modulus compared to HVO blend fuels and HVO. Bulk modulus of H20, H50, H80 and HVO were lower at 1.10%, 3.75%, 6.40% and 7.19%, respectively compared to diesel. Bulk modulus is proportional to the density of each fuel [34]. Lowered densities resulting from increased HVO blend percentages had the effect of decreasing bulk modulus.

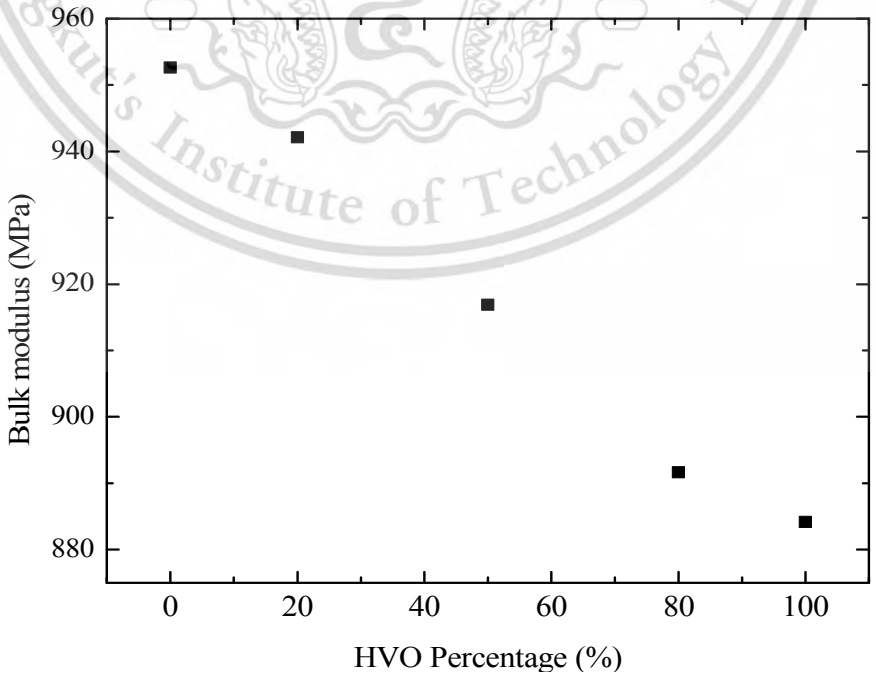

Fig. 4.1 Bulk modulus

4.1.2 Injection rate profile

Fig. 4.2 shows the effects of blending percentage of HVO into diesel fuel on injection rate profile under constant injection pressure. The injection rate profile is presented in several stages. The injection delay stage from start of energizing to 0.4 ms after energizing. Injection delay including with injector electric delay and mechanical delay. The needle rising stage from 0.4 to 0.7 ms after energizing largely depends on fuel viscosity [35]. Injection rate during 0.7 to 1.0 ms after energizing was dip due to the bounce-back of the needle in command chamber of injector. The next stage is the fully open stage form 1.0 to 3.0 ms after energizing. The last stage is the closing stage from 3.0 to 3.4 ms after energizing. In closing stage a small amount of fuel is injected after the closing due to the needle bounce back. However the effects of blending percentage of HVO into diesel fuel still not clearly observe in this figure.

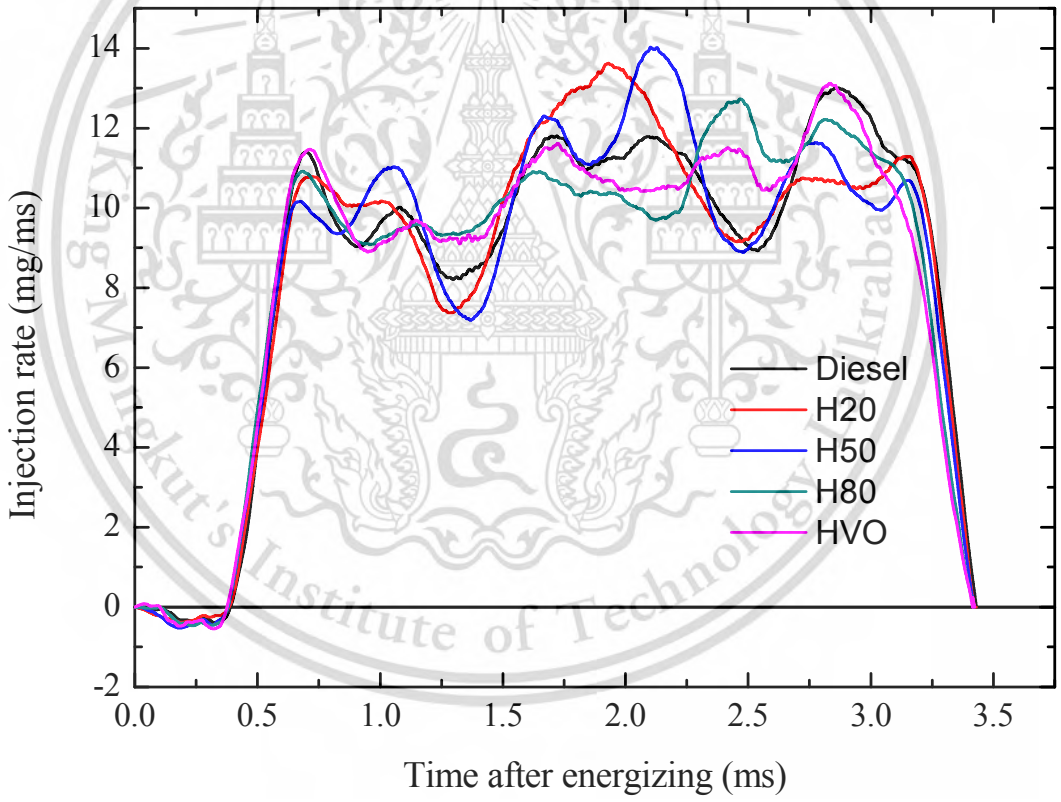

Fig. 4.2 Injection rate profile

4.1.3 Injection delay

Fig. 4.3 shows the effects of blending percentage of HVO into diesel fuel on injection delay under constant injection pressure. The injection delay was determined as shown in Fig. 3.1. Diesel showed the highest injection delay compared to HVO blend fuels and HVO. Injection delays of H20, H50, H80 and HVO were lower by 0.42%, 1.31%, 1.60% and 2.48%, respectively compared to diesel. Injection delay differences were caused by differing fuel viscosities. Lower viscosity from increasing HVO blend percentages resulted in lower resistance force to needle lift, making injection delay shorter [36].

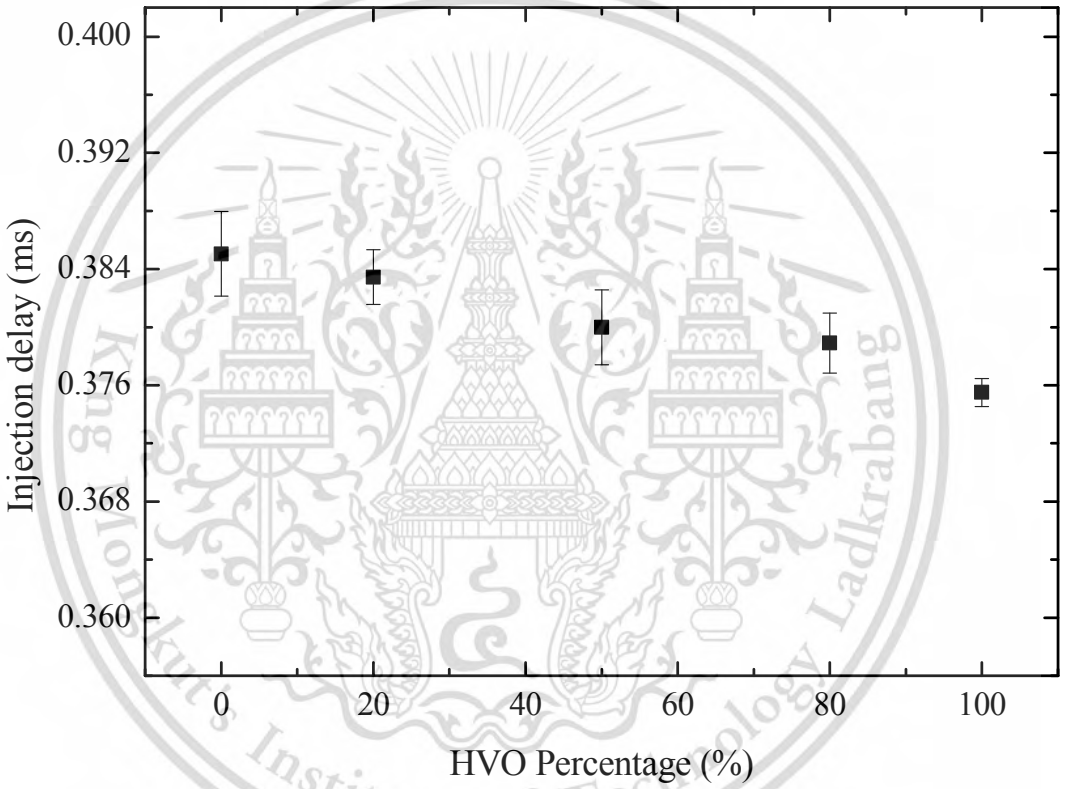

Fig. 4.3 Injection delay

4.1.4 Injection duration

Fig. 4.4 shows effects of blending percentages of HVO into diesel fuel on injection duration under constant injection pressure. The injection duration was determined as shown in Fig. 3.1. Injection duration of H20, H50, H80 and HVO varied from diesel by less than 0.1% leading to the conclusion that injection duration of HVO blended fuels and HVO had the same trends with diesel.

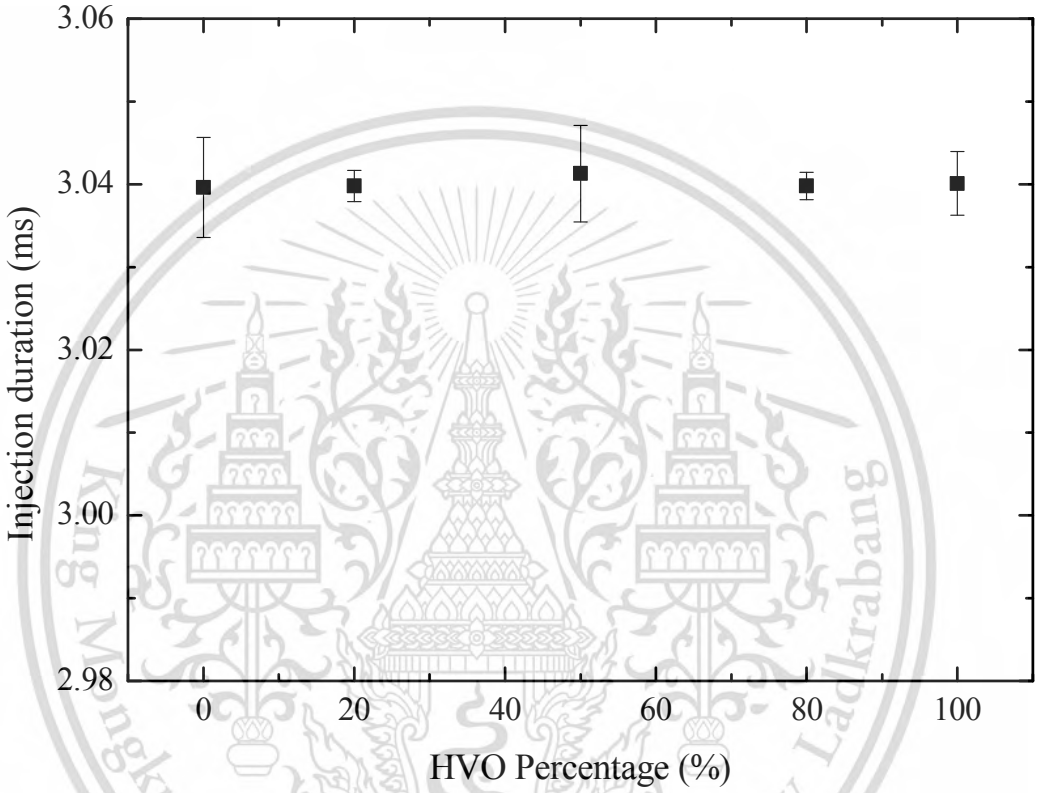

Fig. 4.4 Injection duration

4.1.5 Injection quantity

Fig. 4.5 shows the effects of different blend percentages of HVO into diesel fuel on injection quantity under constant injection pressure. The injection quantity was calculated by integration under injection rate curve area, as shown in Fig. 3.1. Injection quantity of H20, H50, H80 and HVO were lower by 0.07%, 0.74%, 0.79% and 0.81%, respectively compared to diesel. The conclusion is that injection quantity of HVO blend fuels had the same trend with diesel.

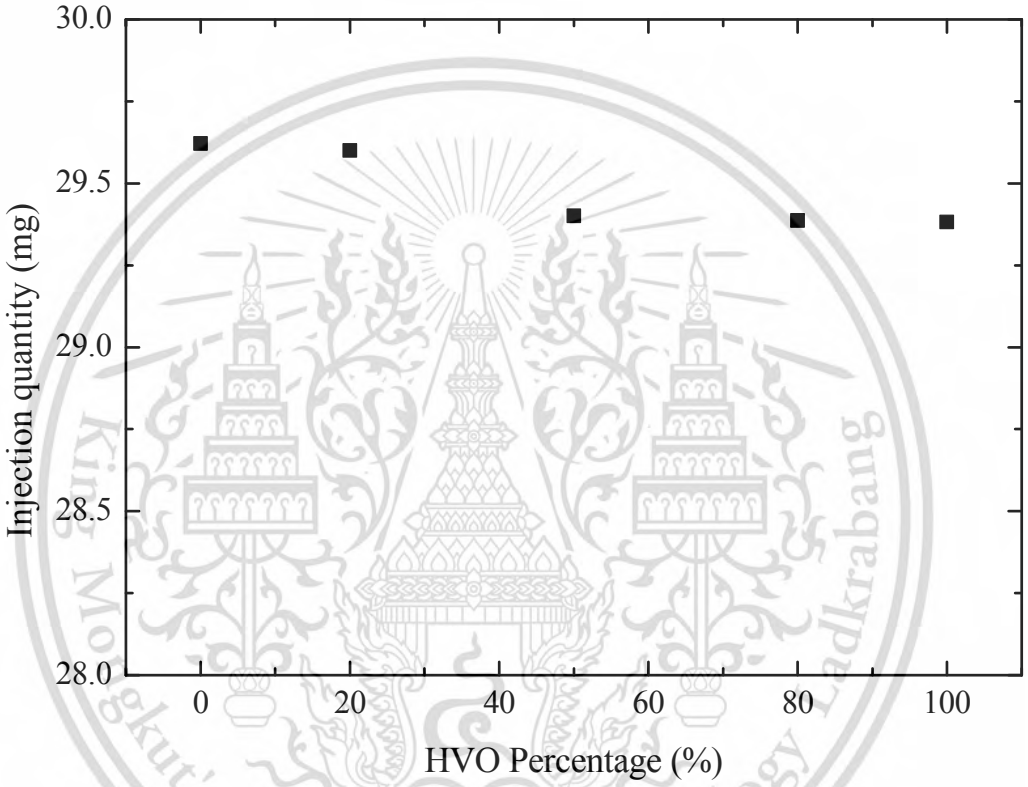

Fig. 4.5 Injection quantity

4.1.6 Injection rate

Fig. 4.6 shows the effects of blending percentage of HVO into diesel fuel on injection rate under constant injection pressure. The injection rate was calculated using Equation (2). HVO shows the highest injection rate compared to HVO blend fuels and diesel. Injection rates of H20, H50, H80 and HVO were higher by 0.25%, 0.79%, 0.84% and 1.43%, respectively compared to diesel. Increasing HVO blend percentages decreased viscosity reducing friction loss [37]. However decreasing viscosity also increased cavitation but the experimental were done on Non-cavitation condition. The effect of friction loss from decreasing viscosity is greater than cavitation making slightly increase in injection rate.

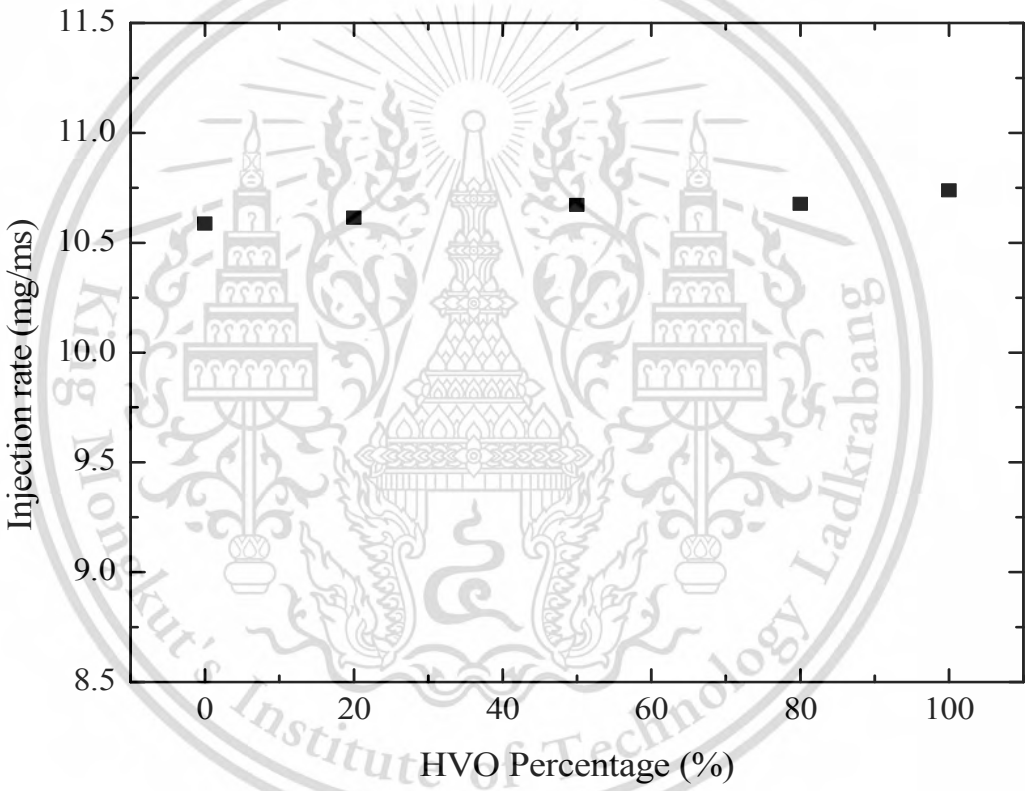

Fig. 4.6 Injection rate

4.1.7 Discharge coefficient

Fig. 4.7 shows the effects of blending percentage of HVO into diesel fuel on discharge coefficient under constant injection pressure. The discharge coefficient was calculated from Equation (3). HVO shows the highest discharge coefficient compared to HVO blend fuel and diesel. Discharge coefficient of H20, H50, H80 and HVO were higher by 0.83%, 2.27%, 3.18% and 4.45%, respectively compared to diesel. With increasing HVO blend percentage decreasing density, this resulted in a theoretical injection rate decrease. It also lead to decreased viscosity making friction loss lower and an increasing discharge coefficient with increased HVO blend percentage.

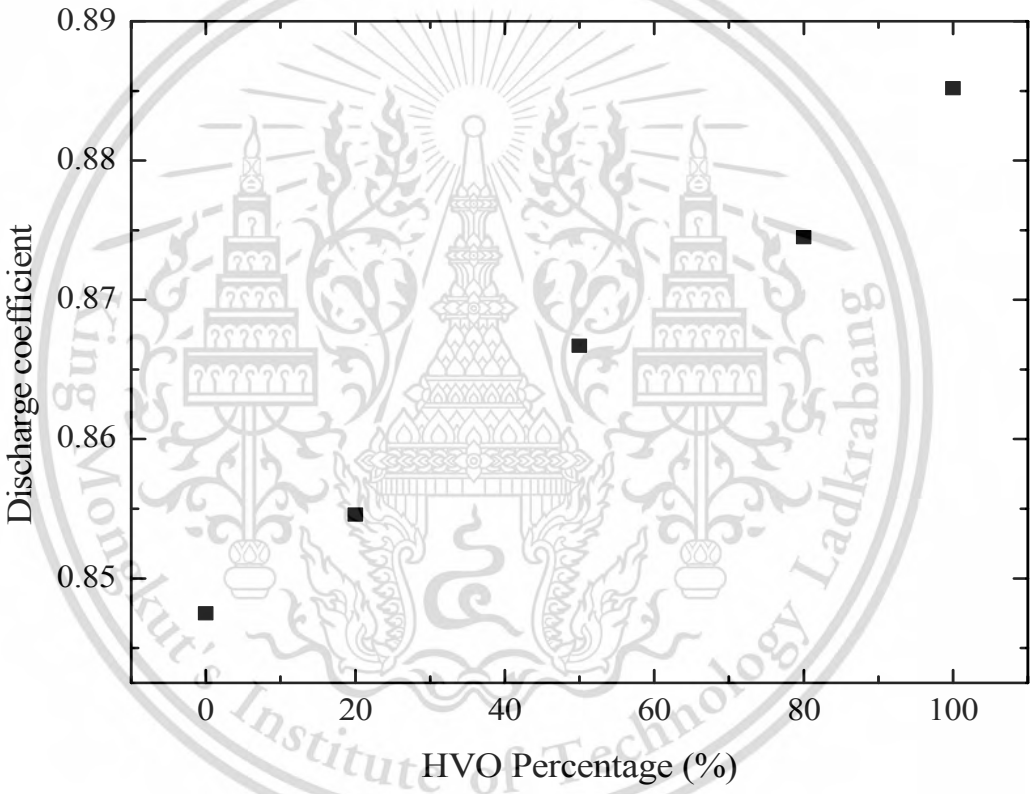

Fig. 4.7 Discharge coefficient

4.1.8 Discharge coefficient and Reynolds number

Fig. 4.8 shows the relationship between discharge coefficient and Reynolds number of blending percentages of HVO into diesel fuel on discharge coefficient and Reynolds number under constant injection pressure. The Reynolds number was calculated using Equation (5). HVO shows the highest Reynolds number compared to HVO blend fuels and diesel. Reynolds number of H20, H50, H80 and HVO were higher by 6.25%, 15.71%, 24.66% and 31.94%, respectively compared to diesel. Increasing HVO blend percentage increased Reynolds number due to decreasing density and viscosity. An increasing Reynolds number means increased mass flow rate. For this reason the effect is an increased discharge coefficient.

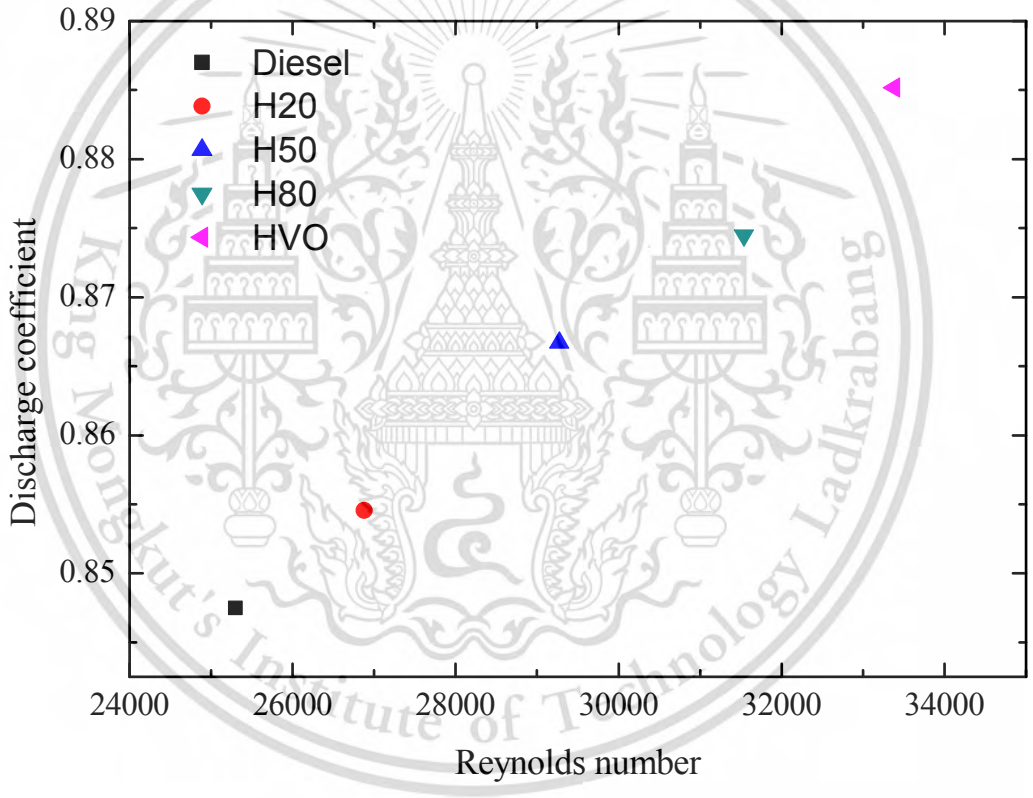

Fig. 4.8 Discharge coefficient and Reynolds number

4.1.9 Energy input

Fig. 4.9 shows the effects of blending percentage of HVO into diesel fuel on input energy under constant injection pressure. The input energy was calculated using Equation (6). HVO shows highest input energy compared to HVO blend fuels and diesel. Input energy of H20, H50, H80 and HVO were higher by 0.32%, 0.37%, 0.70% and 1.35% respectively compared to diesel. Even though injection quantity of HVO blended fuels were similar to diesel, higher heating values due to increasing HVO blend percentages made input energy higher. The higher energy input possibility to make higher heat release from combustion.

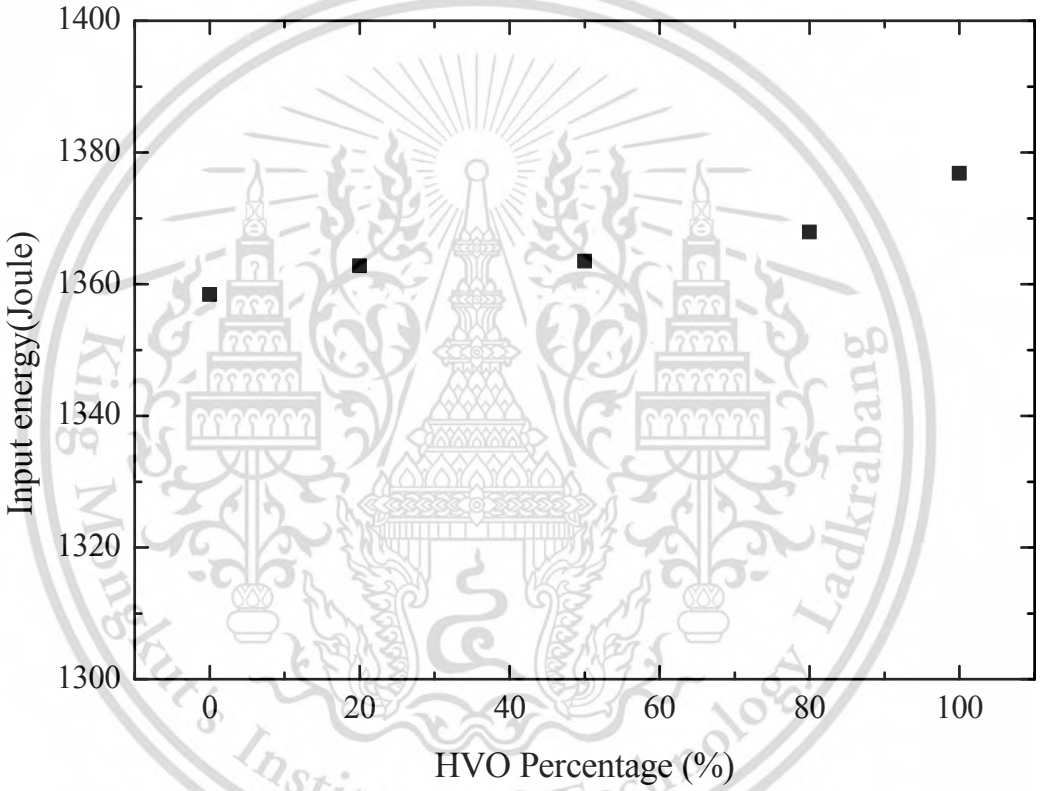

Fig. 4.9 Energy input

4.2 Spray characteristics

In this experiment, spray characteristics were conducted using five different fuels- commercial diesel, H20, H50, H80 and HVO. Other conditions were a nozzle exit orifice diameter of 0.2mm, solenoid injector 2.0 ms energizing time, 100 MPa injection pressure and 4.0 MPa ambient pressure. Result of spray characteristics experimental are present in terms of spray image, spray penetration, spray velocity, spray cone angle and spray volume.

4.2.1 Spray image

Fig. 4.10 shows the effects of blending percentage of HVO into diesel fuel on spray penetration under constant ambient pressure and injection pressure. At 0.5 ms after energizing Diesel, H20 and H50 have a similar spray penetration but the penetration length with HVO and H80 are shorter than the other fuels at the start of injection. From 1.0 to 3.0 ms after energizing HVO and HVO blended fuel have a similar spray penetration with diesel. From 2.5 to 3.0 ms after energizing HVO and H80 show better air entrainment around tip of spray comparison to diesel, H20 and H50. Spray cone angle during 1.0 to 3.0 ms after energizing HVO and HVO blended fuel have a same trend with diesel.

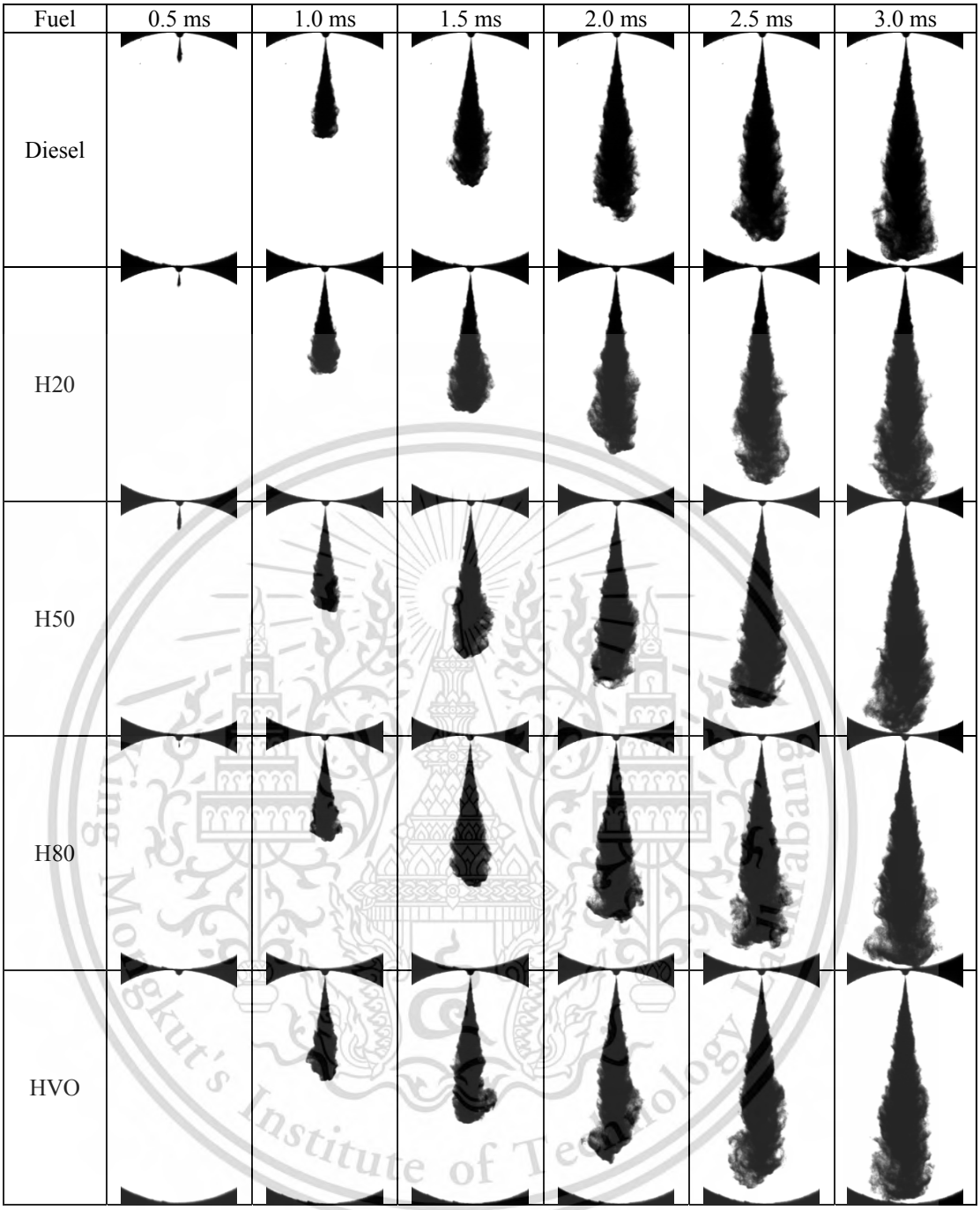

Fig. 4.10 Development of spray image

4.2.2 Spray penetration

Fig. 4.11 shows spray penetration of diesel and HVO as representative. HVO shows slightly lowest spray penetration compared to diesel. Increasing HVO blend percentage decreasing density and viscosity this resulted in a Sauter mean diameter (SMD) decrease [29]. Decreasing SMD had the effect of decreasing spray penetration due to less fuel dropped momentum.

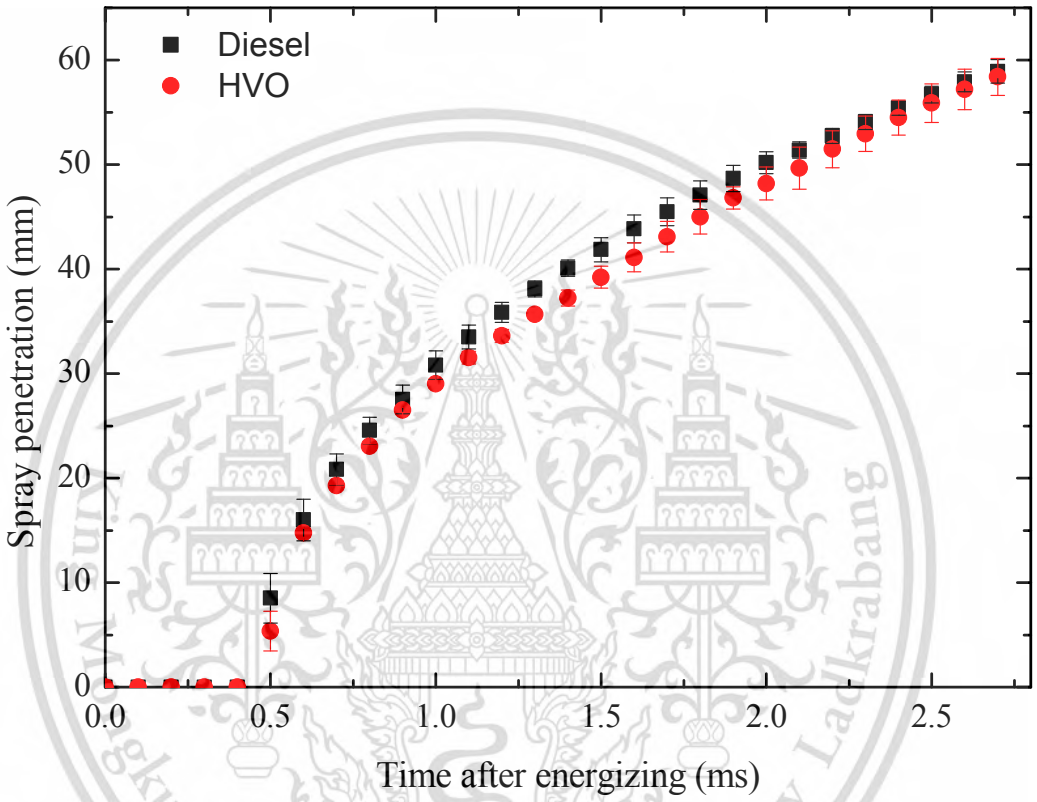

Fig. 4.11 Spray penetration

4.2.3 Spray velocity

Fig. 4.12 shows the effects of blending percentage of HVO into diesel fuel on spray velocity under constant injection pressure. Spray velocity results are presented as function of spray penetration. Spray tip accelerates at start of injection. After spray velocity reaches to highest value then spray velocity decrease. HVO shows lowest spray velocity compared to HVO blend fuels and diesel. Increasing HVO blend percentage decreases spray velocity due to spray penetration.

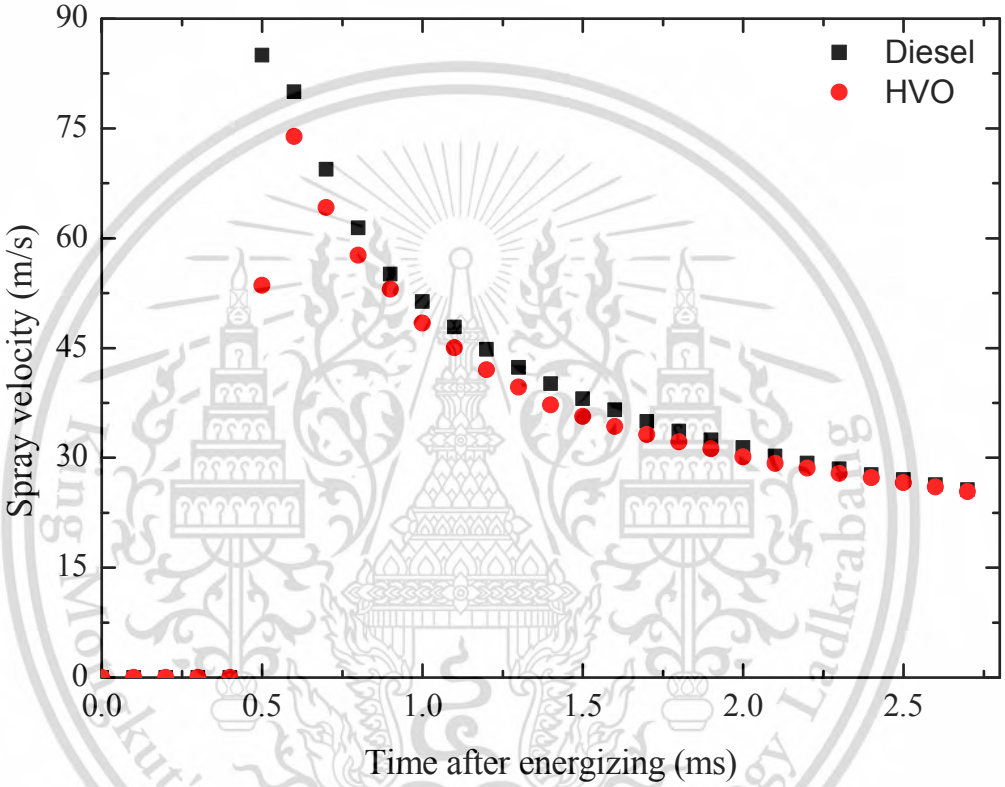

Fig. 4.12 Spray velocity

4.2.4 Spray cone angle

Fig. 4.13 shows spray cone angle of diesel and HVO as representative. There are transient phase and constant phase over 1.0ms. During the transient phase, HVO shows higher spray cone angle compared to diesel. For the constant phase the spray angles of HVO slightly higher than diesel. Increasing HVO blend percentage increases slightly spray cone angle due to decreased viscosity. Decreasing viscosity had the effect to increasing spray cone angle due to increases turbulence at the nozzle exit making a wider spray angle [29]. This coincides with results from previous work [38].

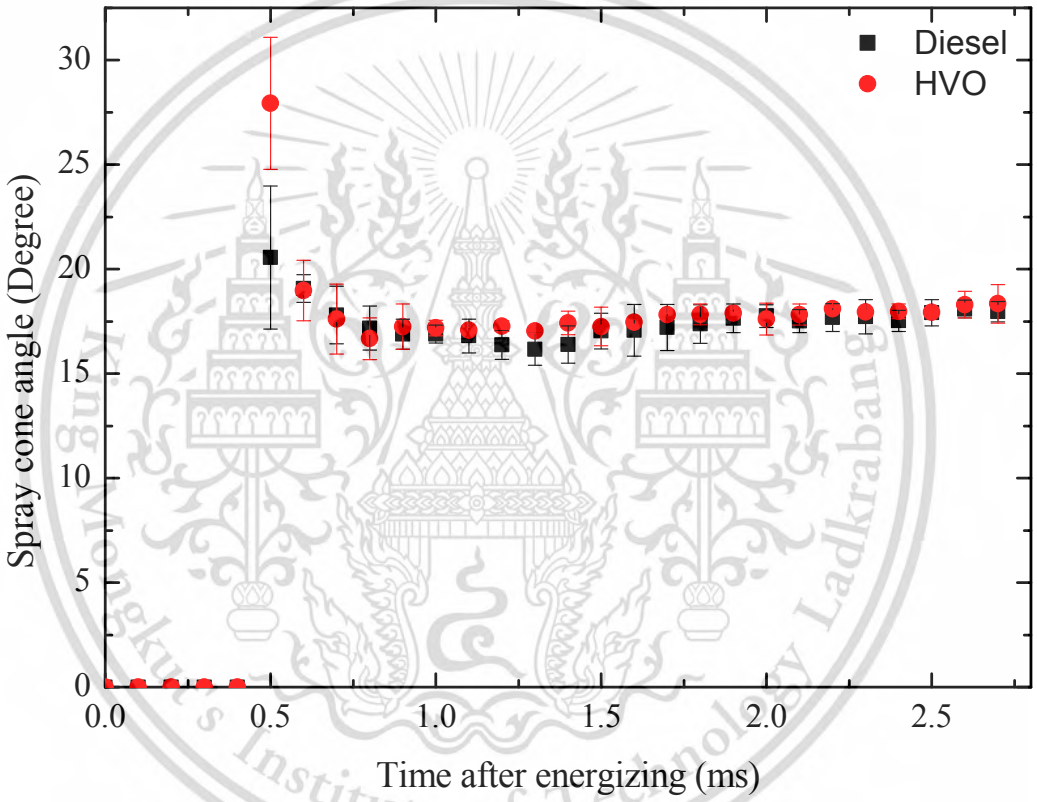

Fig. 4.13 Spray cone angle

4.2.5 Spray volume

Fig. 4.14 shows spray volume of diesel and HVO as representative. HVO shows similar to diesel. Increasing HVO effect to slightly increasing spray cone angle. It also led to decreased density, this resulted in spray penetration slightly decrease. However the difference in spray penetration of HVO is less than spray cone angle that increased. For this reason made spray volume of diesel and HVO are similar.

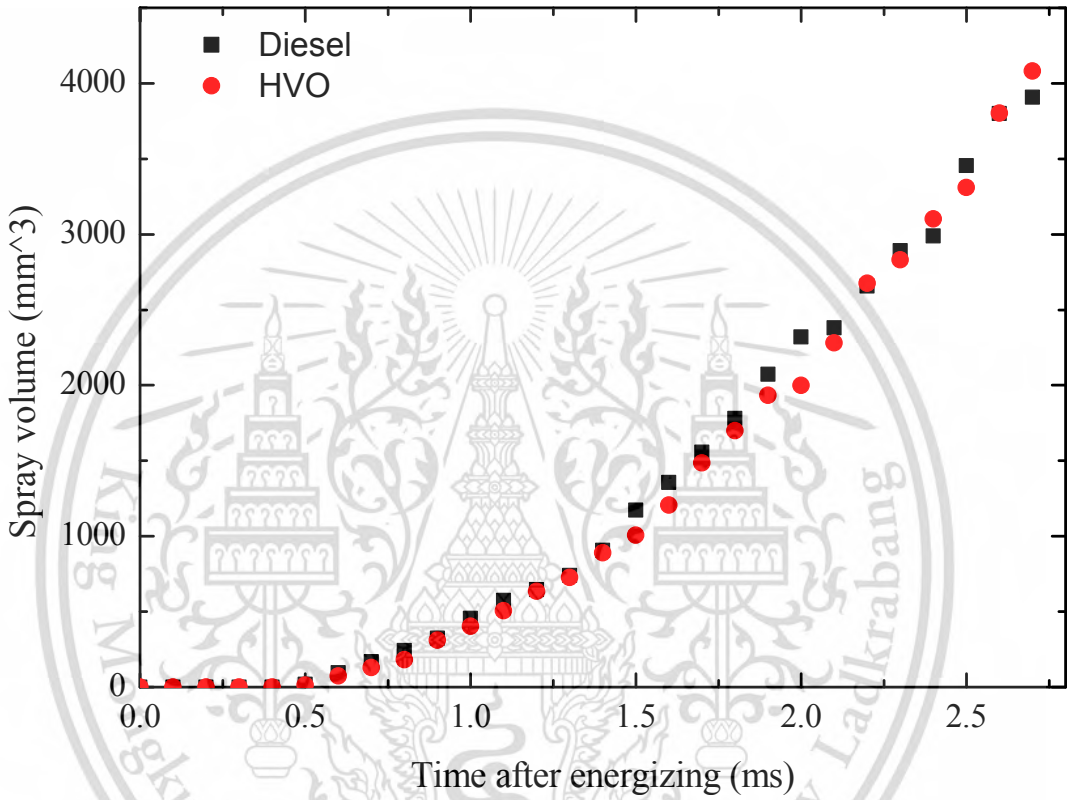

Fig. 4.14 Spray volume

4.3 Combustion characteristics

In this experiment, combustion characteristics were conducted using five different fuels- commercial diesel, H20, H50, H80 and HVO. Other conditions were a nozzle exit orifice diameter of 0.2mm, solenoid injector 2.0 ms energizing time, 100 MPa injection pressure and 800K ambient gas temperature. Oxygen concentrations of 21%, 15% and 10% at 4.0 MPa were used to simulate the effect of EGR under naturally aspirated conditions. For oxygen concentrations of 15% at 5.6 MPa and 10% at 8.4 MPa to investigated the effect of EGR and supercharged. Result of combustion characteristics experimental are present in terms of heat release rate, ignition delay, heat release, flame temperature, soot concentration and NO_x concentration.

4.3.1 Heat release rate

Fig. 4.15 and 4.16 show heat release rates of diesel and HVO as representative. Heat release rates are calculated from pressure rise after injected fuel by using Equation (8). In both after injection the evaporation of fuel into the hot environment causes a dramatically reduce to negative value in the heat release rates curves [23].

Fig. 4.15 shows heat release rates of EGR under naturally aspirated condition. HVO shows a lower peak heat release rate curve compared to diesel in all test conditions due to a higher cetane number making ignition delay shorter [6]. Lower oxygen concentrations resulted in lower increase and lower peak value. They also resulted in a longer ignition delay. Consequently, more premixed combustion occurred in the chamber [15]. Lower oxygen concentrations also had the effect of making the heat release rate more gradual [39]. Two stage ignition were observed in both diesel and HVO at O_2 21% at 4.0MPa. Two stage ignition profile is commonly observed in diesel combustion system [3]. Two stage ignition process were low temperature heat release (LTHR) and High temperature heat release (HTHR). The timing of the LTHR profile was similar under different ambient oxygen concentration. However, the HTHR shifted largely depend on ambient oxygen concentration [40].

Fig. 4.16 shows the heat release rate of the EGR and supercharged conditions. HVO also shows a shorter ignition delay and lower peak heat release rate curve during the EGR condition. During the diffusion combustion phase, heat release rate increased compared with the naturally aspirated condition [18].

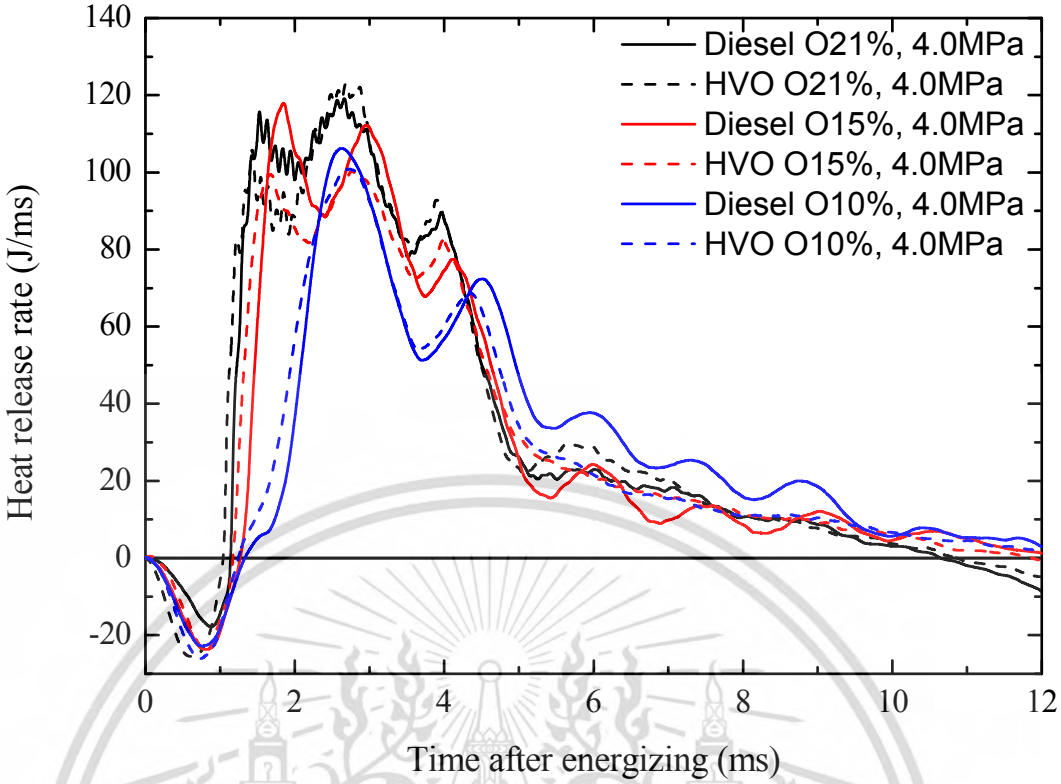

Fig. 4.15 Heat release rate of EGR condition

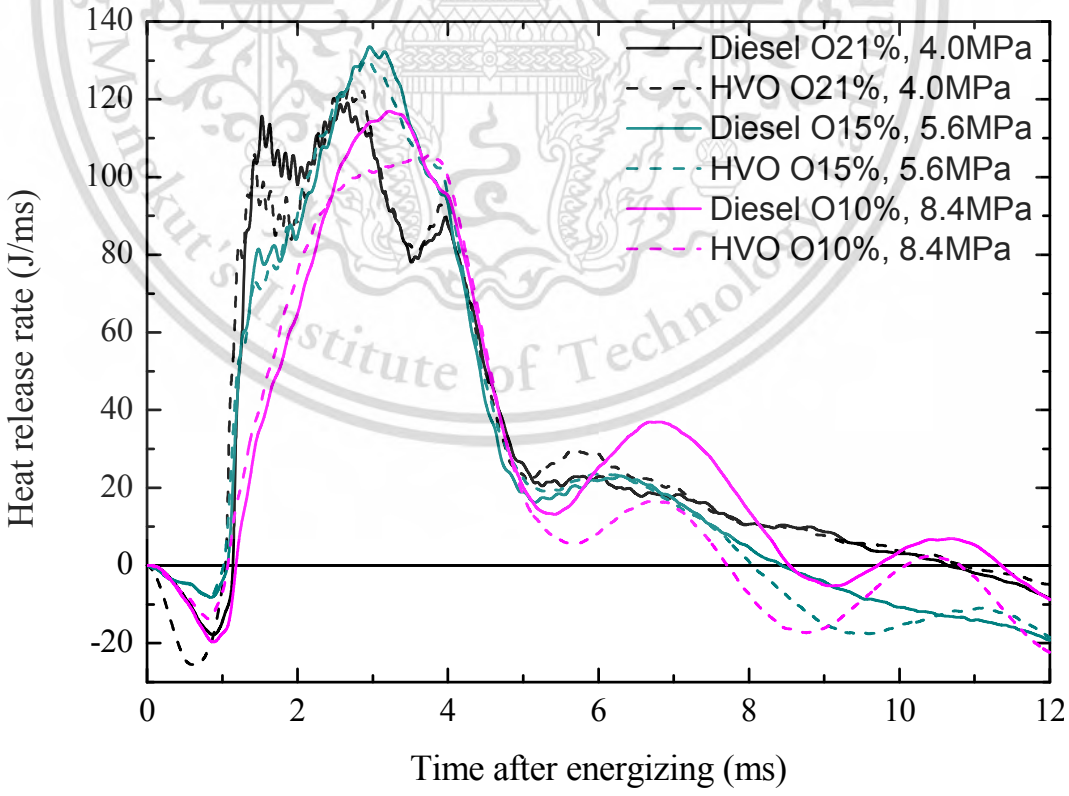

Fig. 4.16 Heat release rate of EGR and supercharged conditions

4.3.2 Ignition delay

Fig 4.17 and 4.18 show ignition delay. Ignition delay is mainly dependent on the fuel cetane number [41].

Fig 4.17 show the effects of oxygen concentration on ignition delay. HVO shows shorter ignition delays of 12.24%, 9.44% and 10.54%, respectively, compared to diesel at ambient O_2 conditions of 21%, 15% and 10%, at 4.0MPa. Increasing HVO blend percentage decreases ignition delay due to an increased cetane number. This coincides with results from previous work [7]. Decreasing oxygen concentrations had the effect of increasing ignition delay due to less oxygen availability during the air entrainment process [42].

Fig 4.18 shows the effects of ambient pressure under constant equivalent ratio on ignition delay. HVO also shows shorter ignition delays of 8.03% and 12.19% compared to diesel at an ambient condition of O_2 15% at 5.6MPa and $O_2$10% at 8.4MPa. EGR and supercharged conditions show shorter ignition delays, 20.49% and 19.90%, compared to EGR conditions at oxygen concentration 15% and 10%. At ambient condition, O_2 15% at 5.6MPa shows the shortest ignition delay compared to other cases. Increasing ambient pressure and density increases the spray volume [43] and improves mixture formation. High ambient pressure also decreases ignition delay from oxygen entrainment due to increasing ambient density [12]. However, at constant oxygen amount and the highest ambient pressure compared to other cases, O_2 10% at 8.4MPa showed longer ignition delay compared to O_2 21% at 4.0MPa. There is a point at which ignition delay is not affected by increasing the ambient pressure. This is due to the fact that the O_2 condition becomes too lean [44].

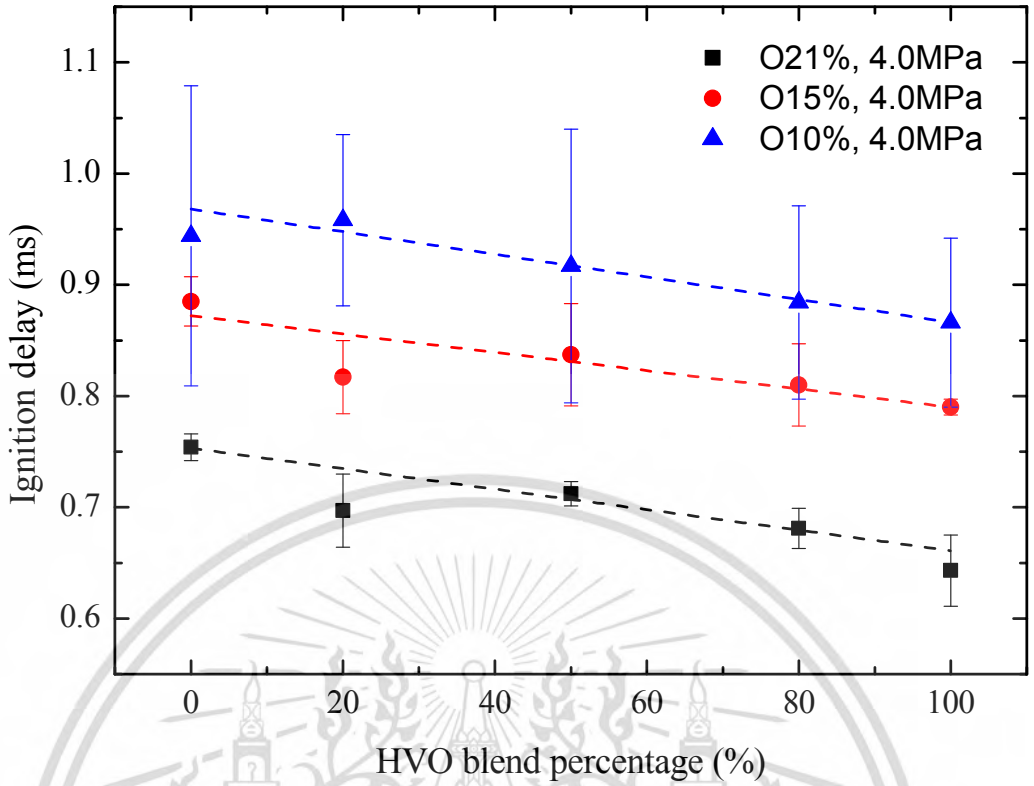

Fig. 4.17 Ignition delay of EGR condition

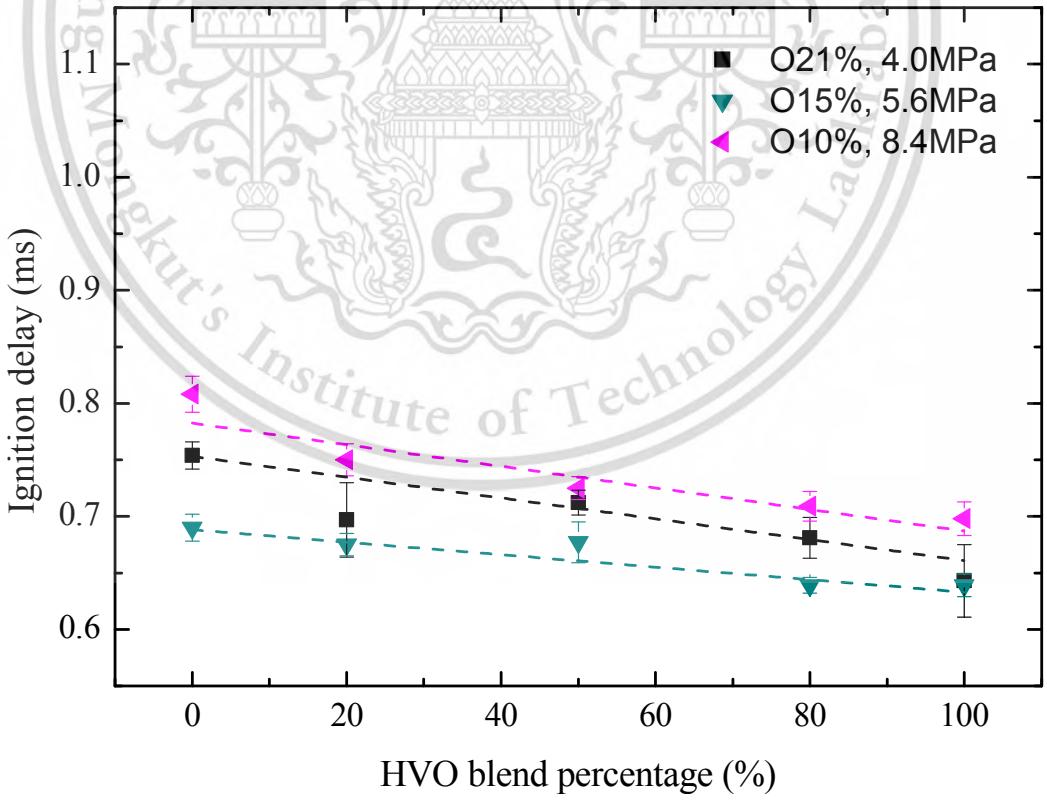

Fig. 4.18 Ignition delay of EGR and supercharged conditions

4.3.3 Integral heat release

Fig 4.19 shows the effects of oxygen concentration on heat release. Significant differences between the integral heat release rate of diesel and HVO were not found under ambient conditions of O_2 21%, 15% at 4.0MPa. On the other hand, at ambient condition, O_2 10% at 4.0MPa, HVO showed a lower integral heat release of 8.93% compared to diesel. The primary reason for a decrease in integral heat release is the changing fuel cetane number, which shortens the ignition delay. That results in the formation of a less combustible mixture, and the extra reactions do not have a chance to occur- especially at low oxygen concentrations [45, 46]. Decreasing the oxygen concentration had the effect of a decrease in integral heat release due to decreased reaction intensity [15]. Another effect of increasing the EGR rate was an increased heat capacity of ambient gas making a lower integral heat release [16].

Fig. 4.20 shows the effects of ambient pressure under constant equivalent ratio on heat release. Significant differences between integral heat release rate of diesel and HVO also were not found at ambient condition of O_2 15% at 5.6MPa. At ambient condition O_2 10% at 8.4MPa, HVO showed a lower heat release of 12.34% compared to diesel. EGR with supercharged showed a higher integral heat release of 7.58% and 4.86% compared to EGR condition under oxygen concentration 15% and 10%, respectively. Increasing ambient pressure increased mixture formation and oxygen entrainment, but heat release was still proportional to oxygen concentration.

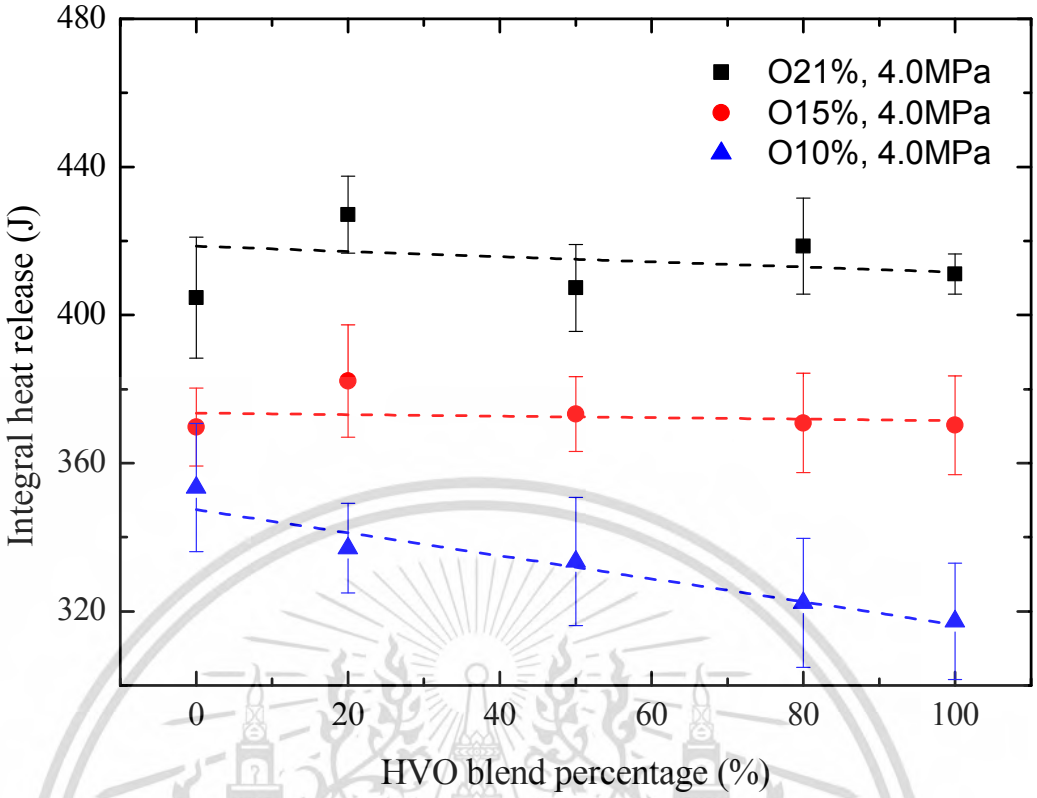

Fig 4.19 Integral heat release of EGR condition

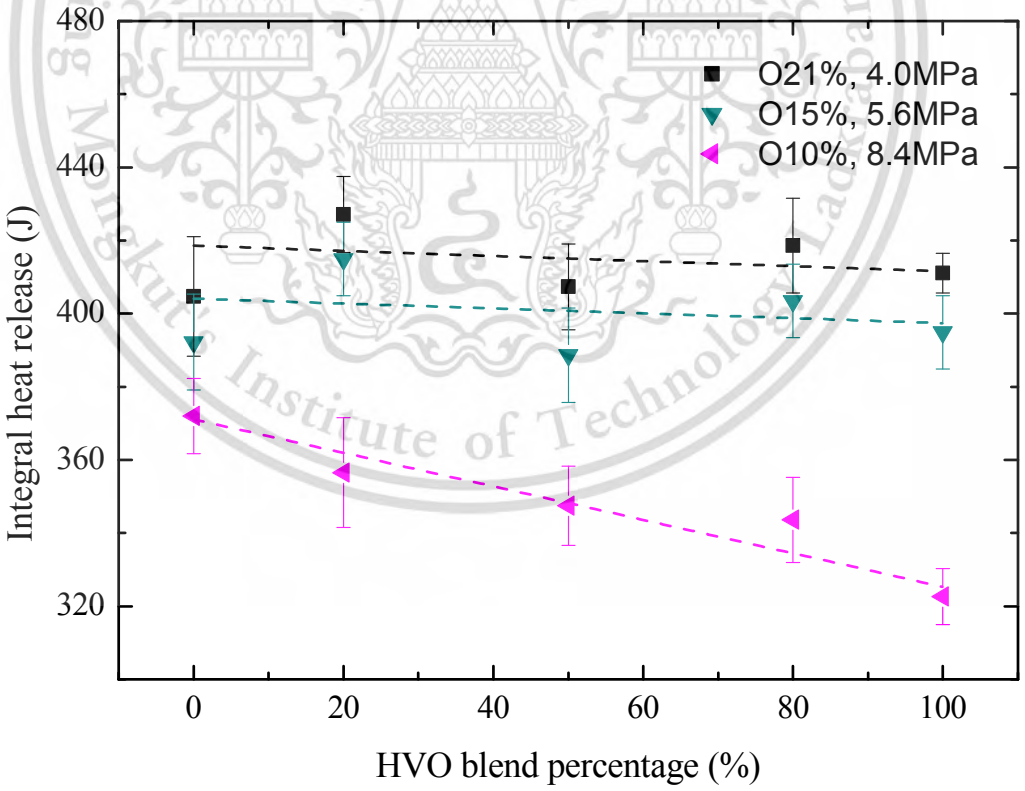

Fig 4.20 Integral heat release of EGR and supercharged conditions

4.3.4 Flame temperature

Fig. 4.21 and 4.22 show flame temperature image calculated by the two color method of diesel and HVO as representative.

Fig. 4.21 shows the effects of oxygen concentration on flame temperature. HVO shows slightly lower flame temperature compared to diesel. This is due to a higher cetane number. HVO shows slightly wider flame image under ambient condition O_2 21% at 4.0MPa during 2.5 to 3.5ms after energizing. This is due to a wider spray angle [38]. The lower viscosity of HVO increases turbulence at the nozzle exit making a wider spray angle [29]. Also contributing to making the flame image of HVO wider than diesel, is a lower distillation temperature which results in better vaporization and mixture formation at the flame border. Both diesel and HVO at O_2 21% at 4.0MPa were the first conditions that show flame temperature image at 1.5 ms after energizing, followed by O_2 15% at 2.0 ms after energizing, and 10% at 7.0 ms after energizing. At ambient condition, O_2 21% at 4.0MPa shows the highest flame temperature among other ambient conditions from 1.5 to 7.0 ms after energizing. At ambient condition, O_2 15% at 4.0MPa shows significantly lower flame temperature compared to O_2 21%, from 2.0 to 7.0 ms after energizing. Late combustion flame area during 5.0 to 7.0 ms after energizing were wider in this condition. At ambient condition, O_2 10% at 4.0MPa, no diffusion flame image appeared during 1.5 to 5.0 ms after energizing. Only late combustion flame image with the lowest flame temperature was captured at 7.0 ms after energizing, in this condition. Flame image of HVO under O_2 10% at 4.0MPa during 1.5 to 7.0 ms after energizing were not obtained in this experiment. This due to combustion reaction at O_2 10% were very weak [47]

Fig. 4.22 shows the effects of ambient pressure under constant equivalent ratio on flame temperature. HVO also shows slightly lower flame temperature compared to diesel. At ambient condition O_2 15% at 5.6MPa shows the same trend as O_2 15% at 4.0MPa. However, in this condition the start of flame image was obtained earlier at 1.5 ms after energizing. Flame temperature during 1.5 to 7.0 ms after energizing also was slightly higher in this condition. At ambient condition, O_2 10% at 8.4MPa shows the same trend with O_2 10% at 4.0MPa, but in this condition flame image also was obtained earlier at 5.0 ms after energizing and flame temperature during 5.0 to 7.0 ms after energizing were slightly higher. Increasing ambient pressure promoted oxygen enhancement in spray

volume improve mixture formation, thus better combustion, result flame temperature was increased.

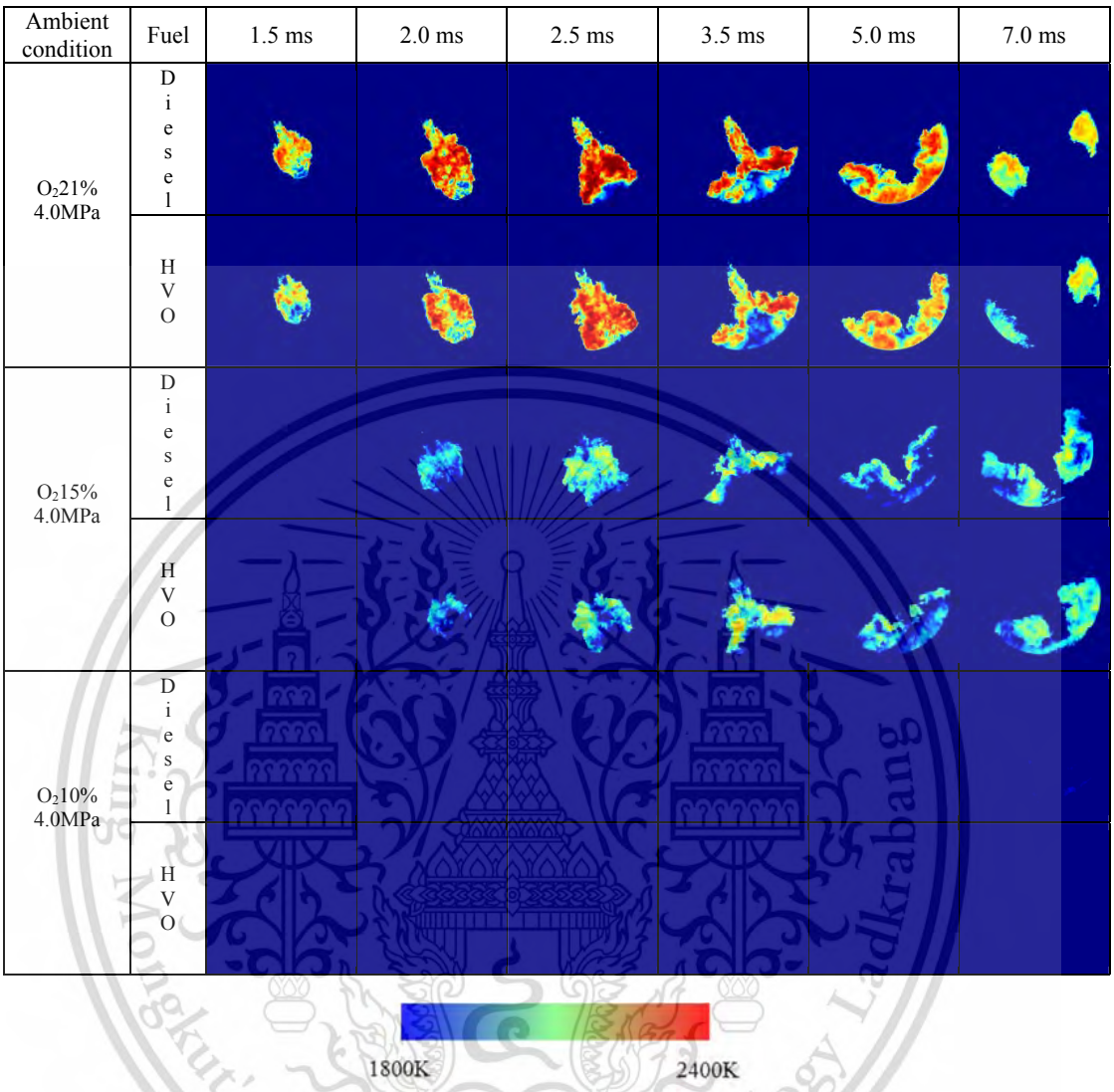

Fig 4.21 Flame temperature image of EGR condition

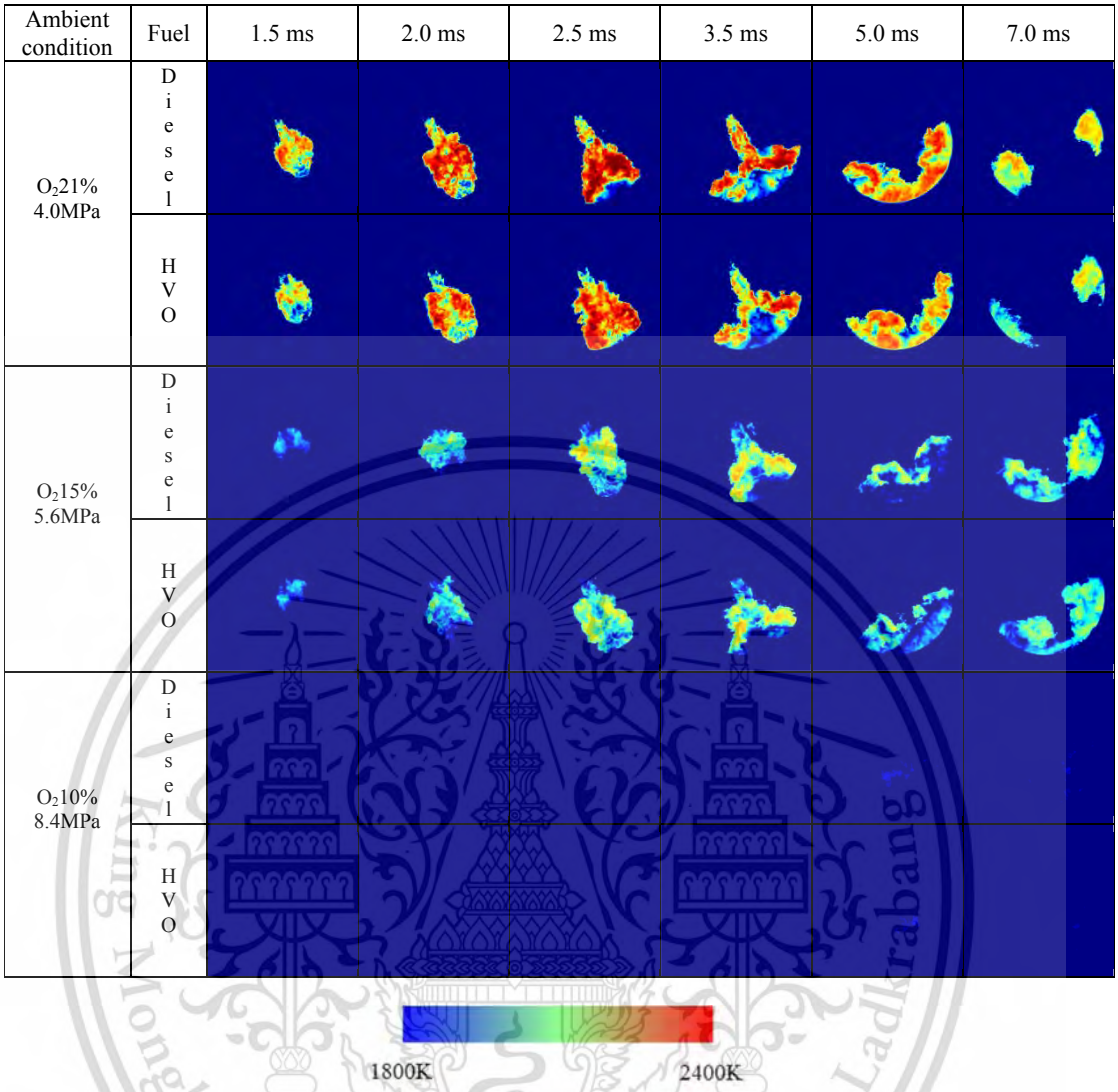

Fig 4.22 Flame temperature image of EGR and supercharged conditions

Fig. 4.23 and 4.24 show average flame of diesel and HVO as representative. Average flame temperature is calculated by summarizing the flame temperature of each pixel in the flame area and dividing by the total pixels [27].

Fig. 4.23 shows the effects of oxygen concentration on average flame temperature. HVO shows slightly lower average flame temperature under ambient condition O_2 21%, 15% and 10% at 4.0MPa due to a higher cetane number of HVO which shortens the ignition delay. The short ignition delay makes a less combustible mixture and the extra reactions did not occur. Decreasing oxygen concentration resulted in less combustion reaction intensity.

Fig. 4.24 shows effects of ambient pressure under constant equivalent ratio on average flame temperature. HVO also showed slightly lower average flame temperature under ambient conditions of O_2 15% at 5.6 MPa and 10% at 8.4MPa. Increasing ambient pressure promoted oxygen enhancement making a better mixture formation and increasing flame temperature.

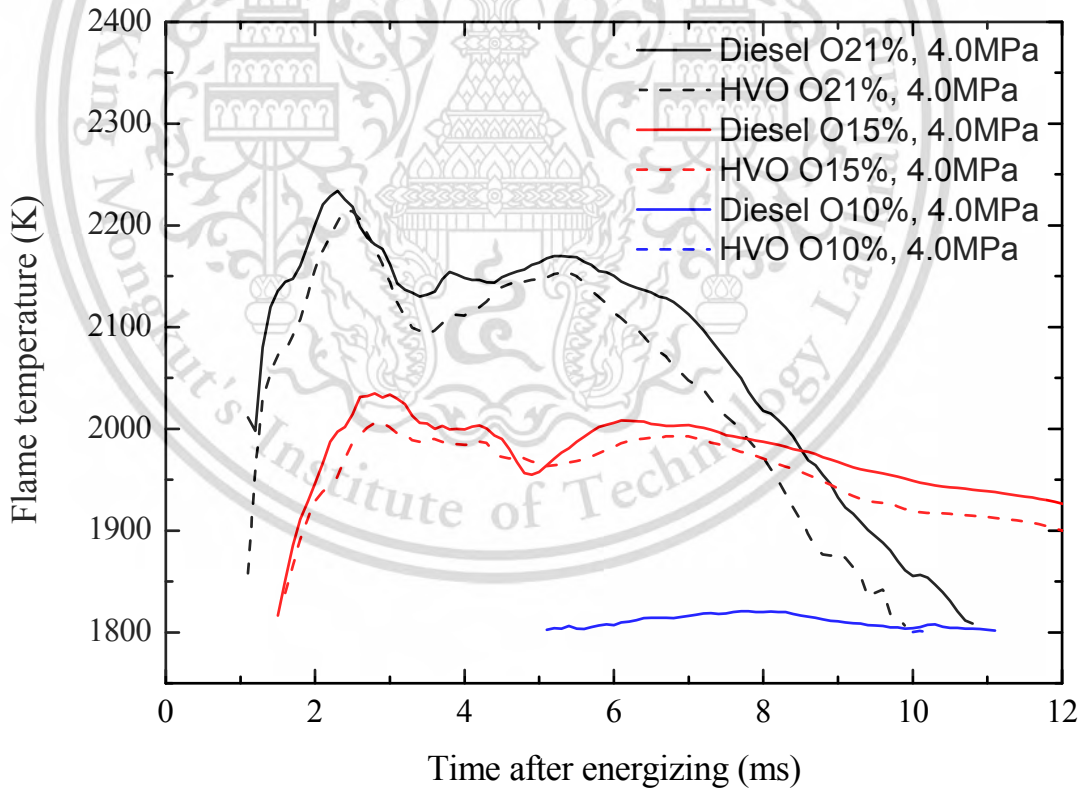

Fig. 4.23 Flame temperature of EGR condition

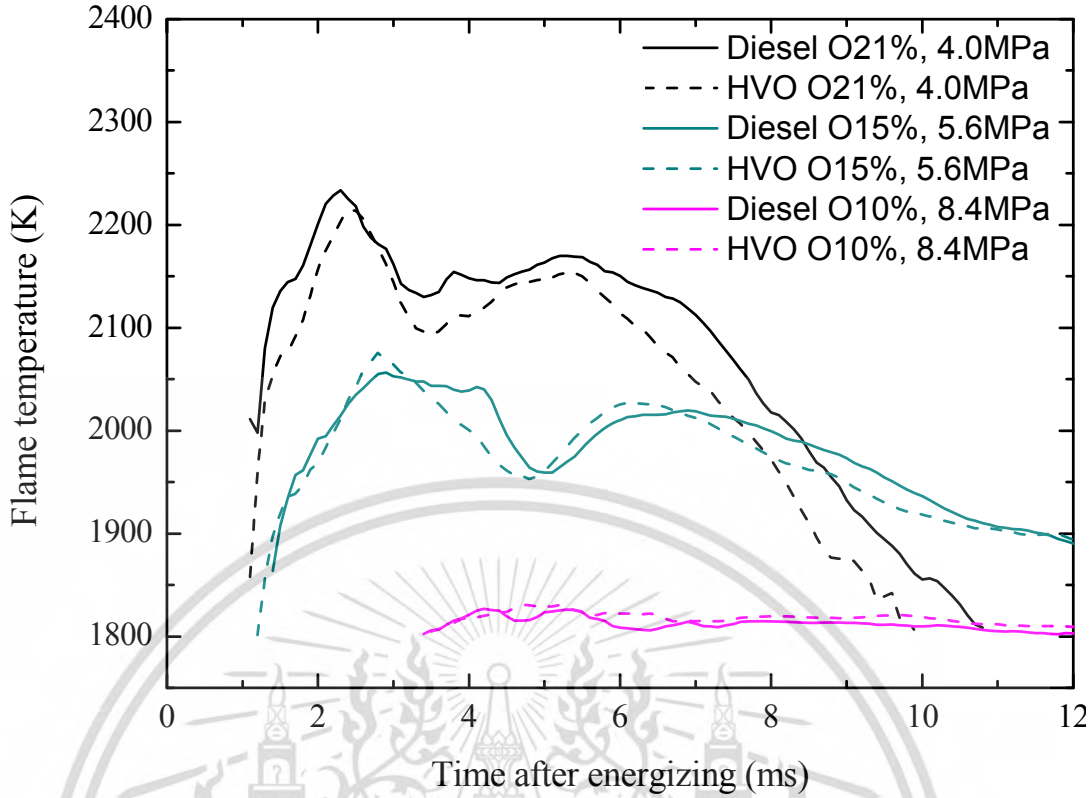

Fig. 4.24 Flame temperature of EGR and supercharged conditions

4.3.5 Soot concentration

Fig. 4.25 shows the effects of oxygen concentration on soot concentration. HVO shows lower soot concentration 16.57%, 14.07% and 14.78%, respectively, compared to diesel, with ambient condition O_2 21%, 15% and 10% at 4.0MPa. Increasing HVO blend percentage also increased the cetane number resulting in a reduction of the unburned fractions. Low distillation temperature of HVO improved fuel evaporation and mixing with surrounding gas. In addition the aromatic compounds which represent to the soot precursor are absent in HVO [7]. Decreasing oxygen concentration makes less oxygen available during the air entrainment process. The O_2 15% at 4.0MPa shows higher soot concentration than O_2 10% at 4.0MPa. This is caused by an EGR rate that exceeds the threshold point, resulting in incomplete combustion [48].

Fig. 4.26 shows the effects of ambient pressure under constant equivalent ratio on soot concentrations. HVO also show lower soot concentrations of 10.49% and 11.24% compared to diesel at ambient condition 15% at 5.6MPa and 10% at 8.4MPa. EGR with supercharged shows lower soot concentrations, 20.59% and 2.50%, compared to EGR conditions under oxygen concentrations of 15% and 10%, respectively. Increasing ambient pressure improves mixture formation and also promotes oxygen enhancement leading to soot reduction.

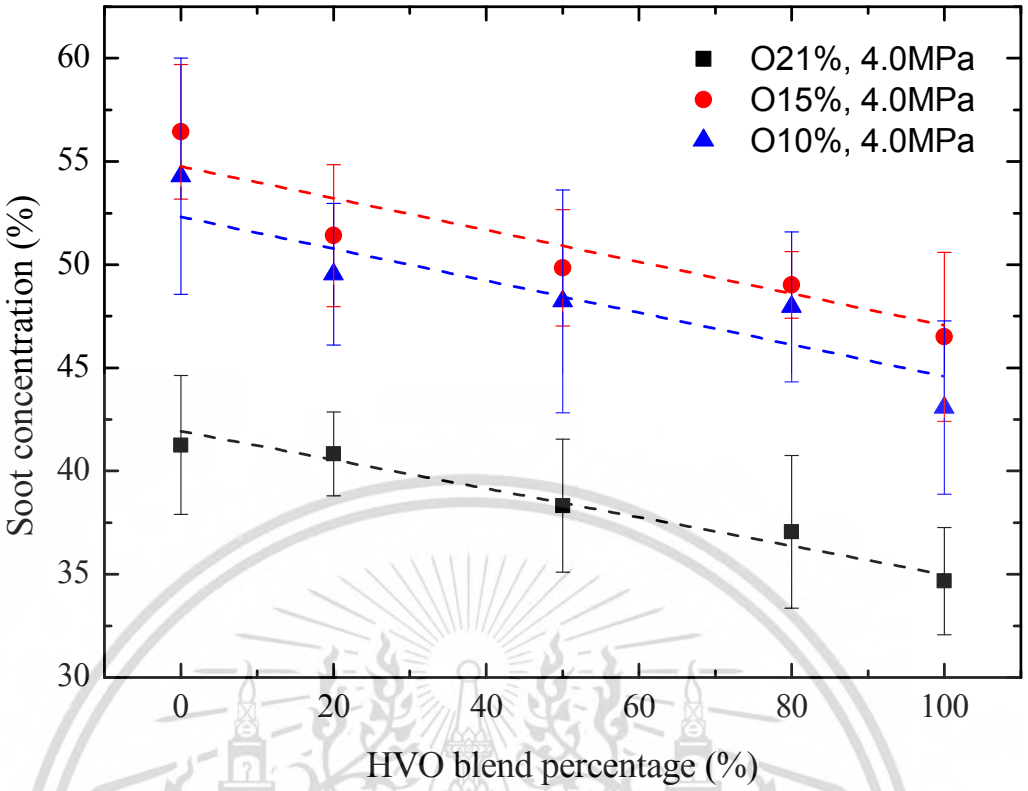

Fig. 4.25 Soot concentration of EGR condition

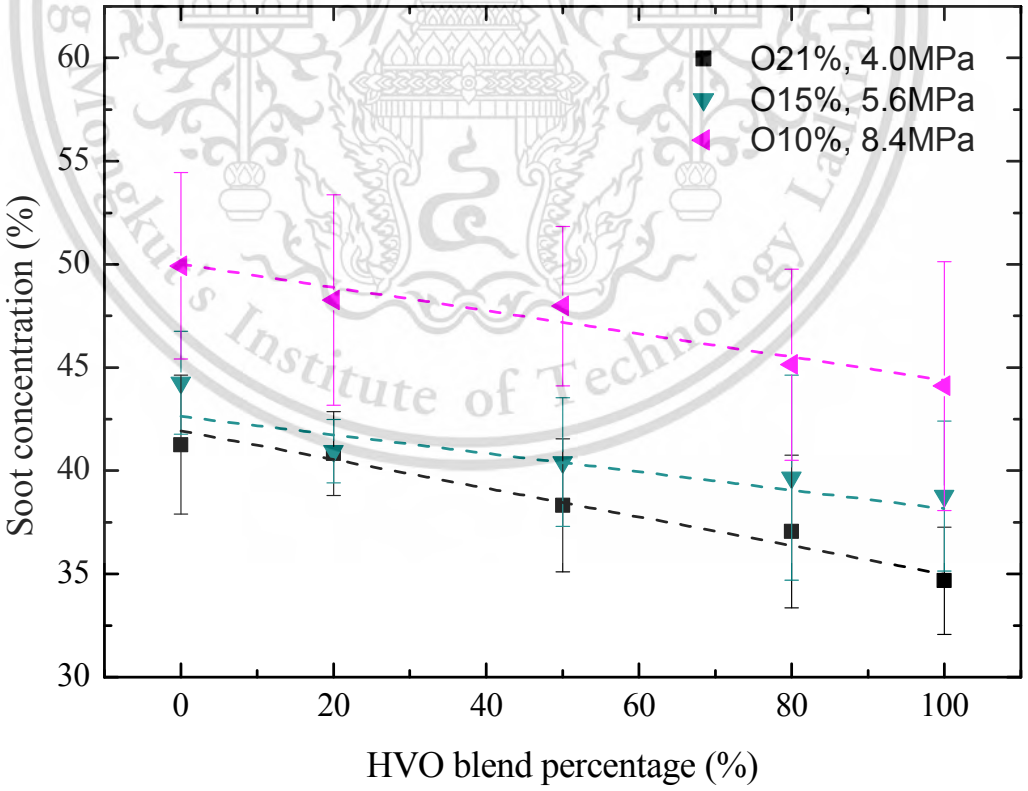

Fig. 4.26 Soot concentration of EGR and supercharged conditions

4.3.6 NO_x concentration

Fig. 4.27 shows that using HVO shows lower NO_x concentrations of 17.46%, 32.65% and 54.29% compared to diesel at ambient conditions of O_2 21% at 4.0MPa, 15%at 4.0MPa, and 15% at 5.6MPa. However, at ambient conditions O_2 10% at 4.0MPa and 8.4MPa did not show a significant difference between diesel and HVO due to a NO_x concentration value of only 2-4ppm. EGR with supercharged showed a higher NO_x concentration of 14.42% compared to EGR condition at oxygen concentration of 15%. Increasing HVO blend percentage led to decreased NO_x concentration due to decreased flame temperature. Decreasing oxygen concentration resulted in a decrease in flame temperature making NO_x emissions decrease [49, 50] as shown in Fig. 4.23 and 4.24.

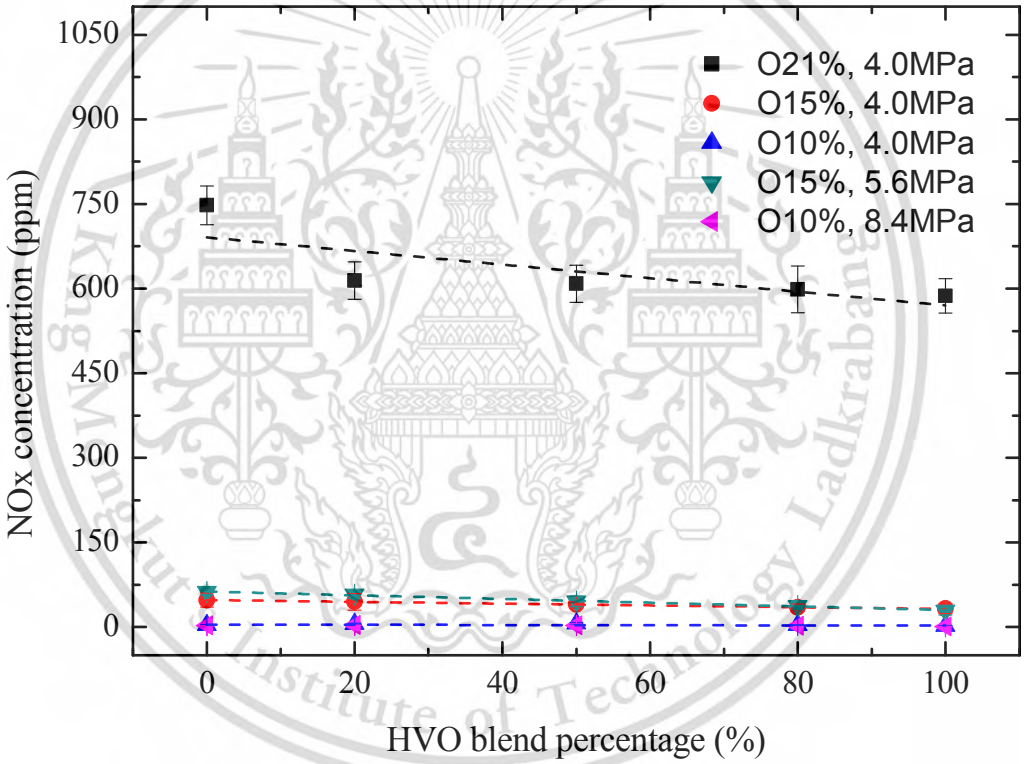

Fig. 4.27 NO_x concentration under EGR and EGR with supercharged condition

CHAPTER 5
Conclusions

5.1 Conclusions

This research investigates effect of Hydrotreated vegetable oil – diesel blend to combustion characteristics under EGR and supercharged conditions. However injection and spray characteristic are require in order to clearly explain combustion characteristics. A single hole injector was tested with five different fuels commercial diesel, HVO - diesel blends by mass: 20%, 50%, 80% and pure HVO under constant injection pressure and injection duration to investigate the effects of HVO percentage on injection, spray and combustion characteristics under simulate CI engine condition.

5.1.1 Injection characteristic conclusions

(1) Injection delay differences were caused by differing fuel viscosities. Lower viscosity from increasing HVO blend percentages resulted in shorten injection delay.

(2) Injection duration of HVO blended fuels and HVO had the same trends with diesel.

(3) Injection quantity of HVO blended fuels and HVO had the same trend with diesel.

(4) Injection rate slightly increased by decreasing the viscosity due to an increased HVO blend percentage. Decreasing viscosity had the effect of increasing injection rate.

(5) Discharge coefficient increased due to increased HVO blending percentage that decreased density, this resulted in a theoretical injection rate decrease. It also led to decreased viscosity making friction loss lower.

(6) Reynolds number increased due to increased HVO blending percentage that decreased density and viscosity.

(7) Injection quantity of HVO blended fuels were similar to diesel, higher heating values due to increasing HVO blend percentages made input energy higher.

5.1.2 Spray characteristic conclusions

(1) Spray penetration slightly decreased by decreasing the density due to an increased HVO blend percentage. Decreasing density had the effect of decreasing spray penetration due to less fuel dropped momentum.

(2) Spray velocity slightly decreased by decreasing the density due to an increased HVO blend percentage. Decreasing density had the effect of decreasing spray velocity due to less fuel dropped momentum.

(3) Spray cone angle slightly increased by decreasing the viscosity due to an increased HVO blend percentage. Decreasing viscosity had the effect of decreasing spray penetration due to increases turbulence at the nozzle exit making a wider spray angle.

(4) Spray volume of HVO is similar to diesel. Increasing HVO effect to slightly increasing spray cone angle. It also led to decreased density, this resulted in spray penetration slightly decrease. However the difference in spray penetration of HVO is less than spray cone angle that increased.

5.1.3 Combustion characteristic conclusions

(1) Peak HVO heat release rate was lower than diesel in all test conditions due to a higher cetane number which shortened ignition delay. Decreasing oxygen concentration resulted in an extended ignition delay and more premixed combustion. Increasing ambient pressure resulted in increasing the heat release rate during the diffusion combustion phase.

(2) Ignition delay decreased by increasing the cetane number due to an increased HVO blend percentage. Decreasing the oxygen concentration had the effect of increasing ignition delay due to less oxygen availability. Increasing ambient pressure decreased ignition delay from oxygen entrainment due to increasing ambient density. However, at one point ignition delay is not affected by increasing the ambient pressure as the ambient condition becomes too lean.

(3) Heat release decrease due to increased HVO blending percentage that increased cetane number made shortens the ignition delay. This results in less combustible mixture formation, which means that the extra reactions do not have a chance to occur. Decreasing the oxygen concentration had the effect of decreasing heat release due to a decreased reaction intensity. This also increased the heat capacity of the ambient gas. Increasing ambient pressure increased heat release, but the effect was less than from varying oxygen concentration.

(4) Flame temperatures of HVO are lower than diesel in every condition due to higher cetane numbers. HVO showed a slightly wider flame image caused by lower distillation temperature resulted in better vaporization and mixture formation. Increasing ambient pressure, slightly, resulted in an increase in flame temperature.

(5) Soot concentration decreased with increasing HVO blend percentage due to an increased cetane number. This lead to a reduction in the unburned fractions. A low distillation range of HVO improved fuel evaporation and mixing with the surrounding gas. In addition the aromatic compounds which represent to the soot precursor are absent in HVO Decreasing oxygen concentration made less oxygen available during the air entrainment process. When the EGR rate exceeds the threshold point, incomplete combustion occurs which decreases soot concentration.

(6) NO_x concentration decreased with increasing cetane number. This showed a decrease in flame temperature due to increasing HVO blending percentage. Decreasing oxygen concentration correlated with a decrease in flame temperature and NO_x emission.

5.2 Suggestions

(1) Investigate on effect of HVO to needle lift in side injector by using needle lift sensor.

(2) Investigate on effect of HVO to SMD by using laser measurement techniques.

(3) Investigate on effect of HVO to combustion characteristic under low temperature condition.

Reference

[1] Fulton L., Lah O. and Cuenot F. (2013). Transport pathways for light duty vehicles: towards a 2° scenario. *Sustainability.* **5**, **5**, 1863-1874.

[2] Kosaka H. (2015). Lecture slide Advance of Internal combustion engine for TAIST Automotive Engineering Course, NSTDA, Thailand .

[3] Dec J. (1997). A conceptual model of DI diesel combustion based on laser-sheet imaging*. *SAE Paper No.* 970873.

[4] Atola H., Larmi M., Sarjovaara T., and Mikkonen S. (2008). Hydrotreated vegetable oil (HVO) as a renewable diesel fuel: trade-off between NO_x, particulate emission, and fuel consumption of a heavy duty engine. *SAE Paper No.* 2008-01-2500.

[5] Rantanen L., Linnaila R., Aakko P., and Harju T (2005). Hydrotreated NExBTL - biodiesel fuel of the second generation. *SAE Paper No*. 2005-01-3771.

[6] Sugiyama K., Goto I., Kitano K., Mogi K., and Honkanen M (2011). Effects of Hydrotreated Vegetable Oil (HVO) as Renewable Diesel Fuel on Combustion and Exhaust Emissions in Diesel Engine. *SAE Paper No*. 2011-01-1954.

[7] Jaroonjitsathian S., Saisirirat P., Sivara K., Tongroon M. and Chollacoop N. (2014). Effects of GTL and HVO blended fuels on combustion and exhaust emissions of a common-rail DI diesel technology. *SAE Paper No.* 2014-01-2763.

[8] Mizushima N., Kawano D., Ishii H., Takada Y. and Sato S. (2014). Evaluation of real- world emissions from heavy-duty diesel vehicle fueled with FAME, HVO and BTL using PEMS, *SAE Paper No*. 2014-01-2823.

[9] Jaroonjitsathian S., Tipdecho C., Sukajit P., Namthirach N. and Suppatvech, S. (2013). Bio-Hydrogenated Diesel (BHD): renewable fuel for advanced diesel technology. *SAE Paper* No. 2013-01-0070.

[10] Lapuerta M., Villajos M., Agudelo J., R. and Boehman A. L. (2011). Key properties and blending strategies of hydrotreated vegetable oil as biofuel for diesel engines. *Fuel Processing Technology.* **92**, **12**, 2406−2411.

[11] No S. (2014). Application of hydrotreated vegetable oil from triglyceride based biomass to CI engines – A review. *Fuel.* **115**, 88-96.

[12] Kitamura Y., Mohammadi A., Ishiyama T., and Shioji M. (2005). Fundamental investigation of NO_x formation in diesel combustion under supercharged and EGR conditions. *SAE Paper No*. 2005-01-0364.

[13] Brijesh P. and Sreedhara S. (2013). Exhaust emissions and its control methods in compression ignition engines: A review. *Int. J. Automotive Technology*. **14**, **2**, 195–206.

[14] Agarwal D., Singh S. and Agarwal A. K. (2011). Effect of exhaust gas recirculation (EGR) on performance, emissions, deposits and durability of a constant speed compression ignition engine. *Applied Energy*. **88**, **8**, 2900–2907.

[15] Zhang J., Jing W., Roberts W. L. and Fang T. (2013). Effects of ambient oxygen concentration on biodiesel and diesel spray combustion under simulated engine conditions. *Energy*. **57**, 722−732.

[16] Pierpont D., Montgomery D., and Reitz R. (1995). Reducing particulate and NO_x using multiple injections and EGR in a D.I. diesel. *SAE Paper No*. 950217.

[17] Adachi T., Aoyagi Y., Kobayashi M., Murayama T., Goto Y. and Suzuki H. (2009). Effective NO_x reduction in high boost, wide range and high EGR rate in a heavy duty diesel engine. *SAE Paper No*. 2009-01-1438.

[18] Uchida N., Daisho Y., Saito T. and Sugano H. (1993). Combined effects of EGR and supercharging on diesel combustion and emissions. *SAE Paper No*. 930601.

[19] Aoyagi Y., Osada H., Misawa M., Goto Y. and Ishii, H. (2006). Advanced diesel combustion using of wide range, high boosted and cooled EGR system by single cylinder engine. *SAE Paper No*. 2006-01-0077.

[20] Hiroyasu H. and Arai M. (1990). Structures of fuel spray in diesel engine. *SAE Paper No*. 900475.

[21] Pulkrabek, W. W. (2014). Engineering fundamentals of the internal combustion engine. 2nd edn. Pearson education limited. London.

[22] Kegl B., Kegl M. and Pehan H. (2013). Green diesel engines. 1st edn. Springer. London.

[23] Heywood, J. B. (1988). Internal combustion engine fundamentals. 2nd edn. McGraw-Hill. New York.

[24] Borhanipour M., Karin P., Tongroon M., Chollacoop N. and Hanamura K. (2014). Comparison Study on Fuel Properties of Biodiesel from Jatropha, Palm and Petroleum Based Diesel Fuel. *SAE Paper No*. 2014-01-2017.

[25] Jing W., Roberts W. and Fang T. (2014). Comparison of soot formation for diesel and jet-a in a constant volume combustion chamber using two-color pyrometry. *SAE Paper No*. 2014-01-1251.

[26] Arcoumanis C. and Baniasad M. (1993). Analysis of consecutive fuel injection rate signals obtained by the Zeuch and Bosch methods, *SAE Paper No*. 930921.

[27] Munsin R., Laoonual Y. Jugjai S. Matsui M.and Kosaka H. (2015). Effect of glycerol ethoxylate as an ignition improver on injection

and combustion characteristics of hydrous ethanol under CI engine condition, *Energy Conversion and Management*. **98**, 282-289.

[28] Dernotte J., Hespel C., Houille S. Foucher F., Houille S. and Rousselle C. M. (2012). Influence of physical fuel properties on the injection rate in a Diesel injector, *Fuel*. **96**, 153-160.

[29] Dernotte J., Hespel C., Houille S. Foucher F. and Rousselle C. M. (2012). Influence of fuel properties on the diesel injection process in nonvaporizing condition, *Atomization and Spray*. **22**, 461–492.

[30] Chen P. C. Wang W., Roberts W. L. and Fang T. (2013). Spray and atomization of diesel fuel and its alternatives from a single-hole injector using a common rail fuel injection system, *Fuel*, **103** 850–861.

[31] Munsin, R., Laoonual, Y., Jugjai, S., Matsuki, M. and Kosaka H. (2012). Investigation of effects of ignition improvers on ignition delay time of ethanol combustion with rapid compression and expansion machine. *SAE Paper No.* 2012-01-0854.

[32] Matsui, Y., Kamimoto, T. and Matsuoka S. (1979). A study on the time and space resolved measurement of flame temperature and soot concentration in a D. I. diesel engine by the two-color method. *SAE Paper No.* 790491.

[33] Kobori, S. and Kamimoto, T. (1995). Development of a rapid compression-expansion machine simulating diesel combustion. *SAE Paper No*. 952514.

[34] Boehman A. L., Morris D. and Szybist J. (2004). The impact of the bulk modulus of diesel fuels on fuel injection timing. *Energy Fuels*, **18**, 1877–1882.

[35] Wang Z., Wyszyski M. L., Xu H., Abdullah N. R. and Piaszyk J. (2015). Fuel injection and combustion study by the combination of mass flow rate and heat release rate with single and multiple injection strategies, *Fuel Processing Technology* **132**, 118-132.

[36] Payri R., Garcia A., Domenech V., Durrett R. and Plazas A. H. (2012). An experimental study of gasoline effects on injection rate, momentum flux and spray characteristics using a common rail diesel injection system, *Fuel* **97**, 390-399.

[37] Millo F., Mallamo F., Vlachos T., Ciaravino C., Postrioti L. and Buiton G. (2013). Experimental investigation on the effects on performance and emissions of an automotive Euro 5 diesel engine fuelled with B30 from RME and HVO, *SAE Paper No*. 2013-01-1679.

[38] Hulkkonen T., Hillamo H., Sarjovaara T., and Larmi M. (2011). Experimental study of spray characteristics between hydrotreated vegetable oil (HVO) and crude oil based EN 590 diesel fuel. *SAE Paper No*. 2011-24-0042.

[39] Yin, B., Wang, J., Yang, K. and Jia, H. (2014). Optimization of EGR and split injection strategy for light vehicle diesel low temperature combustion. *Int. J. Automotive Technology.* **15**, **7**, 1043−1051.

[40] Mayo M. P. and Boehman A. L. (2015). Ignition behavior of biodiesel and diesel under reduced oxygen atmospheres, *Energy Fuels.* **29**, **10**, 6793-6803**.**

[41] Jung S., Ishida M., Yamamoto S. and Sukaguchi D. (2010). Enhancement of NO_x-PM trade-off in a diesel engine adopting bio-ethanol and EGR. *Int. J. Automotive Technology*. **11**, **5**, 611−615.

[42] Malbec L., Egusquiza J., Bruneaux G. and Meijer M. (2013). Characterization of a set of ECN spray an injectors: nozzle to nozzle variations and effect on spray characteristics. *SAE Paper No.* 2013-24-0037.

[43] Wang X., Huang Z., Kuti O. A., Zhang W. and Nishida K. (2010) Experimental and analytical study on biodiesel and diesel spray characteristics under ultra-high injection pressure. *International Journal of Heat and Fluid Flow* **31, 4,** 659-666.

[44] Asad U. and Zheng M. (2009). Efficacy of EGR and boost in single-injection enabled low temperature combustion. *SAE Paper No*. 2009-01-1126.

[45] Kook S., Bae C., Miles P., Choi D. and Pickett L., M. (2005). The influence of charge dilution and injection timing on low-temperature diesel combustion and emissions. *SAE Paper No.* 2005-01-3837.

[46] Azimov U. B., Roziboyev E. A., Kim S. K., Jeong D. S., Lee Y. G., and Yun J. E. (2008). Investigation of soot formation in diesel - GTL fuel blends under quiescent conditions. *Int. J. Automotive Technology.* **9**, **5**, 523−534.

[46] Zhang J., Jing W., Roberts W. L. and Fang T. (2013). Effects of ambient oxygen concentration on biodiesel and diesel spray combustion under simulated engine conditions. *Energy*. **57**, 722−732.

[48] Chen Z., Wu Z., Liu J. and Lee C. (2014). Combustion and emissions characteristics of high n-butanol/diesel ratio blend in a heavy-duty diesel engine and EGR impact. *Energy Conversion and Management.* **78**, 787−795.

[49] Azimov U. B., Kim S. K., Jeong D. S., and Lee Y. G. (2009). Evaluation of low-temperature diesel combustion regimes with n-Heptane fuel in a constant-volume chamber. Int. J. Automotive Technology. 10, 3, 265−276.

[50] Nguyen L. D. K., Sung N. W., Lee S. S. and Kim H. S. (2011). Effects of split injection, oxygen enriched air and heavy EGR on soot emissions in a diesel engine. Int. J. Automotive Technology. **12**, **3**, 339−350.

Appendix

Injection experimental pressure sensor specification

Pressure

KISTLER
measure. analyze. innovate.

Miniature Measuring Probe

Type 6053CC...

for Non-Cooled Cylinder Pressure Measurement, M5 Thread

Patent No. US 6,105,434

The miniature measuring probe with very small dimensions and M5x0,5 mounting thread is particularly suitable for direct installation in small-capacity combustion engines with more than two valves per cylinder. The measuring element is identical to the standard sensor Type 6052C... .

- Good temperature stability of the sensitivity
- Acceleration-compensated
- Needs only 6 mm mounting bore
- Low thermal shock error and long life thanks to the front seal
- Very high sensitivity

Description

Type 6053CC... uses a new type of PiezoStar® crystal which achieves high sensitivity in conjunction with an extremely small sensor structure. The sensitivity drifts by a maximum of ±0,5 % over the temperature range of 200 ±50 °C. The passive acceleration compensation patented by Kistler keeps the influence of engine vibrations to a minimum.

The front seal allows very good heat dissipation and thus briefly a maximum operating temperature of 400 °C. The diaphragm, optimized by finite element calculation, produces good measuring results and ensures a long service life.
The shape of the probe allows mounting with a very small access bore. The cable connection has to be outside the cylinderhead, in an area free of oil mist. O-rings also permit mounting through coolant passages. The probe can be manufactured in custom lengths between 30 and 120 mm.

Application

The sensor Type 6053CC... is an excellent all-rounder. Its rugged construction makes it suitable for measurements at the knock limit as well as for thermodynamic investigations. This sensor is used mainly on multi-valve engines, motor cycle and other small engines and for combustion analysis.
This sensor should be used when there is insufficient mounting space available for the Type 6052C... .
At high speeds (vibrations), the Type 6053CC...U40 should be used. For applications mainly in the knocking range or at very high peak pressures, use of Type 6053CC...U20 with reinforced diaphragm (heavy duty version) is recommended.
The probe is supplied without a cable. See Accessories for the various cables available for different applications.

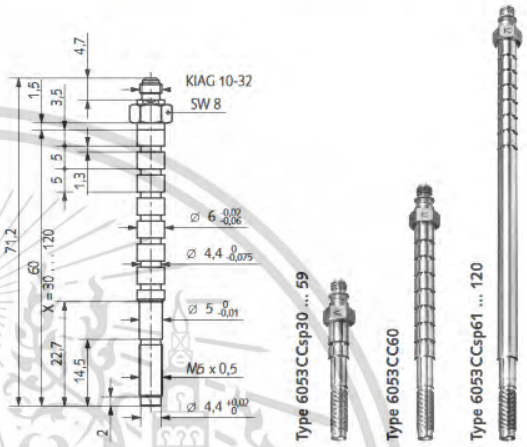

Technical Data

Measuring range	bar	0 ... 250
Calibrated sub-ranges	bar	0 ... 50, 0 ... 100, 0 ... 150, 0 ... 250
Overload	bar	300
Sensitivity	pC/bar	≈–20
Natural frequency, nominal	kHz	≈160
Linearity in all ranges (at 23 °C)	%/FSO	≤±0,3
Acceleration sensitivity		
axial	bar/g	<0,0002
radial	bar/g	<0,0005
Operating temperature range	°C	–20 ... 350
Temperature min./max	°C	–50 ... 400
Connector	°C	200

Technical Data (Continuation)

Sensitivity change		
200 °C ±50 °C	%	≈±0,5
23 ... 350 °C	%	≤±2
Thermal shock error		
(at 1 500 1/min Δp_{mi} = 9 bar)		
Δp_{mi} (short time drift)	bar	≤±0,5
Δp_{mi}	%	<±2
Δp_{max}	%	<±1
Insulation resistance		
at 23 °C	Ω	$>10^{13}$
Shock resistance	g	2 000
Tightening torque	N·m	1,5
Capacity		
Weight (Type 6053CC60)	g	10
Connector (PTFE)	–	KIAG 10-32

Type 6053CC...U20 (other specification as for Type 6053CC...)

Measuring range	bar	0 ... 300
Calibrated partial ranges	bar	0 ... 100, 0 ... 200, 0 ... 300
Overload	bar	350
Acceleration sensitivity		
axial	bar/g	<0,0005
radial	bar/g	<0,0005
Thermal shock error		
(at 1 500 1/min, p_{mi} = 9 bar)		
Δp (short time drift)	bar	≤±0,7
Δp_{mi}	%	≤±3
Δp_{max}	%	≤±1,5

Type 6053CC...U40 (other specification as for Type 6053C...)

Calibrated partial ranges	bar	0 ... 100, 0 ... 200, 0 ...250
Operating temperature range	°C	–20 ... 200
Temperature min./max.		–50 ... 200
Sensitivity shift		
23 ... 200 °C	%	≤±2

Mounting

Direct mounting:
Sensor Type 6053CC... can be mounted directly in the cylinder head, see Fig. 1. Machining of the bore must correspond exactly to the bore specifications shown in Fig. 2.

The Kistler tools:
Step drill Type 1300A53
Special tap Type 1357A and the
Finishing tool for bore Type 1300A79 or 1300A79Q01
must be used in order to comply with the tolerances required. The bore must be machined in one clamping. Before mounting the sensor, the sealing surface in particular must be checked; use of the finishing tool (reamer) Type 1300A79 is mandatory. When mounting the sensor, it is essential to comply with the tightening torque of 1,5 N·m. The sensor should therefore be mounted with the torque wrench Type 1300A17. You will find additional information for machining the bore and mounting in the instruction manual. Your Kistler distributor will provide you with information, for example concerning the preferred position of the indicating bore in the combustion chamber.
The shape of the probe and O-ring sealing allow mounting through coolant passages (see Figure 1). Reliable sealing requires a bore diameter of $6^{+0.03}_{+0.01}$, which can also be achieved with the drill Type 1300A53.

Mounting sleeve:
When space allows or if the water jacket of the cylinder head will be breached, a mounting sleeve Type 6525AQ... is recommended. Mounting sleeves are manufactured to customer requirements. An additional advantage of mounting sleeves is that the actual sensor bore in the sleeve can be very precisely machined. On request, Kistler will provide drawings for your particular mounting situation.

Spray experimental high speed VDO camera specification

Photron

Datasheet

FASTCAM Mini UX

Model UX50 / UX100

1.3-Megapixel CMOS Sensor:
Mini UX50
1280 x 1024 pixels at 2,000fps
1280 x 800 pixels at 2,500fps
Mini UX100
1280 x 1024 pixels at 4,000fps
1280 x 1000 pixels at 5,000fps
1280 x 800 pixles at 6,250fps

Maximum Frame Rate:
160,000fps (Mini UX50 type 160K)
204,800fps (Mini UX100 type 200K)
800,000fps (Mini UX100 type 800K)

Class Leading Light Sensitivity:
ISO 12232 Ssat
• ISO 10,000 monochrome
• ISO 5,000 color

Global Electronic Shutter:
Minimum Shutter speed 3.9µs (to 1µs dependent on frame rate selection)

Dynamic Range (ADC):
12-bit monochrome, 36-bit color

Compact and Lightweight:
120mm (H) x 120mm (W) x 93mm (D)
4.72″ (H) x 4.72″ (W) x 3.66″ (D)
Weight: 1.5Kg (3.13 lbs.)

Internal Recording Memory:
4GB, 8GB, 16GB, or 32GB

Fast Gigabit Ethernet Interface:
Provides high-speed image download to a standard notebook/PC

Flexible Frame Synchronization:
Frame rate may be synchronized to external unstable frequencies

1-Inch C-mount Compatible Sensor Size:
Also supplied with integrated Nikon G-type lens mounts.

High-G Rated:
Suitable for application in high-G environments; operation tested to 100G, 10ms, 6-axes

Compact high-speed camera system

For use with a wide range of general scientific and industrial applications the Photron FASTCAM Mini UX high-speed camera provides outstanding imaging performance at a very attractive price performance ratio.

Two Mini UX camera models provide 1.3-megapixel (1280 x 1024 pixels) image resolution with frame rates up to 2,000fps from the Mini UX50 and 4,000fps from the Mini UX100. Both models are available with recording memory options up to 32GB providing extended recording times and triggering flexibility.

Using innovative proprietary CMOS image sensor technology, the FASTCAM Mini UX achieves high light sensitivity from a small image sensor (10µm pixel pitch) through the utilization of microlenses to increase effective Fill Factor. At maximum image resolution the image sensor is fully compatible with readily available 1-inch C-mount lenses offering a wide choice of small, light weight, rugged and high aperture objective lenses.

The FASTCAM Mini UX features a rugged design suitable for operation in high shock and vibration environments and a compact camera body (120mm x 120mm x 93mm) weighing just 1.5kg.This small and rugged camera design makes the FASTCAM Mini UX ideally suited to on-board and off-board automotive safety testing and many other applications where a compact size and compatibility with standard optical systems is required.

Standard operational features of the FASTCAM Mini UX include a Gigabit Ethernet Interface for reliable system control with high-speed data transfer to PC, and the ability to remotely switch off cooling fans to eliminate vibrations when recording at high magnifications.

Light Sensitivity:
Expressions of light sensitivity in high-speed cameras can be confusing as a variety of differing measurement techniques are used. Photron publishes light sensitivity figures for its products using the ISO 12232 Ssat Standard.

FASTCAM MINI UX	ISO 12232 Ssat
Monochrome models	ISO 10,000
Color models	ISO 5,000

ISO 12232 Ssat values published by Photron for both monochrome and color cameras are measured excluding infrared sensitivity as defined by the ISO standard measurement procedure ISO 14524.

Monochrome sensors used in the FASTCAM Mini UX cameras are supplied without an IR absorbing filter, extending the camera spectral response beyond 900nm. When the sensitivity of the FASTCAM Mini UX camera is measured to tungsten light including near IR response an equivalent value of ISO 25,000 is obtained.

Image Sensor:
The FASTCAM Mini UX system uses an advanced CMOS image sensor optimized for light sensitivity and high image quality that is unique to Photron.

A 10-micron pixel pitch gives a sensor size at full image resolution of 12.8 x 10.24mm (diagonal 16.39mm).

Lenses designed for both 1-inch C-mount and FX / DX (APS-C digital SLR) formats are compatible with the FASTCAM Mini UX at full image resolution.

Sensor Type	Proprietary Design Advanced CMOS
Maximum Reolution (pixels)	1280 x 1024 pixels
Sensor Size / Diagonal	12.80 (H) x 10.24mm (V) / 16.39mm (D)
Pixel Size (microns)	10µm x 10µm
Quantum Efficiency	62.6% at 630nm
Fill Factor	80%
Color Matrix	Bayer CFA (single sensor)
ISO 12232 Ssat sensitivity	ISO 10,000 monochrome ISO 5,000 color (monochrome sensor equivalent ISO 25,000 including near IR response)
Shutter	Global Electronic Shutter 3.9µs up to 1.01µs at maximum frame rates

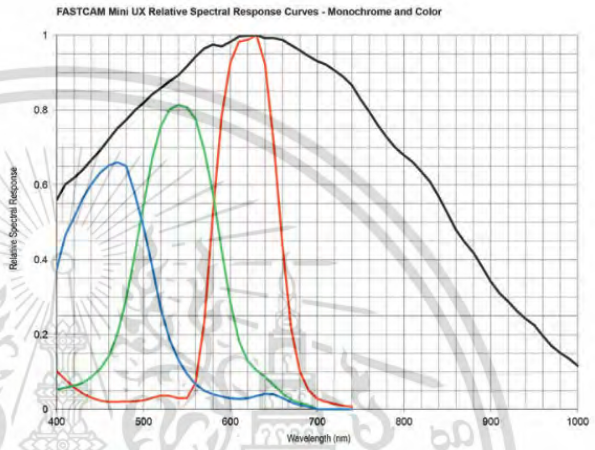

Combustion experimental pressure sensor specification

GU22CK

TIGG1355A.01

The GU22CK is an accurate and robust 6.2 mm plug-type sensor. It is based on a well established design concept that allows high accuracy. It has thermally optimized piezoelectric elements and no influence from the mounting bore on the pressure signal due to minimized mechanical contact between mounting bore and the sensor housing. A thermo protection can improve the cyclic drift down to ± 0.3 bar. The sensor is equipped with built in SID for SDM.

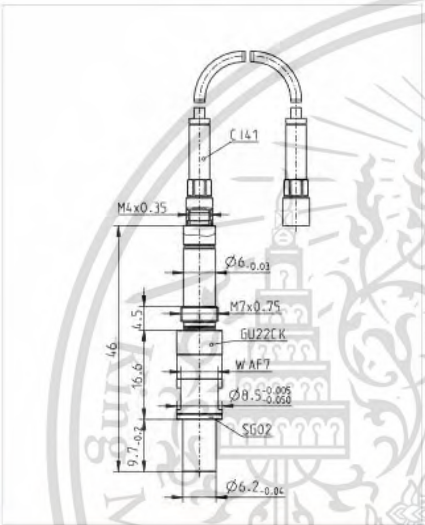

Scope of Supply

- Sensor GU22CK
- Piezo-input cable CI41-1
- Coupling CC41
- Gasket SG02
- Accessory kit (protection cap + 2 spare O-rings)
- Spare gasket SG02
- Calibration sheet
- Documentation

Specifications

Measuring range		0 ... 350 bar	
Overload		400 bar	
Sensitivity		34 pC/bar	nominal
Linearity	≤ ±	0.3 %	FSO
Calibrated ranges		0 ... 80 bar 0 ... 150 bar 0 ... 300 bar	
Natural frequency		96 kHz	
Acceleration sensitivity	≤	0.001 bar/g	axial
Shock resistance	≥	2000 g	
Insulation resistance	≥	10^{13} Ω	
Capacitance		8 pF	
Operating temperature range [1]		- 40 ... 400°C	
Thermal sensitivity change	≤	1 %	20 ... 400 °C and 0 ... 300 bar
	≤ ±	0.25 %	250 ± 100 °C and 0 ... 300 bar typ.
Load change drift		1.5 mbar/ms	max. gradient typ.
Cyclic temperature drift [2]	≤ ±	0.6 bar	
Thermo shock error Δp [3]	≤ ±	0.3 bar	typ.
Mounting bore		6.3 mm	shoulder sealed
Cable connection		M4 x 0.35	negative
Weight		12.5 grams	without cable
Mounting torque		10 Nm	

Combustion experimental high speed VDO camera specification

Image Technology

the most experienced name in high speed cameras

MEMRECAM GX-1

High Speed Camera System

The Memrecam GX series: The workhorse family of ruggedized 1.3 Mega Pixel high speed camera systems.

Memrecam GX-1 FEATURES

CMOS Sensor: 1280 X 1024 — all Active Pixels

Bit Depth: 12/10/8-bit (customer selectable)

Electronic Shutter: OPEN to 1µsec

Variable Framing Profile: Test using a variety of frame rates, sequentially or in parallel.

Versatile Recording: Burst, multi-trigger and image trigger.

Multi-Camera Download: Download images from up to seven cameras simultaneously in same time it takes to download a single camera.

Hi-G Operation: Specifically designed to function effectively in Hi-G environments (to 100G shock).

Ultra-High Light Sensitivity

Ruggedized for Range Use: Sealed camera core, uses no fans.

NAC's Memrecam GX-1 boasts a 1.3 Mega Pixel sensor and the most light sensitive images in its class. The Memrecam GX-1 supports wide screen viewing of critical high-speed imaging events, keeping the subject in frame longer. The Memerecam GX-1 records brilliant color images or crisp monochrome images at full 1.3 Mega Pixel resolution at more than to 2,000 fps, 1 Mega Pixel resolution at more than 2,550 fps and 720p HD resolution at more than 2,780 fps.

The rugged Hi-G GX-1 is perfect for a variety of applications, including: Automotive Crash, Ballistics, Combustion, Materials Research, Machine Design, Microscopy, PIV, Flow Visualization, Spray Analysis, and many more...

When it comes to reliable, high-quality, high-speed camera systems, make the proven choice with NAC and you'll see the visible difference!

MEMRECAM GX-1
High Speed Camera System

Memrecam GX-1 Full Screen Mode		
Max Res (pixels)	1280 X 1024	
Optical Format	35.57 mm	
fps @ Max Res	2,078	
Gpix/ sec @ Max Res	2.72	
	Mono	Color
ISO Rating	20,000	5,000
Memory Options	2GB, 4GB, 8GB	
Max fps	245,098	

Imaging Formats	Max fps @ Full Res.
1 Mega Pixel	2,559
1280 X 720	2,789
XGA (1024 X 768)	3,293
768 X 768	4,359
768 X 576	5,477
VGA (640 X 480)	7,485
512 X 512	8,831
512 X 384	10,837
QVGA (320 X 240)	22,371
256 X 192	30,600
128 X 96	69,444
64 X 64	117,371
64 X 32	128,866

AUTHOR BIOGRAPHY

Author: Mr. Pop-Paul Ewphun

Date of Birth: 18th March 1991

Address: 218 Lapprao 130 Klongchan Bangkapi Bangkok Thailand 10240

Education:

2009 – 2012: Bachelor Degree in Automotive Engineering, Faculty of Engineering, Thai-Nichi Institute of Technology.

2014 – 2016: Master Degree in Automotive Engineering (International Program), International College, King Mongkut's Institute of Technology Ladkrabang.

Publications:

1) P. Ewphun, V. T. Chau, P. Srichai, C. Charoenphonphanich, S. Sato and H. Kosaka. Combustion characteristics of Hydrotreated vegetable oil – diesel blend under EGR and supercharged conditions. International Journal of Automotive Technology 18, 4, (2017) 643-652.

2) P. Ewphun, V. T. Chau, S. Saeo, S. Marasri, P. Srichai, P. Karin, C. Charoenphonphanich, N. Chollacoop, H. Kosaka. Investigate effect of Hydrotreat vegetable oil – diesel blend percentage to injection characteristic. 2016. JSAE Annual Congress (Spring) No. 20165382. Yokohama, Japan, May 25th-27th, 2016.